EUPHAUSIID ECOLOGY AND WATER MASS ASSOCIATIONS IN ROSEWAY BASIN MEASURED FROM AN OCEAN GLIDER

by

Gennavieve Shaanti Ruckdeschel

Submitted in partial fulfillment of the requirements
for the degree of Master of Science

at

Dalhousie University
Halifax, Nova Scotia
September 2017

I had met Neptune in his wrath, but he found that I had not treated him with contempt, and so he suffered me to go on and explore.

– Captain Joshua Slocum, *Sailing Alone Around the World* (1900)

Table of Contents

List of Tables

List of Figures

Abstract

The goal of this thesis is to quantify spatial and temporal variation in the concentration and distribution of zooplankton, with an emphasis on euphausiid krill, in Roseway Basin, on the Scotian Shelf. We used an autonomous ocean glider with an integrated echosounder and CTD to continuously monitor variation in zooplankton and water masses over two months in autumn 2015. The glider data revealed intra-seasonal variation in euphausiid concentrations that depended upon water mass presence in the basin. I provide evidence that the Nova Scotia Coastal Current plays a significant role in transporting euphausiids in Roseway Basin. Glider-derived estimates of euphausiid concentration were similar in magnitude with those in known baleen whale feeding habitats, indicating that Roseway Basin may represent a viable feeding habitat for whales on the Scotian Shelf. The process-based information provided by the glider is critical for identifying feeding habitat for whales and for determining if prey-field variation explains the presence and persistence of whales to support monitoring and conservation efforts.

List of Abbreviations and Symbols Used

Abbreviation	Description	Units
α	Acoustic attenuation coefficient	dB m^{-1}
A_{taxa}	Taxon abundance	ind
BBL	Background backscatter level	dB re m^{-1}
Cal_{coeff}	Calibration coefficient	dB re m^{-1}
df	Degrees of freedom	
g	Density contrast relative to seawater	
$GAIN$	Acoustic gain setting	dB re m^{-1}
h	Sound speed contrast relative to seawater	
LB	Lower boundary	m
N	Sample size	count
N_{cop}	Estimated copepod concentration	ind m^{-3}
N_{eup}	Estimated euphausiid concentration	ind m^{-3}
N_{net}	Net-specific taxon concentration	ind m^{-3}
$\overline{N}_{SL}$	Scattering layer average euphausiid concentration	ind m^{-3}
$\sum N_{SL}$	Scattering layer integrated euphausiid concentration	ind $layer^{-1}$ m^{-2}
p	Probability value	
r	Range	m
R^2	Coefficient of determination	
S	Salinity	psu
SD	Standard deviation	
SE	Standard error	
SF_{taxa}	Taxon split fraction	
S_v	Mean volume backscattering strength	dB re m^{-1}
$S_{v(cop)}$	Expected copepod backscatter	dB re m^{-1}
$S_{v(eup)}$	Expected euphausiid backscatter	dB re m^{-1}
$S_{v(eup+cop)}$	Expected euphausiid and copepod backscatter	dB re m^{-1}
$S_{v(obs)}$	Observed backscatter	dB re m^{-1}
T	Temperature	ºC
t	Student's test statistic	
TS	Target strength	dB re m^{-1}
TS_{amph}	Amphipod target strength	dB re m^{-1}
TS_{cop}	Copepod target strength	dB re m^{-1}
TS_{eup}	Euphausiid target strength	dB re m^{-1}
TS_{pter}	Pteropod target strength	dB re m^{-1}
UB	Upper boundary	m
Vol_{net}	Filtered net volume	m^3
ΔZ_{SL}	Scattering layer thickness	m
AIC	Akaike's Information Criterion	
$ANOVA$	Analysis of Variance	

$\boldsymbol{BIONESS}$	Bedford Institute of Oceanography Net and Environmental Sampling System
$\boldsymbol{CBS-CIL}$	Cabot Straight Cold Intermediate Layer
$\boldsymbol{CBSs}$	Cabot Straight subsurface water
$\boldsymbol{CCGS}$	Canadian Coast Guard Ship
$\boldsymbol{CCS}$	California Current System
$\boldsymbol{CIL}$	Cold intermediate layer
$\boldsymbol{CSW}$	Cabot Straight water
$\boldsymbol{CTD}$	Conductivity-temperature-depth sensor
$\boldsymbol{DFO}$	Department of Fisheries and Oceans
$\boldsymbol{DVM}$	Diel vertical migration
$\boldsymbol{DWBS}$	Distorted-wave Born approximation
$\boldsymbol{GoM}$	Gulf of Maine
$\boldsymbol{GoSL}$	Gulf of St. Lawrence
$\boldsymbol{GPS}$	Global Positioning System
$\boldsymbol{LCW}$	Labrador current water
$\boldsymbol{LSW}$	Labrador slope water
$\boldsymbol{NSC}$	Nova Scotia Current
$\boldsymbol{PAM}$	Passive acoustic monitoring
$\boldsymbol{R01}$	Roseway BIONESS station 1
$\boldsymbol{R02}$	Roseway BIONESS station 2
$\boldsymbol{SL}$	Scattering layer
$\boldsymbol{SLE}$	St. Lawrence Estuary
$\boldsymbol{VIF}$	Variance inflation factor
$\boldsymbol{WAP}$	Western Antarctic Peninsula
$\boldsymbol{WSW}$	Warm slope water

Acknowledgements

This thesis would not have been possible without an able-bodied crew of people who make it their purpose to better understand, and thus better protect, the ocean.

My deepest gratitude to my supervisors, Tetjana Ross and Kim Davies for their enduring support and mentorship during my time with them. I have learned from you how to begin navigating as a researcher, through both calm and rough seas. I also want to acknowledge my committee members, Anna Metaxas, Julie LaRoche, and Johannes Karstensen. Thank you for your time and commitment. Thanks to Carly Buchwald for agreeing to take part in my defence.

Special thanks to the Ocean Tracking Network (OTN) glider team, Adam Comeau, Sue L'Orsa, Brad Covey, and Richard Davis, for making a glider dataset possible. I am also grateful to the Aquatron team, Jon Batt and Jim Eddington, for providing space and support for the echosounder calibration. Many thanks to the Dalhousie oceanography graduate students, the other TOSST students, and especially my first lab mates, Dylan DeGrâce and Nick Dourado, for their camaraderie, friendship, and keeping a sense of humor during this whole voyage.

To WHaLE, I hope this thesis is of benefit for improving what we know about whale habitat. My warmest thanks to Chris Taggart, Delphine Durette-Morin, Hansen Johnsen, Danielle Moore, Caroline Fox, and Tara Howatt. I'm lucky to have landed in such a good bunch.

Thanks to my family, especially my Mom, Dad, brother, and sisters. You believed in me before I did. I've come a long way from Virginia Beach, but maybe I never really left.

This research was made possible through funding by the Transatlantic Ocean System Science and Technology Research School (TOSST) and The Marine Environmental Observation Prediction and Response Network (MEOPAR). Thank you for giving me the opportunity to pursue impactful ocean research.

Chapter 1

Introduction

1.1 Research Motivation

This thesis is a contribution to the Whales Habitat and Listening Experiment (WHaLE project) under the Marine Environmental Observation and Prediction Network (MEOPAR). The primary goal of the WHaLE project is to identify feeding habitats for baleen whales on the Scotian Shelf using autonomous profiling ocean gliders as the primary observational platform. To achieve this, gliders are equipped with a single-frequency echosounder to measure zooplankton (*i.e.,* baleen whale prey), and a hydrophone to listen for the sounds made by five baleen whale species known to be present on the Shelf. Each glider is deployed for several months at a time to concurrently measure whale acoustic presence/absence, zooplankton abundance and distribution, and the physical conditions (temperature, salinity) in the habitats surveyed. The goal of WHaLE is to use this novel remote-sensing data to determine whether variation in the zooplankton prey-field and associated physical environment (transport, water masses, bathymetry) can explain whale acoustic presence in time and space. To achieve this goal, it must first be determined what kind of relevant information the glider-mounted single-frequency echosounder can provide about the baleen whale prey-field; namely the presence, abundance, and distribution of euphausiids and copepods. If the sensor can provide useful information on the baleen whale prey-field, then the question of how baleen whales associate with this prey-field in time and space can be addressed. It is therefore critical to the WHaLE project to quantify variability in zooplankton abundance and distribution derived from the glider echosounder data, and this is the goal of this thesis.

1.2 Background

Zooplankton are a critically important group of organisms in marine ecosystems. By preying on tiny primary producers and being preyed on by animals at higher trophic levels, zooplankton are a fundamental energetic link in marine food webs. Further, because many species perform diel vertical migration (DVM), zooplankton can impact biogeochemical cycling at the scale of ocean basins by transporting organic material between the surface and the deep ocean (*Hays* 2003; *Ringelberg* 2009). Among the myriad groups of zooplankton in the oceans, euphausiids (krill) are particularly important because they constitute a substantial proportion of the total zooplankton biomass in many marine habitats, particularly at temperate to polar latitudes (*Mauchline & Fisher* 1969). Because of this, euphausiids are a primary food-source for pelagic fish, seabirds, and marine mammals in these habitats (*Mauchline* 1980).

The largest euphausiid predators are the baleen whales, who rely on biological and physical aggregation processes to concentrate krill into prey-fields dense enough to sustain the costs of foraging and metabolism (*Kenney et al.* 1986; *Piatt & Methven* 1992). Studying habitat use and explaining variation in baleen whale prey abundance is an important research focus for conservation and management efforts (*e.g.,* defining Critical Habitat), because many species of baleen whales are endangered or have unknown conservation status (*Hoyt* 2012). Three important components of baleen whale feeding habitat are (1) the absolute concentrations of prey, which affects the carrying capacity of the habitat (*Michaud & Taggart* 2007; *Michaud & Taggart* 2011; *Davies et al.* 2014); (2) the spatial distribution of prey concentrations, which defines the spatial habitat boundaries (*Davies et al.* 2014); and (3) the temporal persistence of prey distributions (*Michaud & Taggart* 2007; *Michaud & Taggart* 2011), which can define the occupancy period of whales in the habitat. Variation in the concentration, distribution and persistence of prey are likely the most important drivers of baleen whale presence and absence in feeding habitats, thus it is critical to study the biological and environmental processes that cause variation in these aspects of the prey-field.

The physical and biological processes that explain variation in the concentrations, distribution, and persistence of euphausiids in baleen whale habitat are the focus of considerable study in several locations known to be important feeding areas for whales.

For example, absolute concentrations of euphausiids are impacted by physical processes, such as tidal upwelling in the St. Lawrence Estuary (SLE; *Lavoie et al.* 2000), but can also be a result of social behaviour of the euphausiids themselves, such as in the Western Antarctic Peninsula (WAP; *Hamner & Hamner* 2000). The distribution and temporal persistence of elevated euphausiid concentrations are also affected by larger-scale processes, such as dominant currents and their interactions with bathymetry, as in the WAP (*Hofmann & Murphy* 2004; *Lawson et al.* 2008) and in the California current system (CCS; *Mackas et al.* 1997). However, the processes related to baleen whale habitat are poorly studied in many other locations. The Scotian Shelf is one such location, and is the primary region of focus for the WHaLE project.

The Scotian Shelf extends to the east and south along Nova Scotia, and is characterized by relatively shallow banks (~100 m depth) interspersed with deep shelf-basins that can reach more than 300 m in depth. The same species of baleen whales that feed on euphausiids in the nearby SLE (including blue, *Balaenoptera musculus*; fin, *B. physalus*; humpback, *Megaptera novaeangliae*; sei, *B. borealis*; and minke, *B. acutorostrata*) are seasonally detected across the Scotian Shelf (*Woodley & Gaskin* 1996; *Martin et al.* 2014). Previous work over the Shelf has found significant concentrations of northern krill, *Meganyctiphanes norvegica,* in several deep shelf-basins, notably LaHave and Emerald Basins (see; *Cochrane et al.* 1991; *Sameoto et al.* 1993; *Cochrane et al.* 2000). The region is hydrographically linked to the Gulf of St. Lawrence (GoSL) in the north and to the Gulf of Maine (GoM) in the south by the Nova Scotia Current (NSC), which brings cold and fresh water (hereafter Cabot Straight water; CSW) from the Gulf of St. Lawrence, through the Cabot Straight, and along the shelf (*Smith & Schwing* 1991; *Loder et al.* 1997). Intrusions of warm and salty continental slope water (hereafter warm slope water; WSW), cold and salty Labrador Slope water (LSW), as well as mixtures of cold and fresh inshore Labrador Current water (LCW) and a cold intermediate layer (CIL) from the Cabot Straight are also found over the shelf seasonally and in variable proportions (*McLellan* 1954; *Gatien* 1976; *Petrie & Drinkwater* 1993). The Nova Scotia current and intrusions of WSW are sources of zooplankton biomass, including euphausiids, to the Scotian Shelf (*Herman et al.* 1991). Moreover, deep basins can act to aggregate zooplankton at higher concentrations

than over banks (*Cochrane et al.* 1994). Thus, variations in these water masses and their interactions with basin bathymetry can impact prey-fields of baleen whales in this region.

Despite the presence of several baleen whale species, no previous study has sought to characterize variations of euphausiid concentration on the Scotian Shelf or study processes that drive these variations in terms of baleen whale feeding habitat suitability. Further, to our knowledge, no investigation has yet been made into the drivers responsible for the variation in euphausiids within shelf basins. The WHaLE project's efforts are aimed at filling this knowledge gap for the Scotian Shelf region, specifically by using ocean gliders as a novel observing platform to provide increased survey coverage and high-resolution integrated oceanographic and acoustic sampling for purposes of habitat characterization and whale monitoring.

Among the Scotian Shelf basins, Roseway Basin was selected as the study location for the research presented here because it is an area of special interest for characterizing variation in zooplankton. Roseway has previously been characterized as a critical habitat for the highly endangered North Atlantic right whale (*Eubalaena glacialis*), due to dense aggregations of their preferred copepod prey, *Calanus finmarchicus*, which form along the southeast basin margin (*Davies et al.* 2013; *Davies et al.* 2014). Euphausiids have been sampled previously in Roseway (*Doherty & Horsman* 2007, *Brown et al.* 2009), but their baseline concentrations and distributions in the basin have not been studied prior to the current study. In addition to the presence of euphausiid prey in the basin, baleen whales that feed on euphausiids including fin, humpback, and sei whales have been sighted and recorded acoustically in the basin (*Mitchell et al.* 1986, *Davies K. pers. comm.* 2016).

1.3 Research Objectives

The glider data used for this study provided simultaneously measured spatial and temporal information on variation in zooplankton and water masses, which was used to investigate euphausiid concentrations, spatial distributions, and persistence over time in Roseway Basin during a glider survey conducted during autumn 2015. Specifically, this thesis aims to address the following motivating questions:

- Are euphausiids more abundant in particular source water masses in Roseway Basin (*e.g.,* slope vs. shelf water)?

- Does Roseway Basin contain euphausiid concentrations, distributions and temporal persistence necessary to constitute a significant baleen whale habitat?
- What are the primary drivers of variation in euphausiid concentration in the Basin (*e.g.,* advection, bathymetry) and what scales do they occur on?

To address these questions, this thesis has the following research objectives:

1. Characterize intra-basin spatial (*i.e.,* across and along-basin, depth) and temporal (within and between months) variation in (A) the concentration and distribution of euphausiids derived from acoustic scattering layers (SLs) and (B) water mass properties in Roseway Basin.
2. Perform modelling and statistical comparisons to identify glider-measured oceanographic variables that can explain variation in euphausiid SLs, and infer oceanographic processes attributable to identified relationships.

1.4 Thesis Structure

This thesis is divided into four chapters. Chapter 2 provides a summary of the field study, including the glider survey of Roseway Basin and processing of the CTD data. Chapter 3 presents zooplankton observations from two ship-based net tows performed in Roseway, and a comparison of the net sample data to the acoustic measurements from the echosounder to validate the latter by quantifying the extent to which the acoustic measurements can be interpreted as variation in euphausiid concentrations. Chapter 3 also details the development and implementation of an algorithm to identify acoustic scattering layers (SLs) in the glider data and to calculate descriptive metrics from detected SLs. Chapter 4 contains the characterizations of both the acoustic measurements (in the form of SL metrics) and the water mass properties measured by the glider. Chapter 4 also presents results from statistical analysis for modelling variation in the SL metrics and comparisons between identified water masses in the basin. Finally, Chapter 5 sums up with a discussion of the results from the characterizations and modelling in terms of oceanographic processes that can explain variation in euphausiid SL metrics and how the results relate to Roseway's potential as a baleen whale feeding habitat.

Chapter 2

Field Study

2.1 Glider Survey of Roseway Basin

2.1.1 Study Location

Roseway Basin is positioned on the western Scotian Shelf in the Northwest Atlantic Ocean, flanked by neighbouring LaHave Basin and LaHave Bank to the northeast and by Browns Bank to the southwest (Fig. 2.1). In addition to its designation as a right whale critical habitat (DFO 2007; *Brown et al.* 2009), Roseway Basin is also recognized as an area of high fish and invertebrate richness, (*Ward-Paige & Bundy* 2016), and as an important seabird habitat (*Allard & Gjerdrum, in prep.*). The basin is roughly 400 km^2 in size and contains depths of up to 180 m with more sharply sloping bathymetry along the southeast and northwest margins and more gently sloping bathymetry that leads into channels along the northeast and southwest margins (Fig. 2.1, inset). Roseway Basin has a few physical oceanographic features that make it unique among shelf-basins, and that are relevant to this study. The basin contains the strongest tides of anywhere on the Scotian Shelf, with speeds up to 0.5 m s^{-1}, and deep water in the Basin is comprised primarily of WSW (which is warm and salty), while CSW (which is cold and fresh) is typically present on the northern Basin margins, closer to the coast (*Davies et al.* 2013; *Davies et al.* 2014). In some years, LSW can also be found in the Basin due to high transport of the Labrador Current (*Patrician & Kenney* 2010, *Davies et al.* 2015).

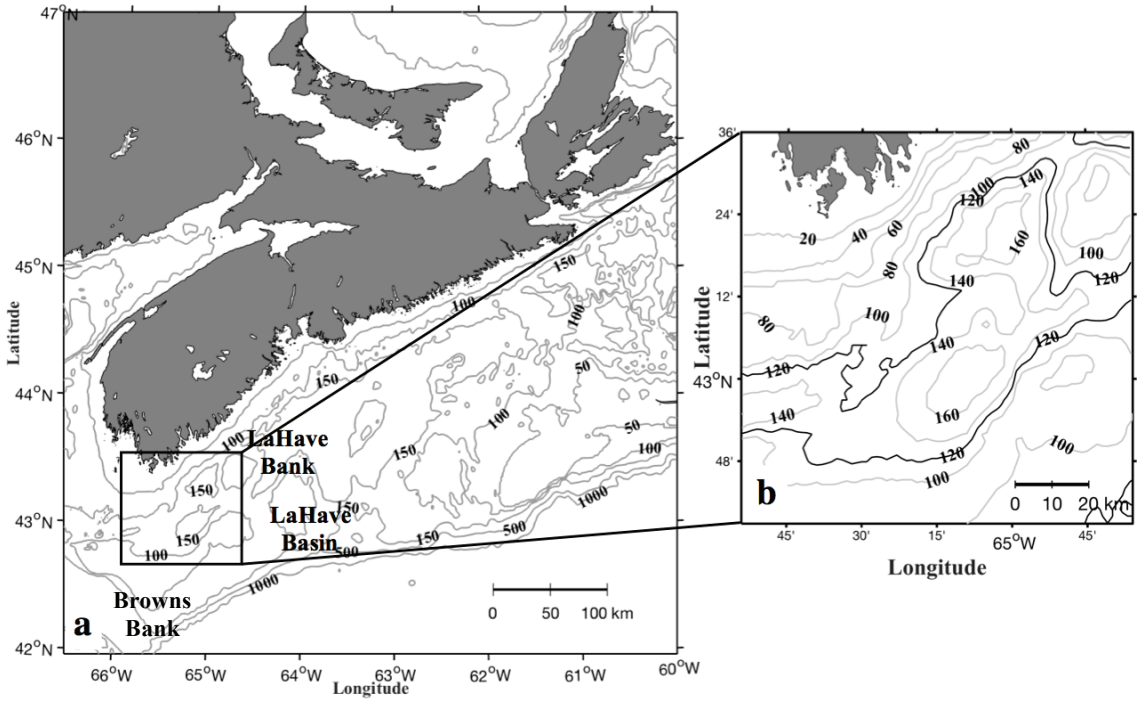

Figure 2.1. Map showing location of Roseway Basin on the Scotian Shelf (a) with the 50, 100, 150, 500, and 1000 m isobaths. Inset (b) shows detailed bathymetry of Roseway Basin. Isobaths are drawn every 20 m. The 120-m isobath is drawn in bold in the inset to indicate the boundary of the basin margins.

2.1.2 Glider and Sensors

This study relied on data collected with an electric G2 Slocum ocean glider (*Schofield et al.* 2007) which collected geo-referenced measurements of hydrography and acoustic backscatter (see 2.1.3 for survey details). Slocum gliders are autonomous underwater vehicles (AUVs) that profile up to 200 m deep by adjusting their internal buoyancy. The gliders have an average horizontal speed of 0.3 m s^{-1} with an angle of attack of 22–26 degrees. Wings on the glider body translate some of the vertical motion into horizontal motion, resulting in a saw-tooth dive pattern. For this study, the glider profiled vertically to between ~ 5–10 m above the seafloor, and surfaced at intervals of approximately 2 hours (equivalently, 2–4 vertical profiles) to send science and diagnostic data, receive navigation commands via the Iridium satellite, and acquire a new GPS fix. Obtaining a GPS fix at each surfacing allows the glider to correct its dead-reckoned course if it drifts off course while underwater and out of contact with satellites. The latitude and longitude were interpolated onto the same high-resolution time axis as the environmental observations, so

may not be exact, but are useful in interpreting the data. It should be noted that an occasional (less than 30% of profiles) malfunction of the glider's altimeter causes an underestimate of the seafloor, and results in an early inflection where the glider returns to the surface mid-way through a profile.

The glider was powered with lithium batteries and was equipped with an un-pumped Seabird (SBE41 modified, *Garau et al.* 2011) conductivity-temperature-depth sensor (CTD) to measure profiles of water temperature, salinity, and density at a sampling rate of 1 Hz, which resulted in data with a vertical resolution of ~ 0.5 m. A downward-looking 300 kHz Imagenex 853 echosounder was integrated on the underside of the glider to record acoustic backscatter at a ping rate of 1 Hz. The 300 kHz frequency was selected to detect backscatter from both small and large targets (*i.e.,* copepods at ~1–2 mm and euphausiids at ~10–20 mm). The raw backscattering returns for each ping from the echosounder were recorded as peak-to-peak voltage amplitudes (V) in two hundred 0.5 m vertical range bins (*e.g.,* distance from transducer beneath the glider). The echosounder collected observations only during glider downcasts, as the transducer was tilted at 26 degrees from the glider's axis so that it would be oriented straight down on the descent.

2.1.3 Survey Design and Implementation

The glider survey plan was designed to characterize the four-dimensional variability of hydrography and acoustic backscatter in the Basin. The glider transited across and along the Basin among 9 waypoints, starting at waypoint A and ending at waypoint I (Fig. 2.2). This plan resulted in 8 across-basin transects, hereafter labeled transect-1 (between waypoints A and B) through transect-8 (between waypoints H and I). The glider completed two transits of the survey plan. The first transit took 32 days to complete and occurred from September 18 to October 21 (hereafter transit 1, Fig. 2.2a). The second transit took 26 days to complete and occurred from October 23 to November 19 (hereafter transit 2, Fig. 2.2b). Transects 7 and 8 were not surveyed during transit 2 (Fig. 2.2b). The glider did not always precisely follow the planned survey track because it moves slowly and can be pushed around by strong currents; for example, the wave-like deviation of the glider path from a

straight line joining consecutive waypoints is due to the influence of strong tidal currents in the Basin (Fig. 2.2).

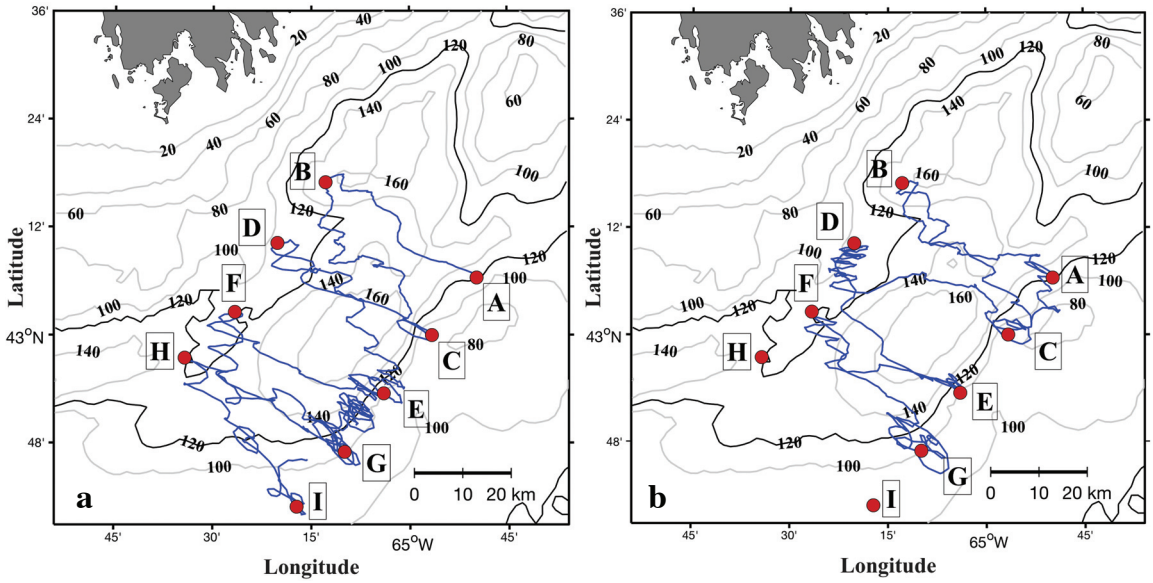

Figure 2.2. Waypoints for survey (A-I; red circles), with realized glider track for transit 1 (a) and transit 2 (b) of Roseway Basin. Isobaths are shown at 20 m intervals, and the 120 m isobath is drawn in bold to indicate the basin boundary.

2.2 CTD Data Processing

Conservative temperature (°C) and absolute salinity (g kg^{-1}) were calculated from the CTD sensor data using the Gibbs Seawater (GSW) Oceanographic Toolbox in MATLAB (*McDougall & Barker* 2011). Because unpumped CTDs can suffer from hysteresis across strong thermal gradients in the water column, a published empirical correction for thermal lag was applied to the salinity data (*Garau et al.* 2011). Briefly, the method finds lag correction parameters using an optimization algorithm that minimizes the difference between pairs of glider upcasts and downcasts in temperature-salinity space. This algorithm assumes that the water masses sampled during consecutive upcast-downcast pairs (equivalent to ~ 1 km spatial scale) are the same. In ~18% of profile pairs, the water masses were too different between consecutive upcast-downcast pairs for the algorithm to correct, and these profiles were removed from the dataset. Following the thermal lag correction, the *in-situ* temperature (°C, hereafter temperature) and corrected Practical

salinity (psu, hereafter salinity) were vertically bin-averaged into 0.5 m bins for the remainder of the analysis.

2.3 Positional Data Processing

Because the Nova Scotia coastal current flows approximately parallel to the along-basin axis, and the across-basin axis is approximately orthogonal to the shelf break, which is the origin of WSW to the basin, a coordinate rotation was applied to the data. The rotated axes are, thus, more relevant to examining the spatial oceanographic variability of the system than latitude and longitude. The latitude and longitude data collected by the glider were rotated by + 0.89 radians to express the glider position in terms of the along- (long dimension) and across-basin (short dimension) coordinates in the basin. The angle of rotation was defined by calculating the angular difference between the latitude and longitude data and the long dimension of the basin (Fig. 2.3).

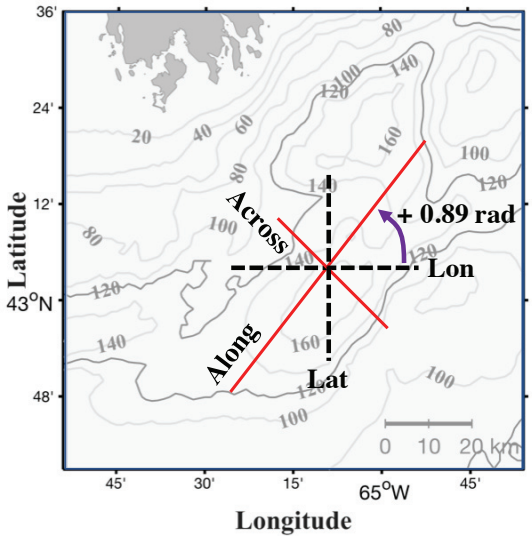

Figure 2.3. Definition of along- and across-basin coordinate axes following a coordinate rotation. Black dashed lines indicate latitude and longitude (original coordinates), solid red lines indicate the long and short dimensions of Roseway Basin (rotated coordinates), and arrow indicates + 0.89 rad rotation applied to the original coordinate data.

The following two chapters contain details of further processing steps applied to the CTD and echosounder data in preparation for analysis; Chapter 3 for the acoustic measurements from the echosounder (section 3.1), and Chapter 4 for the hydrographic measurements from the CTD (section 4.2.1a).

Chapter 3

Validation of Echosounder Data with Zooplankton Samples

My first research objective was to characterize spatial and temporal variation in zooplankton concentration in Roseway Basin using measurements from the glider-mounted echosounder. To achieve this, I first needed to quantify the extent to which the acoustic estimates derived from the echosounder represented the concentration of different zooplankton groups. Much of this chapter deals with this task.

3.1 Acoustic Data Processing

3.1.1 Acoustic Data Preparation

The echosounder recorded peak-to-peak voltage amplitudes (V) at a ping rate of 1 Hz in 200 vertical range bins (r) of 0.5 m. To reduce the volume of data and aid in computationally handling the full two months of data simultaneously, these raw acoustic data were subsampled to 1/10 Hz, and only the first 100 range bins (50 m) of data were retained from each ping. Each subsampled ping was converted to mean volume backscattering strength (S_v, dB re m^{-1}) according to the standard sonar equation (*e.g., Medwin & Clay* 1998):

$$S_v = 20log_{10}(V) + 20log_{10}(r) + 2\alpha r - GAIN + Cal_{coeff} \quad (3.1)$$

Where α is the acoustic attenuation at 300 kHz in dB m^{-1} (-0.09 dB m^{-1} for water of 10 °C; *Francois & Garrison* 1982), *GAIN* is the gain setting applied to the echosounder (40 dB), and Cal_{coeff} is the calibration coefficient (-2 dB). The calibration coefficient was determined through a post-deployment set of calibration measurements collected by suspending the glider at the surface of a 10-m deep seawater tank above tungsten-carbide calibration spheres (*i.e.,* targets with known acoustic properties) that were suspended at variable depths under the echosounder, following the protocol of *Vagle et al.* (1996).

Next, a range-dependent noise floor was applied to the data from each ping to remove all S_v values that were below the noise sensitivity of the echosounder. The noise floor is range dependant because the acoustic signal dissipates through attenuation and spherical spreading as the sound wave (ping) travels away from the echosounder. In general, the effective range of the echosounder (with signal, as opposed to noise, in each ping) is around 10 m. Noisy range bins were found by evaluating each acoustic ping against a threshold for background noise that was determined from the distribution of S_v in a set of profiles with very little signal. Only range bins with values exceeding the background noise were retained for each ping. All remaining S_v data within a single glider profile were then bin-averaged into constant depth horizons with 0.5 m vertical resolution to give a single S_v profile for each glider downcast. An example of the resulting data is shown in Fig. 3.1a.

3.1.2 Eliminating Backscatter Due to the Seafloor, Bubbles, and Fish

Acoustic backscatter resulting from the seafloor, from bubbles at the sea surface, or from fish, were removed so that the resulting processed data represented primarily backscatter from zooplankton. First, S_v at depths > 45 m that exceeded -20 dB re m^{-1} were flagged, since this was the weakest backscatter value that was associated with the seafloor. Because the seafloor produces a strong acoustic signal and can contaminate adjacent range bins with increased backscatter, S_v in depth bins from the identified seafloor depth plus 3 m above this depth were removed from the dataset. Seafloor depth derived from the echosounder data was retained as a separate variable for later analyses (yellow line in Fig. 3.1b).

A second acoustic threshold was used to remove echoes from fish and near-surface bubbles. This threshold was determined through inspection of the S_v echograms (Fig. 3.1a) and using knowledge of three key characteristics of bubbles, large fish, and zooplankton as scattering targets. Bubbles are apparent in echograms as very strong values (around -40 dB re m^{-1} and stronger in this dataset) within the upper 10-15 m of the water column. Fish are often visually apparent in echograms as discrete high S_v areas because fish swim bladders are very strong acoustic scattering targets (ca. -50 to -40 dB re m^{-1}), whereas zooplankton appear in echograms as diffuse layers of weaker backscatter (ca. -70 to -55

dB re m^{-1}) spanning tens to hundreds of meters in the horizontal and from several meters in thickness up to the entire water column vertically (see Fig. 3.1a for example). In addition, many species of zooplankton perform DVM by vertically moving to the surface at sunset and returning deep below the pycnocline at sunrise; this can show up as a banded pattern with a period of 12 hours in echograms (*e.g.,* Fig 3.1 where a deep scattering layer can be seen throughout the water column each night, returning to depths below ~80 m during the day). Taking these acoustic characteristics into account, a fish and bubble exclusion threshold of S_v = -55 dB re m^{-1} was estimated by selecting the maximum S_v value from within the night-time surface scattering layers (*i.e.,* strongest acoustic signal from zooplankton). S_v data exceeding this threshold was removed from the dataset at all depths (see example, Fig. 3.1b).

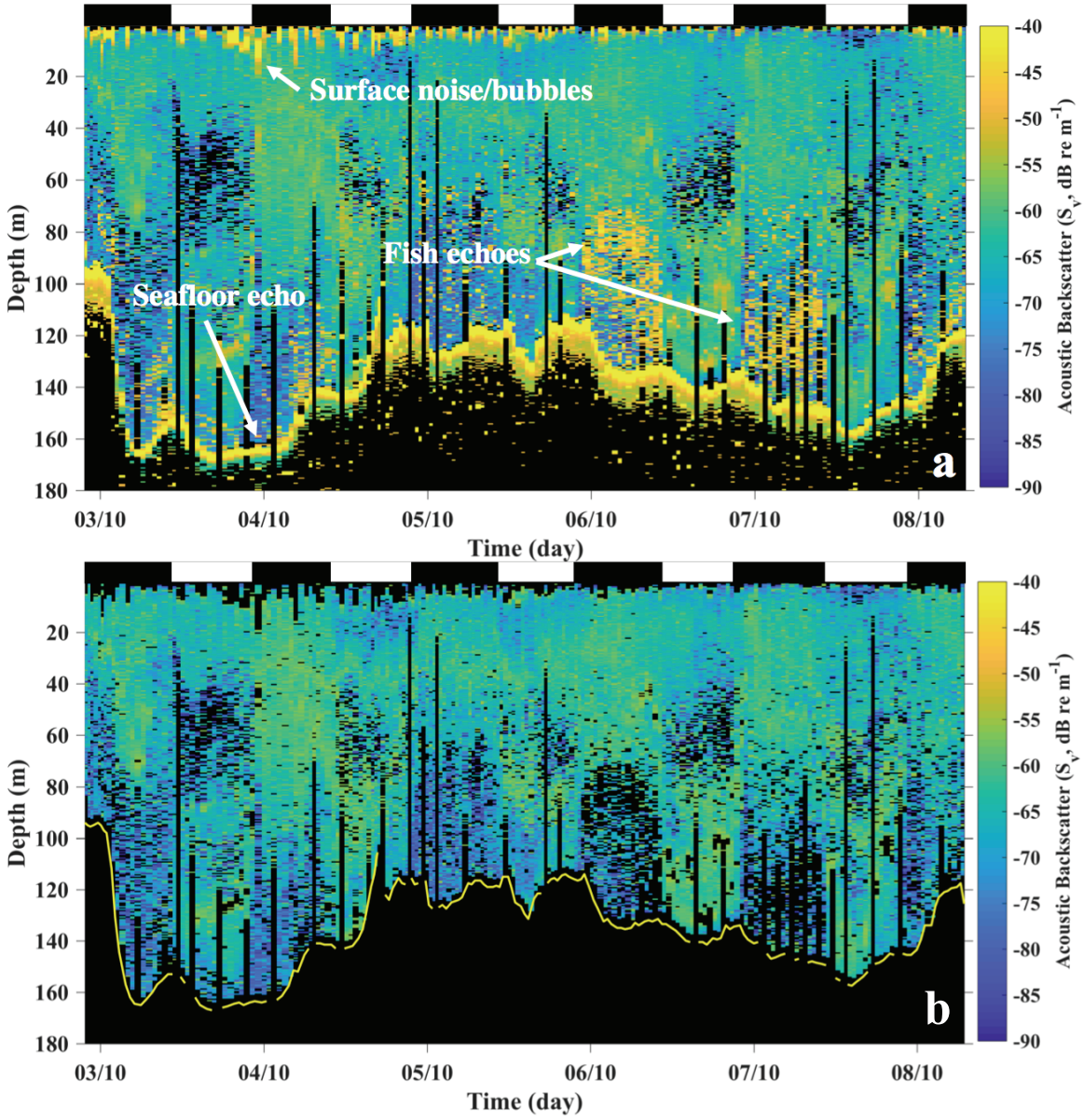

Figure 3.1. Example section plots of glider echosounder-derived S_v (dB re m^{-1}). This example shows vertical profiles collected across Roseway Basin over a five-day period between 2 Oct and 8 Oct 2015. Two panels show the data (a) before and (b) after application of thresholds to remove echoes from the seafloor, bubbles, and fish. Horizontal bars across the top of each panel indicate night (black) and day (white), which helps illustrate the zooplankton DVM signal in the S_v data. Black regions within the S_v plots indicate data removed because it was below the noise threshold. Sporadic vertical black bars in the S_v data show the early inflections made by the glider described in Chapter 2, section 2.1.2. In panel (b), the seafloor is indicated with a yellow line.

3.2 Zooplankton Observations from BIONESS Net Samples and Estimation of Acoustic Target Strengths

Zooplankton net samples collected during the glider survey were analyzed to quantify the species composition and concentrations of zooplankton in Roseway Basin. These data were then used to validate the glider echosounder data by comparing the backscatter measurements collected by the echosounder during the net tows to the backscatter that would be expected given the observed concentrations and species composition of zooplankton present in the nets (Sections 3.3.1–3.3.3). Then, these analyses were used to convert the echosounder data to units of concentration and estimate the uncertainties in the echosounder-derived concentration estimates (Sections 3.3.4–3.3.5).

3.2.1 Zooplankton Concentration and Species Composition from BIONESS Net Tows

Depth-structured zooplankton net samples were collected using the Bedford Institute of Oceanography Net and Environmental Sampling System (BIONESS; *Sameoto et al.* 1980) by the vessel *CCGS Hudson* in Roseway Basin on 9 October 2015. Tows were completed at two stations located 3.5 km apart on the southern Basin margin; the first station (R01) was collected near the 155 m isobath, and the second station (R02) near the 140 m isobath (Fig. 3.2). Both tows were collected at night; station R01 was sampled between 1:15–1:24 am ADT, and station R02 between 3:05–3:16 am ADT. The BIONESS was equipped with six nets each fitted with 243 μm mesh, a flowmeter used to measure the volume of seawater filtered through each net, a CTD, and a strobe light to stun euphausiids and thus reduce net avoidance (*Sameoto et al.* 1993). The first net during each tow was not used for this study because it collected a depth integrated sample during the downcast. Depth integrated samples are of limited use for echosounder calibration because zooplankton aggregate in discrete vertical layers in the water column and a depth integrated tow does not measure that important vertical distribution. On each upcast five remaining nets were opened and closed sequentially to collect depth-structured samples, which were used in this study (Table 3.1).

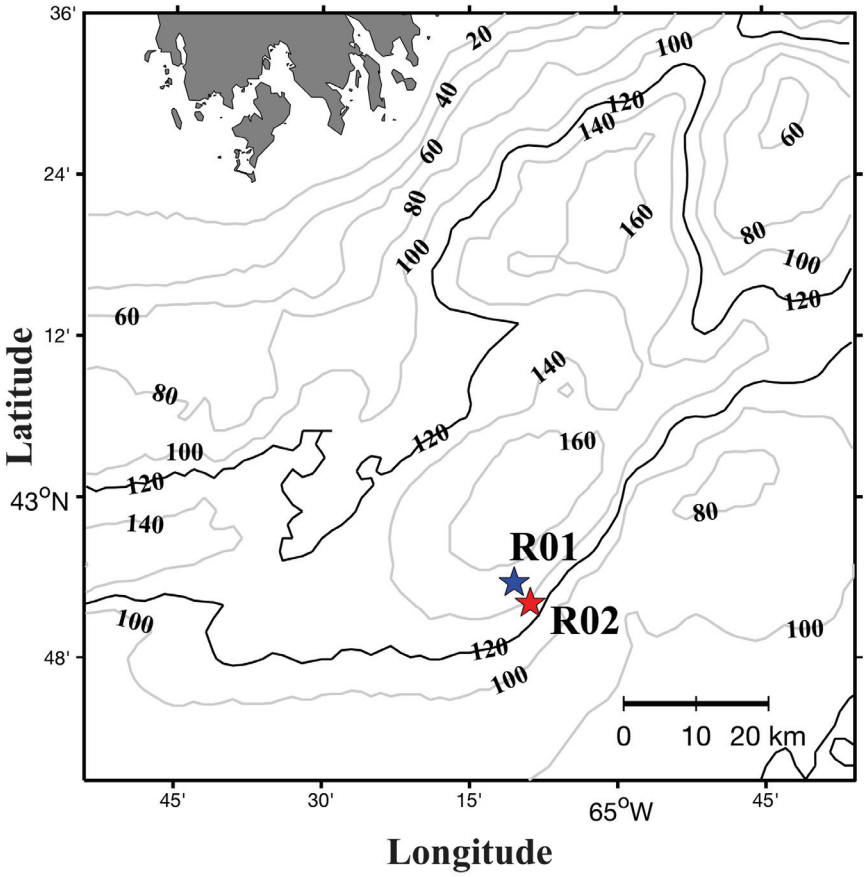

Figure 3.2. Map showing locations of the two BIONESS stations (R01 and R02) where zooplankton net samples were collected in Roseway Basin on 9 Oct 2015 during the glider survey.

Table 3.1. The start and end depths, depth range (m) and filtered volume (m^3) of each BIONESS net collected at two stations (R01 and R02) on 9 October 2015 in Roseway Basin. Location of each station is shown in Fig. 3.2.

Station	Net	Start depth (m)	End depth (m)	Range (m)	Volume Filtered (m^3)
R01	6	50.9	1.4	49.5	69.9
	5	105.7	50.9	54.8	66.47
	4	120.9	105.7	15.2	14.51
	3	137.1	120.9	16.2	14.95
	2	154.6	137.1	17.5	22.18
R02	6	50.7	1.5	49.2	96.28
	5	95.6	50.7	44.9	79.05
	4	110.9	95.6	15.3	37.65
	3	125.7	110.9	14.8	33.3
	2	139.2	125.7	13.5	49.52

Zooplankton in each BIONESS net sample were enumerated and classified to the highest taxonomic resolution possible by a trained technician (*J. Spry*, SpryTech Inc.). All macrozooplankton > 10 mm length were counted in each sample and identified to species (Table 3.2). Mesozooplankton (< 10 mm length) were subsampled by splitting the sample and taking an aliquot then counting and identifying all animals in the aliquot. Mesozooplankton were identified to genus or species, except *Calanus* spp., which were identified to life-stage (I-VI). Net-specific concentration of each taxon (N_{net}, ind m^{-3}) was calculated from the abundance (A_{taxa}), filtered volume (Vol_{net}), and split fraction (SF_{taxa}) as follows:

$$N_{net} = \frac{A_{taxa}}{Vol_{net} * SF_{taxa}} \tag{3.2}$$

Six euphausiid species were found in the net samples: *Meganyctiphanes norvegica*, *Thysanoessa inermis, T. raschii, Euphausia krohnii, T. longicaudata,* and *Nematoscelis megalops.* Euphausiid concentrations at both stations ranged between 0 and 9 ind m^{-3} among nets. Large copepods (> 1.5 mm prosome length) included *Calanus finmarchicus* stages IV-V and stage VI females, *C. hyperboreus* stages III-IV, and *Metridia* sp. Small copepods (≤ 1.5 mm prosome length) primarily included *C. finmarchicus* stages I-III, *Oithona* sp.*, Paracalanus* sp., *Pseudocalanus sp., Centropages typicus,* and *Clausocalanus* sp. Concentrations of large copepods ranged from ~ 35–560 ind m^{-3}, and concentrations of small copepods ranged from ~ 10–1,030 ind m^{-3} over both stations and among nets. Other zooplankton groups potentially important to the study (due to their potential to contribute significantly to acoustic backscatter measured by the echosounder) included amphipods, *Themisto compressa* and *Parathemisto* sp., and pteropods (*Limacina* sp.). These other zooplankton groups ranged in concentration from ~ 0–60 ind m^{-3} over both stations and among nets.

Zooplankton abundance varied among taxon, depth range (net), and station (Fig. 3.3). At station R01, the concentration of euphausiids in the deepest net (net 2; 137.1–154.6 m) was at least four times higher than any other net primarily due to the presence of high concentrations (9 m^{-3}) of a single species, *T. inermis*. In contrast, at R02 the highest concentration of euphausiids in the water column was in the shallowest net (net 6; < 50 m

depth). In net 6 euphausiid concentration at R02 was higher than at R01 due to a high concentration (6 m^{-3}) patch of *M. norvegica*. The concentrations of these two euphausiid species were two orders of magnitude higher in these nets than any other euphausiid species (Tables 3.2–3.3). The vertical distribution of large copepods showed the opposite pattern to euphausiids (Fig. 3.3b); copepod concentrations were highest by a factor of five in the two mid-water nets (net 3 and net 4) at both stations (~ 100–140 at R01 and ~ 100–125 m at R02), compared with either the shallowest or deepest nets. This pattern was driven strongly by variation in a single species and stage, *C. finmarchicus* stage-V**,** whose concentration was an order of magnitude higher in the mid-water nets than any other species. This vertical distribution is typical of diapausing (*i.e.,* dormant and non-migrating) *C. finmarchicus* stage-V in the basin at that time of year (October). The concentrations of all other zooplankton, including small copepod species and stages, were generally highest in the upper 50 m (Fig 3.3c, d), which is consistent with behaviour exhibited by species that perform DVM (*e.g.,* euphausiids, non-diapausing copepods, amphipods, and pteropods). *Limacina* sp. pteropods (a strongly backscattering acoustic target) were present at concentrations between 3-25 ind m^{-3} in the upper 100 m across both stations, and had higher concentrations in the upper 50 mm.

Literature reported values for copepod length by species used to designate 'large' from 'small copepods' are from *Razouls et al.* (2005), and a list of rare species also present in the net samples is presented in Table A.1 (Appendix A).

Table 3.2. Net-specific zooplankton concentration (ind m^{-3}) and species composition from station R01 in BIONESS net-tows collected in Roseway Basin on 9 October 2015. Small copepods were defined as species/stages with prosome lengths ≤ 1.5 mm, and large copepods as species/stages with lengths > 1.5 mm.

	Net:	**2**	**3**	**4**	**5**	**6**
Taxon	**Depth:**	137.1-154.5	120.9-137.1	105.7-105.7	50.9-105.7	1.4-50.9
Euphausiia krohnii		0	0	0	0	0.09
Meganyctiphanes norvegica		0	0	0.14	1	1
Nematoscelis megalops		0.05	0.07	0	1	0
Thysanoessa inermis		9	1	0.34	0	0
Thysanoessa longicaudata		0	0	0.07	0	0
Thysanoessa raschii		0	0	0	0	0
Total euphausiids		**9**	**1**	**1**	**2**	**1**
Calanus finmarchicus IV		20	16	8	2	2
Calanus finmarchicus V		30	484	405	27	5
Calanus finmarchicus VI female		9	16	8	7	5
Calanus hyperboreus III-IV		23	19	11	< 1	< 1
Metridia sp.		41	24	39	15	43
Total large copepods		**122**	**559**	**471**	**51**	**55**
Calanus finmarchicus I-III		0	0	0	0	2
Centropages typicus		0	0	0	3	77
Clausocalanus sp.		2	0	0	1	189
Oithona sp.		52	62	39	3	142
Paracalanus sp.		9	0	14	3	609
Pseudocalanus sp.		11	5	3	2	9
Total small copepods		**74**	**67**	**55**	**12**	**1028**
Limacina sp.		0	0	3	0	9
Parathemisto sp.		11	0	11	33	0
Themisto compressa		3	0	< 1	< 1	47
Total other zooplankton		**14**	**0**	**14**	**33**	**56**

Table 3.3. Net-specific zooplankton concentration (ind m^{-3}) and species composition from station R02 in BIONESS net-tows collected in Roseway Basin on 9 October 2015. Small copepods were designated as species/stages with prosome lengths < 1.5 mm, and large copepods are species/stages with lengths > 1.5 mm.

	Net:	**2**	**3**	**4**	**5**	**6**
Taxon	**Depth:**	125.7-139.2	110.9-125.7	95.6-110.9	50.7-95.6	1.5-50.7
Euphausiia krohnii		0	0	0	0	0.04
Meganyctiphanes norvegica		1	0.45	0.19	1	6
Nematoscelis megalops		0.14	0.15	0	0.01	0.01
Thysanoessa inermis		2	0	0.13	0	0
Thysanoessa longicaudata		0	0	0	0	0
Thysanoessa raschii		0	0	0	0	0.01
Total euphausiids		**3**	**1**	**0**	**1**	**6**
Calanus finmarchicus IV		6	14	6	3	3
Calanus finmarchicus V		97	384	336	37	3
Calanus finmarchicus VI female		6	14	2	3	3
Calanus hyperboreus III-IV		6	7	15	1	5
Metridia sp		11	29	8	30	21
Total large copepods		**127**	**449**	**368**	**73**	**34**
Calanus finmarchicus I-III		0	0	0	1	2
Centropages typicus		2	0	2	1	135
Clausocalanus sp.		2	2	0	32	104
Oithona sp.		19	19	13	12	62
Paracalanus sp.		15	0	0	7	525
Pseudocalanus sp.		1	2	6	4	0
Total small copepods		**38**	**24**	**21**	**57**	**828**
Limacina sp.		1	0	0	0	26
Parathemisto sp.		0	0	0	38	16
Themisto compressa		< 1	< 1	< 1	< 1	0
Total other		**1**	**0**	**0**	**38**	**42**

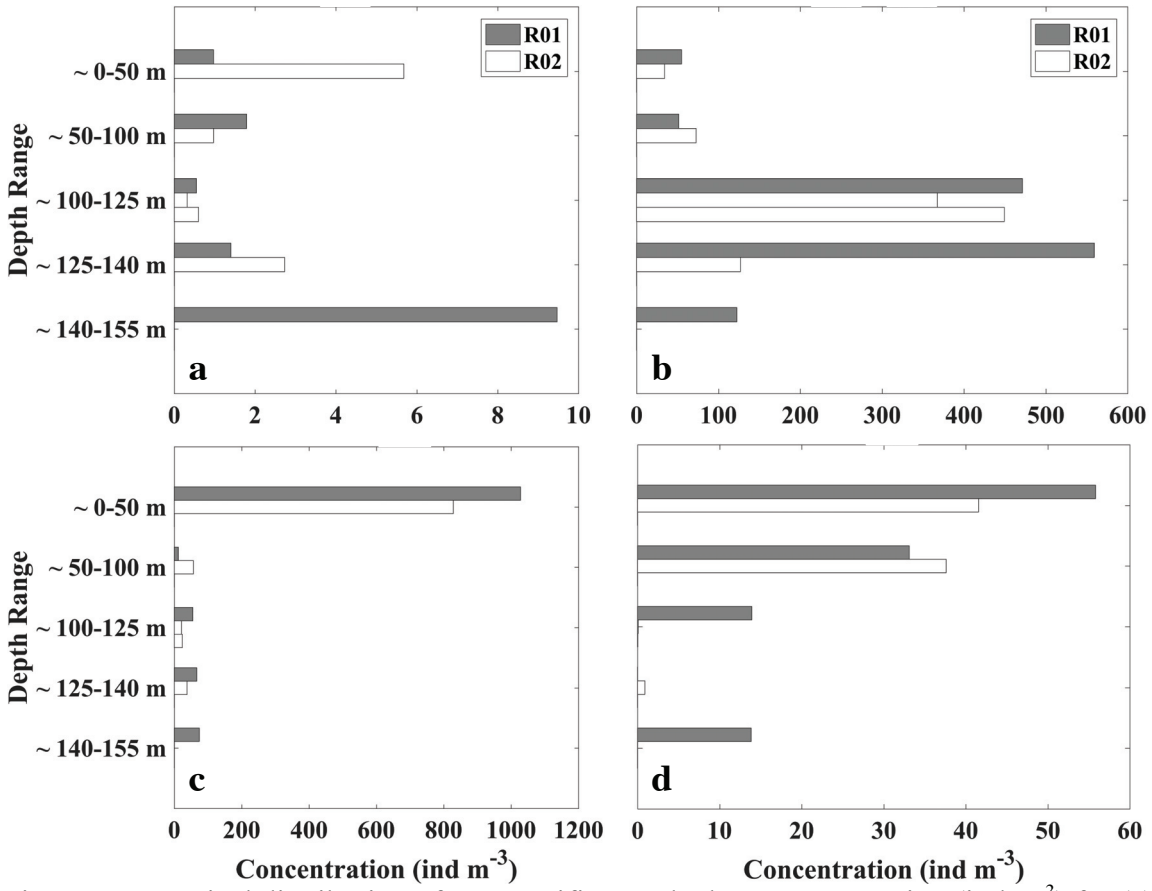

Figure 3.3. Vertical distribution of net-specific zooplankton concentration (ind m^{-3}) for (a) euphausiids, (b) large copepods (> 1.5 mm), (c) small copepods (≤ 1.5 mm), (d) other zooplankton among BIONESS net-tows collected at two stations (R01, R02). Depth ranges shown are approximate; as the ranges were slightly different between stations, see Table 3.1 for actual depth ranges. Note that nets 3-4 for station R02 are within same depth range in the panels, and that the concentration range (x-axis) is different for each panel.

3.2.2 Target Strength (TS) Estimation for Euphausiids and Large Copepods

3.2.2a Use of BIONESS Data in Acoustic Scattering Models

The acoustic measurements from the echosounder provide some information on relative patterns in zooplankton distribution, but it is also of interest to validate this data using biological samples, and estimate the absolute concentration of different groups of zooplankton. For this purpose, acoustic target strengths were estimated for each of the two highest biomass groups of zooplankton – euphausiids and large copepods (> 1.5 mm in length). Acoustic target strength (TS, dB re m^{-1}) is the intensity of backscatter expected

from a single organism (scatterer), and is dependent on the acoustic frequency, the size and orientation of the scatterer relative to an incoming acoustic wave, and the shape and material properties of the scatterer (*Medwin & Clay* 1998). Target strength for each group was estimated using BIONESS zooplankton size distributions, while the shape, orientation and material properties were modeled.

Estimates of TS were for euphausiids (TS_{eup}) and for large copepods (TS_{cop}) because these two common and high-biomass groups typically contribute to the majority of acoustic backscatter over large spatial scales. This assumption is based on the size of euphausiids (an order of magnitude larger than copepods, which increases TS) and the biomass dominance of large copepod concentration in the BIONESS net samples considering their size. The TS for copepods and other zooplankton decreases steeply once the organism is smaller than the acoustic wavelength (< ~2.5 mm for the 300 kHz frequency of the echosounder) and thus small copepods (≤ 1.5 mm in length), despite their numerical dominance in the net samples, contribute little to observed backscatter at 300 kHz (*Greene et al.* 1989; *Medwin* 2005). Some rarer groups of zooplankton such as pteropods may also contribute to the total backscatter, and thus increase uncertainty in estimates of euphausiid or copepod abundance from acoustic data. These sources of uncertainty are discussed in section 3.3.5.

Scattering models based on the distorted-wave Born approximation (DWBA; *Chu et al.* 1993) were used to estimate TS_{eup} and TS_{cop}. This form of scattering model is a standard method used to estimate the TS values of weakly scattering fluid-like zooplankton, including euphausiids and copepods (see *Lavery et al.* 2007; *Stanton et al.* 1998a,b; *Stanton & Chu* 2000). The scattering models assume that both groups are fluid scatterers with small density (g = 1.02, 1.034) and sound speed (h = 1.058, 1.041) contrasts relative to seawater. Additionally, DWBA assumes that euphausiids are uniformly-bent cylinders, that copepods are prolate spheroids, and that both groups are oriented over a normal distribution of angles of incidence. In this study, the models were applied to empirical length and width measurements of euphausiids and large copepods in the BIONESS net samples collected from each station and net.

3.2.2b Measurement of Euphausiid and Large Copepod Size Distributions

The body length and width for euphausiids and large copepods in the BIONESS net samples were measured at each station and in each net as follows. Copepod length was defined as the longest anterior to posterior distance across the prosome, not including the antennae or urosome, and the width as the widest cross-sectional distance across the prosome. Euphausiid length was defined as the distance from the leading edge of the eye to the base of the telson[1] (adapted from *Morris et al.* 1988), and the width as the distance across the body at the posterior edge of the first segment. All size definitions are illustrated in Fig. 3.4. For the measurements, first, all euphausiids in a net sample (unless the total sample size was more than N ~ 50) and a random sample of N = 30 copepods ~ 1 mm and larger for each net sample were photographed under a light microscope (although only copepod lengths > 1.5 mm were used in the scattering models, lengths 1.5 mm and below were included here to show a more accurate depiction of the length distribution for this group). The maximum sample size for euphausiids per net sample was larger than the sample size for copepods because a wider range of lengths were observed for euphausiids, and a larger sample size aided in ensuring a representative random sample. Next, a stage micrometer was photographed at the same magnifications to provide an image size calibration. The lengths and widths of each photographed specimen were then digitally measured using Image J software.

[1] The Discovery standard length for euphausiids from Morris et al. (1988) was modified by excluding the length of the telson; this gives a 'reduced acoustic length' consistent with the expected input of the scattering models.

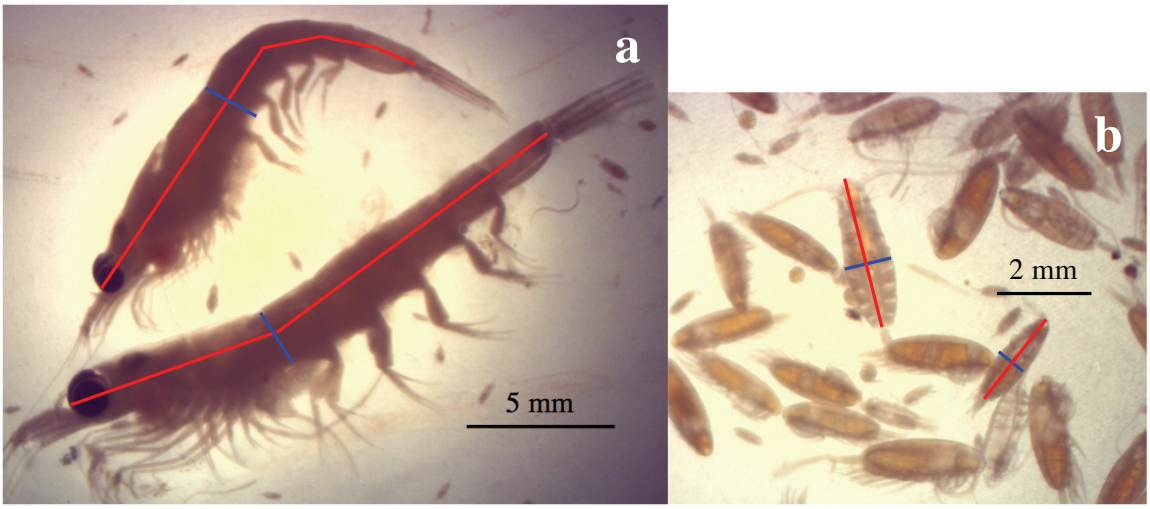

Figure 3.4. Zooplankton length and width definitions used in this study. Body length indicated with a red line, and body width indicated with a blue line for euphausiids (a) and large copepods (b). Images from BIONESS net samples referred to in text.

3.2.2c Statistical Analysis of Euphausiid and Copepod Size Distributions

Euphausiid length distributions differed among nets and stations (Fig. 3.5). Two size-classes were apparent with mean lengths of ~ 13 mm and ~24 mm, respectively. Sometimes both size classes occurred in the same net (*e.g.,* R01 from 50.9–105.7 m, and R02 from 1.5–50.7 m; Fig. 3.5c,b), while sometimes primarily one or the other size class occurred in a net (*e.g.,* R01 from 50.9–105.7 m vs. R02 from 125.7–139.2 m; Fig. 3.5c, j). Individuals in the larger class were relatively more abundant above than below 100 m. The larger class was also found in deeper nets, but at lower abundances than the smaller class. This depth distribution is consistent with larger *M. norvegica* (mean length 26 mm, *Herman et al.* 1993) being more abundant in the shallow nets, whereas smaller *T. inermis* (mean length 10 mm, *Herman et al.* 1993) is more abundant at depth (Tables 3.2-3.3). More individuals in the large size class were found throughout the water column in station R02 than R01. The mean body length at station R01 was 15.5 ± 5.1 mm, at station R02 was 17.3 ± 5.7 mm, and average among all nets and stations was 16.5 ± 5.5 mm.

The vertical distribution of copepods shows an abundance of small individuals (< 2 mm) occurring above 50 m, while larger individuals (~2.1 mm) are found predominantly at depths greater than 50 m at both stations (Fig. 3.6). The larger individuals being found at depth are primarily *C. finmarchicus* stage-CV aggregated in deeper waters during

diapause (Fig. 3.6c-j). The mean length over all nets for copepods was 2.0 ± 0.5 mm at station R01; 1.8 ± 0.7 mm for station R02; and 1.9 ± 0.6 mm overall. The average lengths and widths for large copepods (> 1.5 mm in length) among nets and stations was used in the scattering models, and the error in the size distribution was incorporated into the uncertainty estimation in Section 3.3.5.

Only the euphausiid and copepod body length data are shown here because length and width for both groups were significantly correlated (Fig. 3.7). This is expected, as allometric scaling in body size is commonly exhibited by both copepods and euphausiids (*Blaxter et al.* 1998; *Becker & Warren* 2014). Least-squares linear regressions yielded $R^2 = 0.7$, $p << 0.001$ for euphausiids, and $R^2 = 0.91$, $p << 0.01$ for copepods.

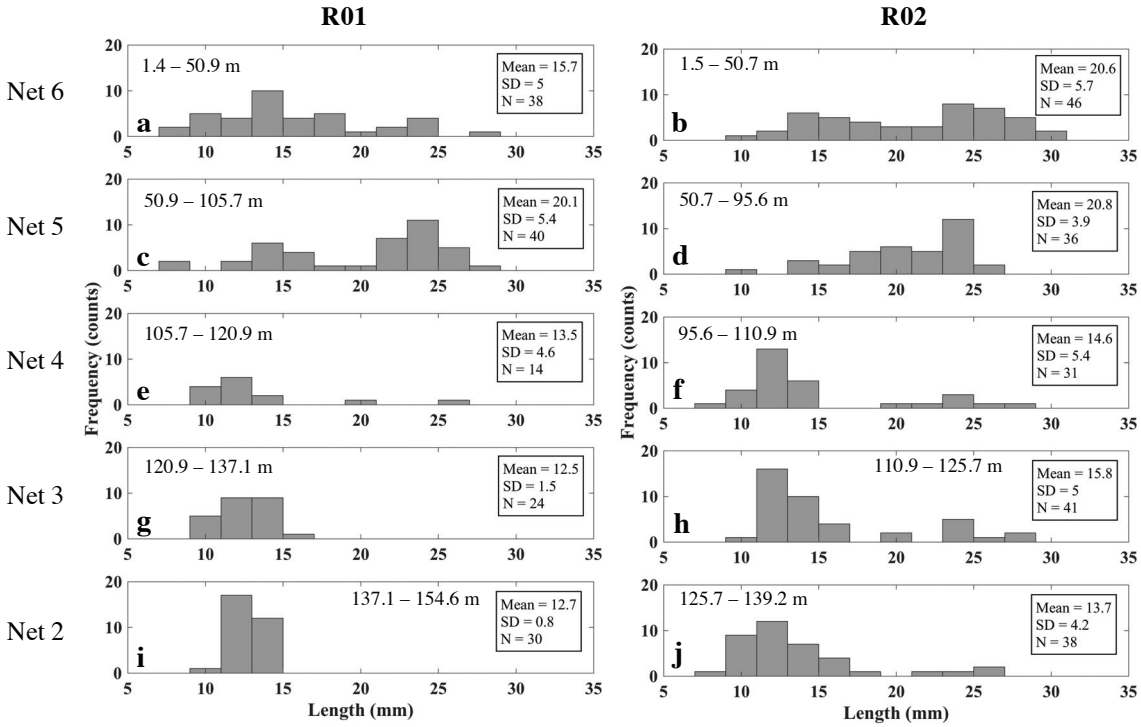

Figure 3.5. Frequency distributions of euphausiid reduced acoustic length (see footnote 1 on page 26) in each BIONESS net at stations R01 (left panels) and R02 (right panels). Net depth range (m), labeled above the histogram, increases from top to bottom panel.

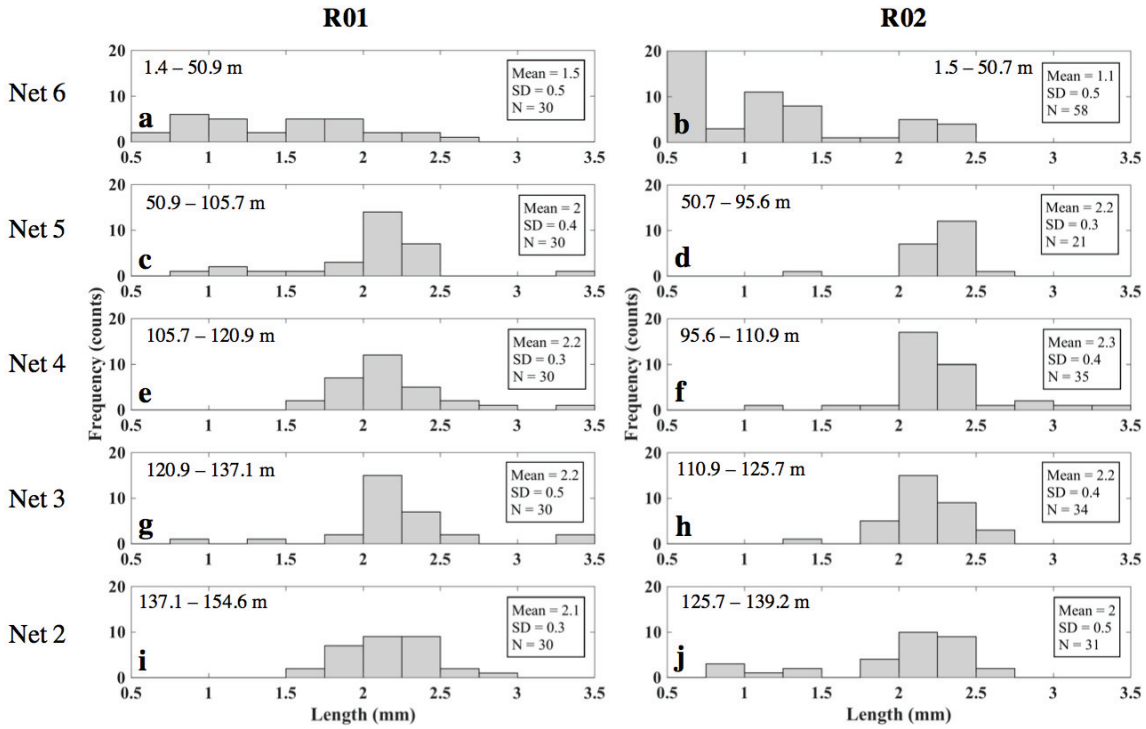

Figure 3.6. Frequency distributions of large copepods in each BIONESS net at stations R01 (left panels) and R02 (right panels). Net depth increases from top to bottom panel. Note that some small copepods (≤ 1.5 mm) were included in the random samples of copepods included in the size distribution measurements. Net depth range (m), labeled above the histogram, increases from top to bottom panel.

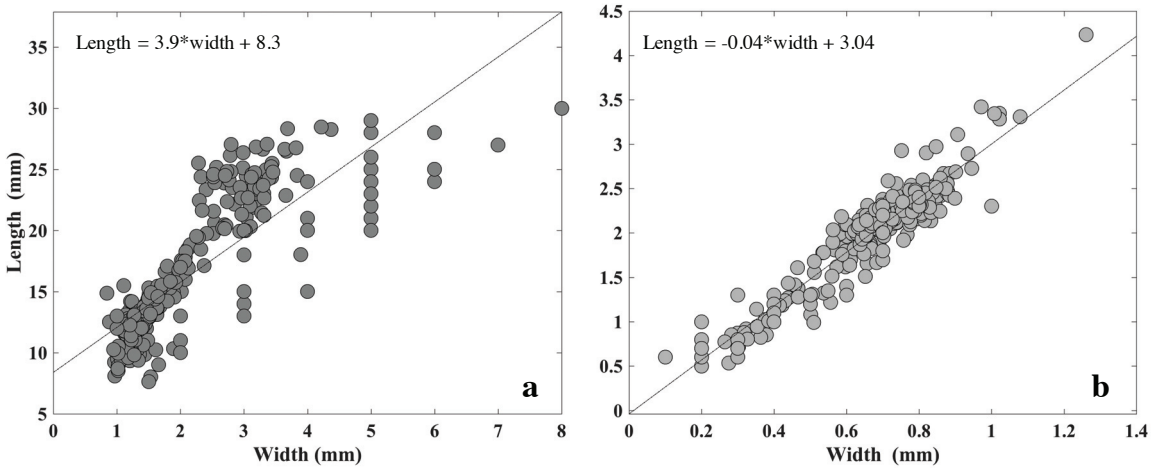

Figure 3.7. Scatterplots of width against length for euphausiids (a) and copepods (b). Data used from measurements taken across both BIONESS stations and all nets. Best-fit line and equation are shown for both least-squares linear regressions. Results for euphausiid length to width: $R^2 = 0.70$, $p << 0.001$; and for copepods: $R^2 = 0.91$, $p << 0.001$.

3.2.2d Statistical Analysis of Zooplankton TS Distributions

The variation in TS distribution over depth and between stations was similar to the length distributions for each zooplankton group; this is expected as the length-width pairs were the only parameters that varied within the acoustic scattering models (shape, acoustic frequency, and material properties were constants). The TS distributions for euphausiids varied strongly, with some nets containing TS estimates spread over 10 dB (*e.g.,* in Fig. 3.8). A difference of 3 dB represents approximately a doubling of concentration in linear space, meaning that size variation is an important source of uncertainty in acoustically-derived concentration estimates. Additionally, the bimodal pattern that was apparent in the length distributions is also present in some of the TS_{eup} distributions (*e.g.,* net 5 at both R01 and R02, and somewhat in R02 net 2). The mean TS estimate for euphausiids at station R01 was -80.6 ± 2.7 dB re m^{-1}, and at station R02 was -79.4 ± 3.6 dB re m^{-1}. The mean estimate for TS_{eup} over both stations and all nets was -79.9 ± 3.2 dB re m^{-1}.

A two-way analysis of variance (ANOVA) was performed to test for significant differences in TS_{eup} between stations and among nets (Table 3.4). The ANOVA revealed a significant difference in TS_{eup} estimates among nets ($p < 0.01$), but no significant difference between stations ($p = 0.2$). A multiple comparisons test on the ANOVA results for TS_{eup} showed that the TS estimates in the shallowest nets (0–50 m) were significantly stronger than those in the deeper nets. This difference can be attributed to the largest euphausiid lengths, and therefore individuals with the largest TS, being in the shallowest net. The variation in TS_{eup} over depth, however, introduces some uncertainty in calculating abundances from acoustic data with a single mean TS value. Even so, considering the range of uncertainty in the TS_{eup} estimates themselves (1.2–4 .7 dB; equivalent to a change of ~ 1.3–3-fold variation in linear space), taking the mean over both stations and all nets provides a reasonable TS approximation for this group and is used in further analysis.

The distribution of TS_{cop} was more consistent across nets than the distributions of TS_{eup}, although some distributions contained strong variance (Fig. 3.9) spanning a factor of four or more. The mean TS estimate for copepods at station R01 was -104.2 ± 2.1 dB re m^{-1}, and at R02 was -103.8 ± 1.9 dB re m^{-1}. The mean estimate for TS_{cop} across both stations and all nets was -104.0 ± 2.0 dB re m^{-1}. For large copepods, the two-way ANOVA over stations and nets showed that TS_{cop} did not vary significantly between stations ($p = 0.1$) or

among nets (p = 0.5). The ANOVA results for TS_{cop} indicate that a single value of TS (as the average over both stations and all nets) is appropriate to use for estimating abundances of large copepods from acoustic data.

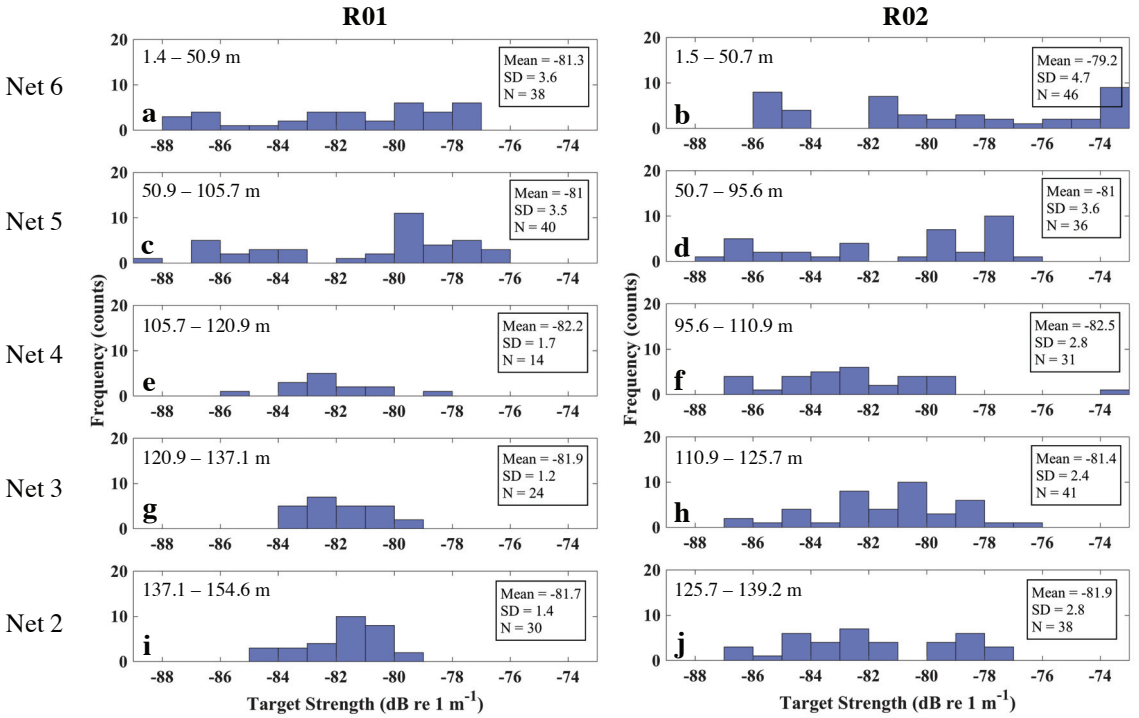

Figure 3.8. Frequency distributions of euphausiid acoustic target strength (TS_{eup}) measured at two BIONESS sampling stations (R01, R02) in Roseway Basin for each BIONESS net (a-j). Net depth range (m), labeled above the histogram, increases from top to bottom panel.

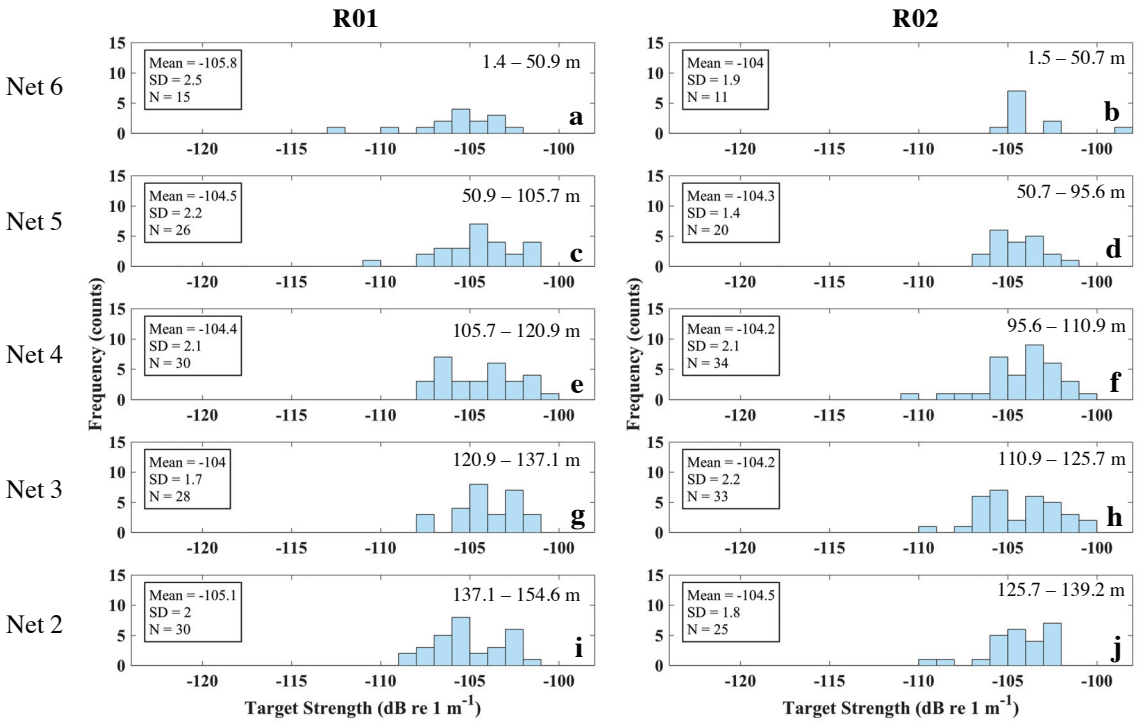

Figure 3.9. Frequency distributions of copepod target strength (TS_{cop}) measured at two BIONESS sampling stations (R01, R02) in Roseway Basin for each BIONESS net (a-j). Net numbers on the y-axis increase from Net 2, collected near the seafloor, to Net 6, collected near the surface. Net depth range (m), labeled above the histogram, increases from top to bottom panel.

Table 3.4. Two-way analysis of variance (ANOVA) testing whether euphausiid TS and large copepod TS varied significantly between BIONESS stations (R01, R02) and among nets (5 nets per station). SS = Sum of squares; DF = degrees of freedom (N - 1); MSE = mean squared error. Asterisk (*) indicates significance at >95% confidence level.

	Source	SS	DF	MSE	F-statistic	P-value
TS_{eup}	*Station*	15.1	1	15.1	1.5	0.2
	Net	165.7	4	41.4	4.1	< 0.01*
	*Station*Net*	70.4	4	17.6	1.8	0.1
	Error	3284.5	328	10.0		
	Total	3578.4	337			
TS_{cop}	*Station*	11.9	1	11.9	2.8	0.1
	Net	14.8	4	3.7	0.9	0.5
	*Station*Net*	5.8	4	1.4	0.3	0.8
	Error	1011.6	242	4.2		
	Total	1046.6	251			

3.3 Validation of Acoustic Data with BIONESS Net Samples

In this section, I validated the echosounder data using the BIONESS-net data. This was achieved by selecting glider-echosounder profiles that co-occurred in time and space with BIONESS collections (Section 3.2.3a), calculating expected acoustic backscatter from copepods ($S_{v(cop)}$) and euphausiids ($S_{v(eup)}$) using BIONESS net-derived zooplankton concentrations and TS estimates (Section 3.2.3b), and then statistically comparing net-specific $S_{v(cop)}$ and $S_{v(eup)}$ with acoustic backscatter averaged over the same depth interval as the nets ($S_{v(obs)}$) (Section 3.2.3c).

3.3.1 Selection of Glider Profiles for Echosounder Validation

During BIONESS tows the glider was navigated as close as possible to the *CCGS Hudson* (Fig. 3.10, Table 3.5). Local currents are extremely strong (tidal velocities ~ 0.5 m s^{-1}) and it is impossible to achieve fine-scale maneuverability with the glider in that environment, so there was a spatial mismatch of up to 5 km between the glider and the vessel locations. Glider profiles selected for comparison with the BIONESS net samples were restricted in time and space to ensure that the acoustic measurements represented as closely as possible the vertical distributions of zooplankton sampled during the net tows (Table 3.5). Only glider profiles collected at night and within three hours of the net collection were used. Four glider profiles per station (profiles 981–984 at Station R01, and profiles 987–988 plus 990–991 at station R02) fit these conditions for comparison to the net samples (Fig. 3.10, Table 3.5).

S_v measured in the four glider profiles per station was averaged among profiles and over the same depth ranges sampled by the BIONESS to match the vertical resolution of the net samples. This variable, which was only used in this validation step, is hereafter referred to as $S_{v(obs)}$ to distinguish it from the rest of the glider-echosounder data. At station R01, the deepest seafloor depth where the glider profiled was ~ 15 m shallower than the seafloor depth at the BIONESS station. This resulted in no glider data to compare with the net sample data from the deepest net at R01 (net 2; 137.1–154.6 m).

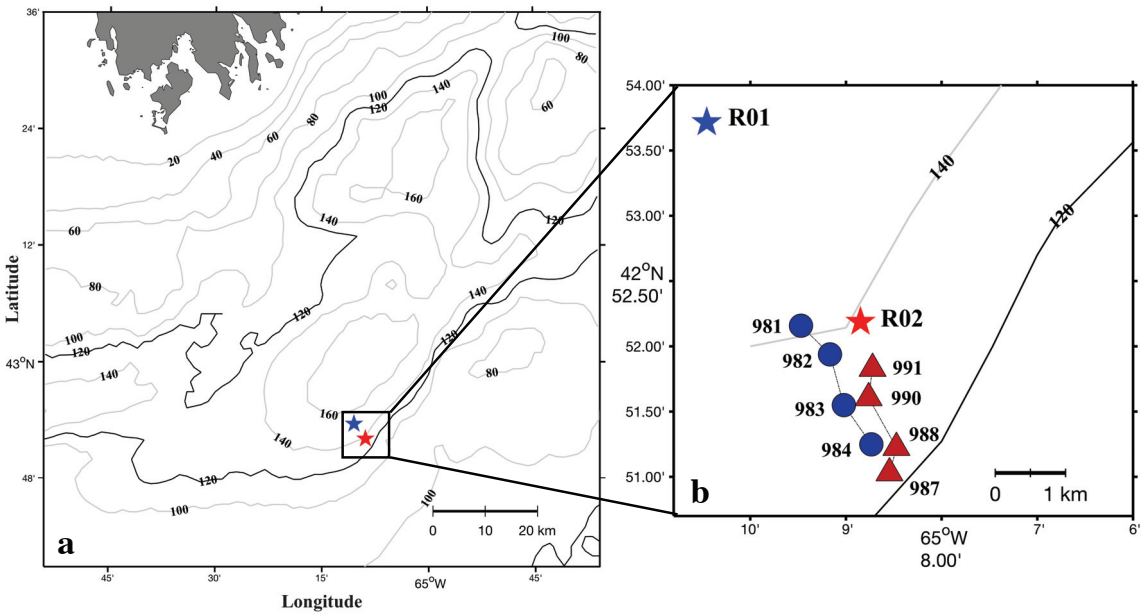

Figure 3.10. Position of BIONESS stations (R01 and R02, stars) in Roseway Basin (a), and inset (b) showing R01, R02 and positions of glider profiles selected for acoustic comparison to net sample data. Blue circles are profiles compared with R01, and red triangles are profiles compared with R02. Glider profiles numbered as shown in Table 3.5.

Table 3.5. Glider position, time, and difference in time and position to corresponding BIONESS tows. Time for all entries are for the average for each profile/tow. Distance between BIONESS stations R01 and R02 = 3.54 km. Note (1) that the reported times and positions of the BIONESS tows are for the beginning of the tow, and (2) that sunrise (beginning of zooplankton DVM) occurred at ~ 6:22 am ADT on October 9, 2015.

Profile/Station	Position (lat, lon)	Time (ADT)	Max profile depth (m)	Time to tow (hr)	Distance to tow (km)
R01	42.89, -65.17	1:14 am	154.6	–	–
981	42.87, -65.16	11:36 pm	141	1.75 before	2.37
982	42.86, -65.15	12:11 am	116	1.0 before	3.71
983	42.86, -65.15	12:57 am	133.5	0.25 before	3.71
984	42.85, -65.15	1:31 am	120	0.25 after	4.74
R02	42.87, -65.15	3:04 am	139.2	–	–
987	42.85, -65.14	3:22 am	116	0.25 after	2.37
988	42.85, -65.14	3:53 am	115	1.0 after	2.37
990	42.86, -65.15	4:48 am	133.5	1.75 after	1.11
991	42.86, -65.14	5:24 am	136.5	2.5 after	1.34

3.3.2 Calculation of Expected S_v from Zooplankton Concentrations and Comparison to Observed S_v from the Glider Profiles

To compare the BIONESS net sample data to the observed acoustic measurements ($S_{v(obs)}$), the net sample concentrations (N) of euphausiids and large copepods (N_{eup} and N_{cop}) and their respective TS estimates (TS_{eup} and TS_{cop}) were used to estimate the 'expected' backscatter from euphausiids, $S_{v(eup)}$, or copepods, $S_{v(cop)}$, using the following relation:

$$S_v = TS + 10log_{10}(N) \tag{3.3}$$

The conversion was made for euphausiids ($S_{v(eup)}$) and large copepods ($S_{v(cop)}$) separately. Additionally, to represent the combined expected backscatter from both euphausiids and copepods, a third variable, $S_{v(eup+cop)}$ was calculated by taking the sum of $S_{v(eup)}$ and $S_{v(cop)}$ in linear space. The agreement between expected backscatter and $S_{v(obs)}$ was quantified with least-squares linear regressions applied to all samples collected at both BIONESS stations and all nets (N = 10). Two regression comparisons were made; $S_{v(eup)}$ vs. $S_{v(obs)}$, and $S_{v(eup+cop)}$ vs. $S_{v(obs)}$. Ideally, if all the acoustic backscatter measured by the echosounder was comprised of euphausiids, then the slope of the $S_{v(eup)}$ vs. $S_{v(obs)}$ regression would be 1. Since copepod and euphausiid concentrations each varied with depth, plots of the three net-specific expected backscatter quantities ($S_{v(eup)}$, $S_{v(cop)}$ and $S_{v(eup+cop)}$) and $S_{v(obs)}$ illustrated the vertical structure in the relationship between observed and expected backscatter.

3.3.3 Statistical Comparisons Between Observed and Expected Backscatter

At both BIONESS stations, $S_{v(eup)}$ dominated the total expected backscatter compared to $S_{v(cop)}$ in the two surface nets and in the deepest net, whereas $S_{v(cop)}$ exceeded $S_{v(eup)}$ in the two mid-depth nets (~ 100–140 m) (Fig. 3.11a,b). In the shallow and deep nets where $S_{v(eup)}$ was a stronger contributor than $S_{v(cop)}$, euphausiid concentrations were one to two orders of magnitude lower than copepod concentrations. This is explained by the difference in TS between euphausiids and copepods, where TS_{eup} is stronger than TS_{cop} by a factor of ~2^8 in linear space; that is, more than 250 copepods m^{-3} would be required for the backscatter intensity that would result from 1 euphausiid m^{-3}. The variation in depth distribution is consistent with the vertical distribution of species composition in the nets (Fig 3.3). Depths where $S_{v(cop)}$ exceeded $S_{v(eup)}$ (*i.e.,* the second and third deepest nets) were consistent with the vertical variation of copepods and euphausiids in the net samples, where the highest

concentrations of copepods (368 - 559 m^{-3}) and the lowest concentrations of euphausiids (0–1 m^{-3}) were sampled at mid-depths at both stations (Tables 3.2-3.3).

$S_{v(obs)}$ was consistently stronger than all measures of expected backscatter over all depths at both stations (Fig 3.11a, b). On average, $S_{v(obs)}$ was 11.5 ± 4.9 dB stronger than $S_{v(eup)}$ and 10.2 ± 3.4 dB stronger than $S_{v(eup+cop)}$. This means that not all of the acoustic backscatter measured by the echosounder could be accounted for by the concentrations of euphausiids and copepods in the net samples. The offset between the observed and expected backscatter was large, as a difference of 10 dB is approximately equivalent to an order of magnitude stronger backscattering intensity. The observed and expected backscatter were in closest agreement at depths greater than 100 m over both stations, with the closest agreement occurring at depth at station R01.

To quantify the agreement between the observed and expected backscatter, least-squares linear regression was used to assess the agreement between $S_{v(obs)}$ and each of $S_{v(eup)}$ and $S_{v(eup+cop)}$ over data for both stations (Fig. 3.11c, d). The regressions showed that $S_{v(eup)}$ was not correlated with $S_{v(obs)}$ ($R^2 = 0.27$, slope = 0.23, $p = 0.15$), and that the addition of copepod expected backscatter in $S_{v(eup+cop)}$ did not improve the fit with $S_{v(obs)}$ ($R^2 = 0.01$, slope = -0.08, $p = 0.80$) (Fig. 3.10c, d).

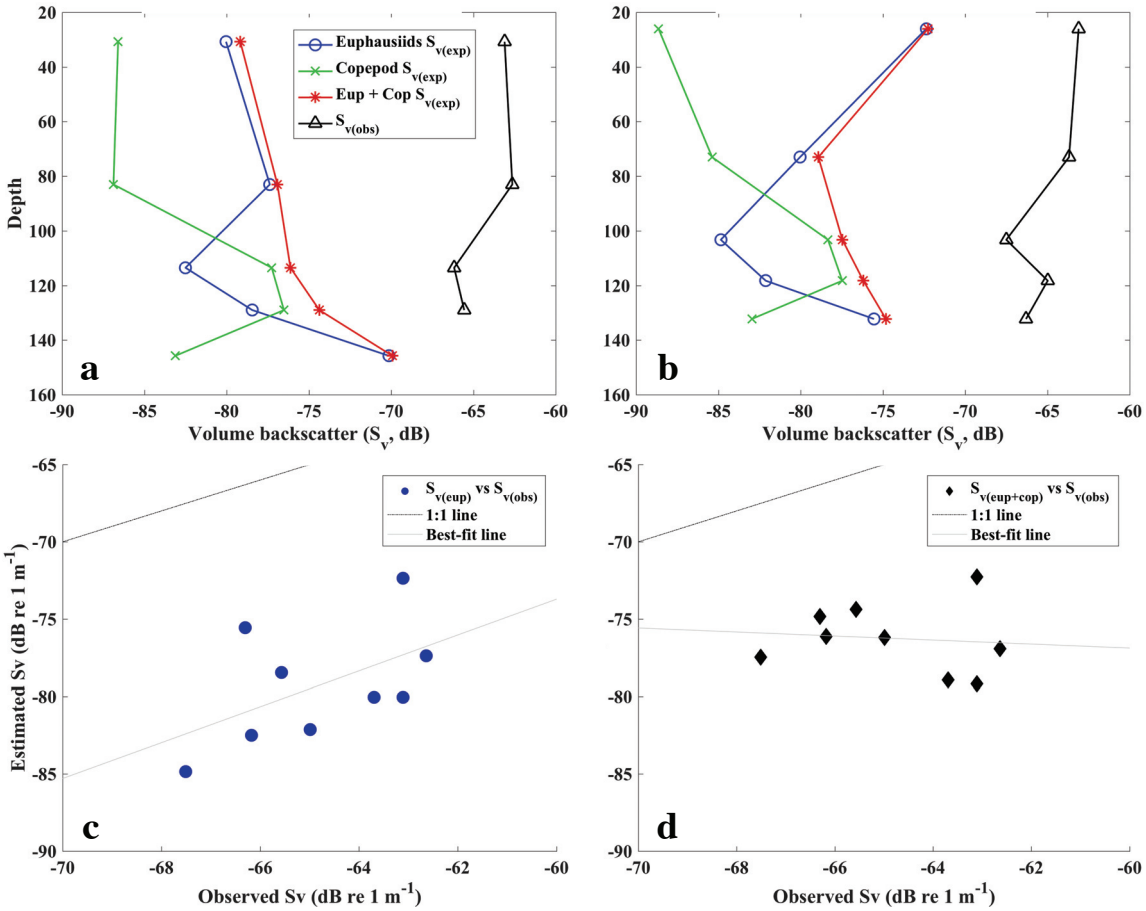

Figure 3.11. Top panels (a,b) show vertical profiles of acoustic backscatter inferred from BIONESS-net data compared to glider-echosounder derived backscatter (averaged over 4 profiles) for station R01 and R02, respectively. Bottom panels (c.d) show least-squares linear regressions for $S_{v(eup)}$ against $S_{v(obs)}$ (c), and $S_{v(eup+cop)}$ against $S_{v(exp)}$ (d). The 1:1 line for both regressions is indicated by a black dashed line, and lines of best fit (though neither regression is significant at the 0.01 confidence level) are shown in grey.

3.3.4 Analysis Decisions Based on Outcome of the Net-Acoustics Comparison

The two-fold objectives of the net-acoustic comparison were, first, to determine how accurately the net sample abundances of zooplankton were represented in the acoustic measurements (*i.e.,* a validation of the echosounder data), and second, to develop a conversion factor to convert the entire echosounder dataset to estimates of zooplankton concentration. The results of the net-acoustics comparison showed (1) that backscatter of euphausiids dominated backscatter over copepods, (2) that the neither the expected backscatter from euphausiids nor that from the combination of expected backscatter from euphausiids and copepods was correlated with the observed backscatter, and (3) that the

observed backscatter was consistently stronger than the expected backscatter for either euphausiids or for euphausiids and copepods combined.

The offset between observed and expected backscatter can be explained by effects of net avoidance in euphausiids, which is a common issue that has been reported on many times (*Hardy* 1936; *Fleminger & Clutter* 1965; *Wiebe et al.* 1982). While the strobe light on the BIONESS is designed to reduce euphausiid net avoidance by temporarily stunning the animals, it has been shown that the use of a strobe is less effective at night than during the day (*Sameoto et al.* 1993). During the day, *Sameoto et al.* (1993) found that a strobe increased net catches by 10-20 times, while at night the catches were only increased 2-3 times. Therefore, it is still likely that the abundances of euphausiids in the BIONESS net samples are an underestimate of the actual concentrations in the water column, possibly by an order of magnitude. Thus, it is possible that euphausiid backscatter dominates copepod backscatter at all depths, and that the majority of acoustic backscatter measured by the echosounder could be inferred to be euphausiids.

Based on the results of the net-acoustics comparison and in combination with the net samples having been only collected at night, the following two decisions were made regarding how the acoustic measurements were handled for subsequent analysis:

1) The entire acoustic dataset was converted to estimates of euphausiid concentration (N_{eup}, m^{-3}), using the following relation:

$$N_{eup} = 10^{\left(\frac{S_v - TS_{eup}}{10}\right)} \quad (3.4)$$

Caveat for Chapter 4: The shallowest net sample from BIONESS station R02 was lost in the sample archive and was only found when the thesis was nearly completely written. Analyses in Chapter 4 used a TS_{eup} value of -80.7 dB re m^{-1}. Including the missing net data, which is included in this chapter, resulted in a TS_{eup} of -79.9 dB re m^{-1}, which represents an increase in estimated euphausiid TS of ~ 18%. All analysis presented in Chapter 3 have been updated to be consistent with the addition of this missing data. However, the analysis presented in the following chapter (Chapter 4) used the initial, weaker, TS_{eup} value for concentration estimates (due to time constraints). The relative changes in concentrations from the acoustic measurements are preserved despite the

universal increase in TS. Moreover, the adjusted TS_{eup} is within the range of uncertainty for the TS_{eup} (average TS_{eup} standard deviation = 3.2 dB re m^{-1}, and revised TS_{eup} is only 0.8 dB re m^{-1} stronger than the initial TS_{euo} value).

2) Only glider profiles collected at night, between local sunset and sunrise, were used for analysis. This kept the data consistent with the net sample times, while euphausiids were vertically separated from the densest concentrations of copepods.

3.3.5 Sources of Uncertainty in Euphausiid Concentration Estimates from S_v

There are several important sources of uncertainty in the estimates of euphausiid concentration derived from the echosounder data. These fall into three categories; (1) uncertainty from the measurement and processing of the acoustic data, (2) the uncertainty from the estimate of TS_{eup} used to convert the backscatter data to estimates of euphausiid concentration, and (3) uncertainty from the contribution of non-target scatterers (*e.g.,* zooplankton other than euphausiids) to the measured backscatter.

For uncertainty from the acoustic measurements, there are two main contributors; the first of these is the calibration measurements performed to estimate a calibration coefficient (Cal_{coeff}, Equation 3.1) which was then used to convert the raw acoustic data (peak-to-peak voltages) to mean volume backscatter (S_v, dB re m^{-1}). The uncertainty in the calibration coefficient was determined to be ± 2 dB (a factor of ± 1.5 in linear space, *e.g.,* concentration). This accounts for differences between multiple measurements taken at different ranges from the acoustic transducer with differently sized standard targets (see section 3.1), along with an estimate of unknown uncertainties (such as the target sphere being systematically off axis or biased to one end of the range bin). The second main source of uncertainty in the backscatter data is from the bin-averaging that produces a single depth-binned glider profile from the returns of many acoustic pings sent out during that profile (section 3.1). This error was estimated by calculating the standard error for each binned profile from the first five days of profiles collected by the glider during transit 1 (176 profiles) and transit 2 (179 profiles). The acoustic measurements have an associated uncertainty estimate of ± 1 dB; or a factor of ± 1.25 in concentration.

The most significant source of uncertainty in the estimates of euphausiid concentration is from the estimated TS for euphausiids. The measurement of body lengths of euphausiid net sample specimens accounts for much of this uncertainty, as there was around a three-fold range of variation in euphausiid lengths (~ 10–30 mm across BIONESS nets). The average standard deviation was taken over all estimates from each of the five BIONESS nets over both stations, and the uncertainty in TS_{eup} is ± 3.2 dB re m^{-1}. This uncertainty is approximately equivalent to a two-fold variation in target strength, and thus the resulting estimates of concentration, in linear space. However, there are also unquantifiable sources of uncertainty, for instance as larger animals are generally more successful in avoiding nets (*Hovekamp* 1989), which can introduce a size bias in the euphausiids used to estimate the target strengths.

Finally, there are the non-target scatterers. Pteropods and amphipods are the most significant zooplankton groups of non-target scatterers in this study. Both groups were present in higher abundances in the near-surface BIONESS nets (upper 100 m) than anywhere else in the water column. Furthermore, both groups have the potential to make significant contributions to acoustic measurements, in addition to backscatter from euphausiids. Pteropods cause more concern, because with their calcareous shells, they are known to be strong scattering targets. Pteropod TS (TS_{pter}) has been estimated at approximately -80 dB re m^{-1} at a 300-kHz sampling frequency for individuals similar in size to those sampled by the BIONESS (*Lavery et al.* 2007), which is very similar to the euphausiid TS estimated in this study. Using the average abundance of pteropods from the BIONESS samples from the upper 100 m (10–20 ind m^{-3}) with TS_{pter} results in an expected backscatter intensity of approximately -70 to -67 dB re m^{-1} at 300 kHz. These expected levels of backscatter are close to those measured throughout the surface depths, meaning that where they occur in high abundances, pteropods could account for a large proportion of measured backscatter. Unlike pteropods, amphipods have a similar material composition to copepods and euphausiids, are generally between the two in terms of size (~4–10 mm), and have been modelled the same as euphausiids and have a TS (TS_{amph}) of approximately -95 dB re m^{-1} at a 300 kHz sampling frequency (*Lavery et al.* 2007). The average abundance of amphipods from the upper 100 m from the BIONESS nets (15–40 ind m^{-3}) with TS_{amph} results in an expected backscattering intensity of approximately -80 to -78 dB re m^{-1}.

It is difficult to assign a single uncertainty range to the estimates of euphausiid concentration. However, acknowledging the main sources of uncertainty, caution should be used when discussing absolute values of the euphausiid concentration estimates, especially because the validation step was completed with a relatively small sample size (only two BIONESS net tows in a single day for a two-month glider survey). The estimates are likely an accurate representation of actual euphausiid concentrations only within an order of magnitude. However, converting the acoustic measurements to estimates of absolute concentration, instead of only relative changes in backscatter, allows comparisons between concentrations sampled or acoustically estimated in other locations.

3.4 Identification and Characterization of Acoustic Scattering Layers (SLs) in the Echosounder Data

Euphausiids aggregate in vertically discrete layers in the water column, and layers with high concentrations of euphausiids are potentially important as prey-fields for foraging whales who seek out these discrete, dense patches. Therefore, to study variability in euphausiid concentration, those layers first had to be identified and delineated in the glider-echosounder dataset in an automated way. An algorithm was developed to identify discrete scattering layers (SLs) of backscatter (S_v) from the full echosounder dataset (Fig.3.1b, Section 3.3.1–3.3.3). The algorithm then calculated three descriptive metrics from the converted euphausiid concentration estimates to characterize the dataset: average concentration (ind m^{-3}), integrated concentration (ind $layer^{-1}$ m^{-2}), and layer thickness (m) (Section 3.3.4).

3.4.1 Preparation of Acoustic Data

Horizontal and vertical 2-D centered moving average low-pass filters were applied to smooth the glider profile data and better resolve SLs over kilometer-scales (*i.e.,* increase the signal to noise ratio). Prior to the application of the filters, missing data from the application of the noise floor curve in the initial processing needed to be filled. This was accomplished by estimating an approximate noise floor constant, as the lowest S_v from the first bin in a single acoustic ping that was not saturated (after a sharp drop from S_v values close to zero). This value, -84.2 dB, was inserted into all bins in the acoustic measurements

with missing data, and was also retained in the data used to calculate the SL descriptive metrics. The filters applied had a vertical window of 5 m and a horizontal window of two glider profiles (approximately 1 km resolution).

3.4.2 Definition of the Background Backscattering Level

A background backscatter level (BBL, S_v) was required as a measure of the backscatter intensity that would be present if the total amount of backscatter was homogeneous throughout the water column (*i.e.,* no SLs present). The BBL, used as a reference to determine the presence of SLs, was calculated for each glider profile as the average S_v over all depths and glider profiles collected within ± 12 hours of the profile being analysed:

$$\overline{\overline{BBL}}(j_t) = \frac{1}{M}\frac{1}{N}\sum_{k=1}^{M}\sum_{i=1}^{N} S_{v\,i_{l(k)}} \tag{3.5}$$

where *j* is the glider profile number, *t* is time, *i* is each depth bin up to *N* (total) depth bins, *k* is each profile up to *M* profiles within the range: $j_{(t)} - 12\ hrs \leq j_t \leq j_t + 12\ hrs$, and *l* is the group of profiles over the range *j* that is being summed over. BBL was variable throughout the survey (Fig. 3.12), and thus this procedure allowed the identification of SL boundaries (as described in the following section) in every glider profile regardless of variability in BBL among profiles. The interval of 12 hours before and after each profile included a full period of DVM variability in zooplankton wherever the profile in question was located, such that the signal of DVM was not included in the BBL values.

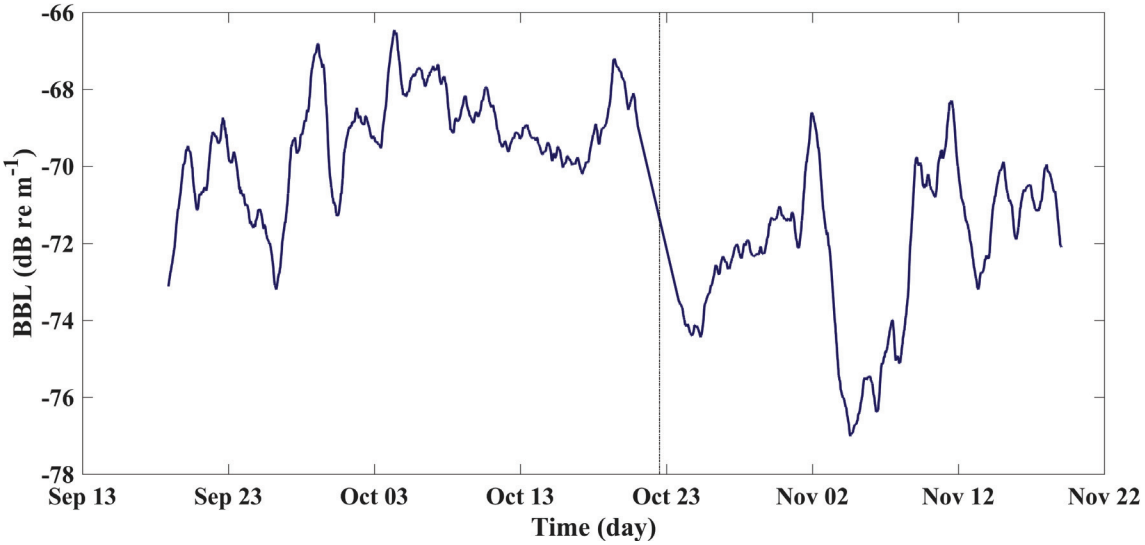

Figure 3.12. Time series of the background backscattering level (BBL, dB re m^{-1}) throughout the full glider survey. Data are shown by profile, as the mean S_v over 12 hours of profiles before and after the profile. Dashed vertical line indicates end of transit 1 and beginning of transit 2.

3.4.3 Identification of SL Boundaries

To identify SLs within each glider profile, first BBL(j_t) was subtracted from the S_v profiles. The boundaries for all SLs within each profile were identified by the zero crossing, *i.e.* the depth (*d*) where ∂ (S_v - BBL(j_t))/ ∂d = 0 (see example for a single profile, Fig. 3.13, and for an echogram showing identified SLs identified over multiple profiles, Fig. 3.14). Any SLs with upper (negative to positive) and lower (positive to negative) boundaries less than 1 m apart were not of interest in this study, and were omitted from further analysis. Additionally, if more than one layer was identified in an acoustic profile and the layers were 10 m or less apart in the vertical, they were combined as a single layer. This step last was applied to account for vertical gaps that can be present in large, 'pancake-shaped' SLs that span multiple glider profiles (*Reid et al.* 2000).

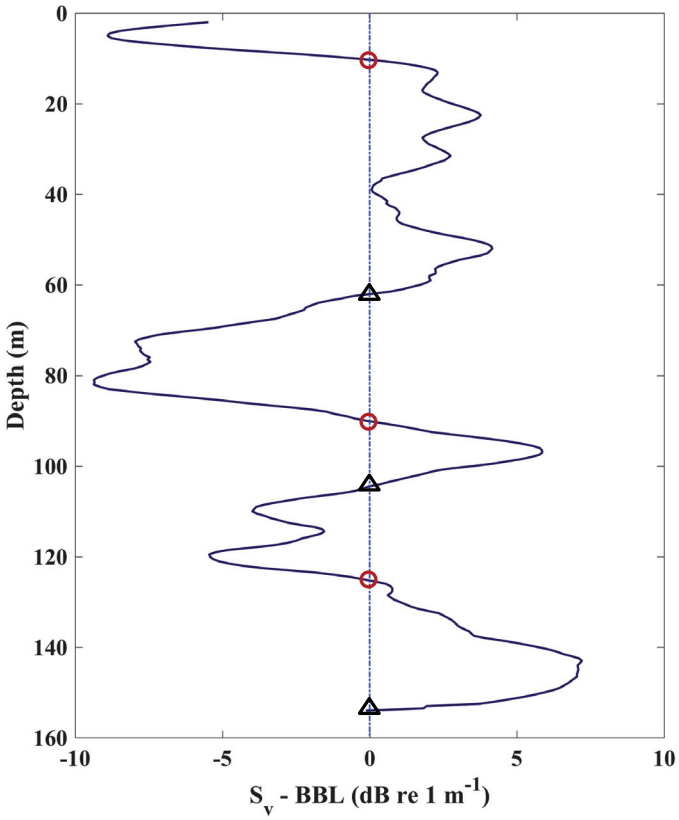

Figure 3.13. Example SL boundary identification for a glider profile collected 7 October 2015 at 11:24 ADT. Three SLs were identified in this profile, where the difference between the profile S_v and the associated BBL value crosses zero. Upper SL boundaries indicated with red circles and lower SL boundaries indicated with black triangles.

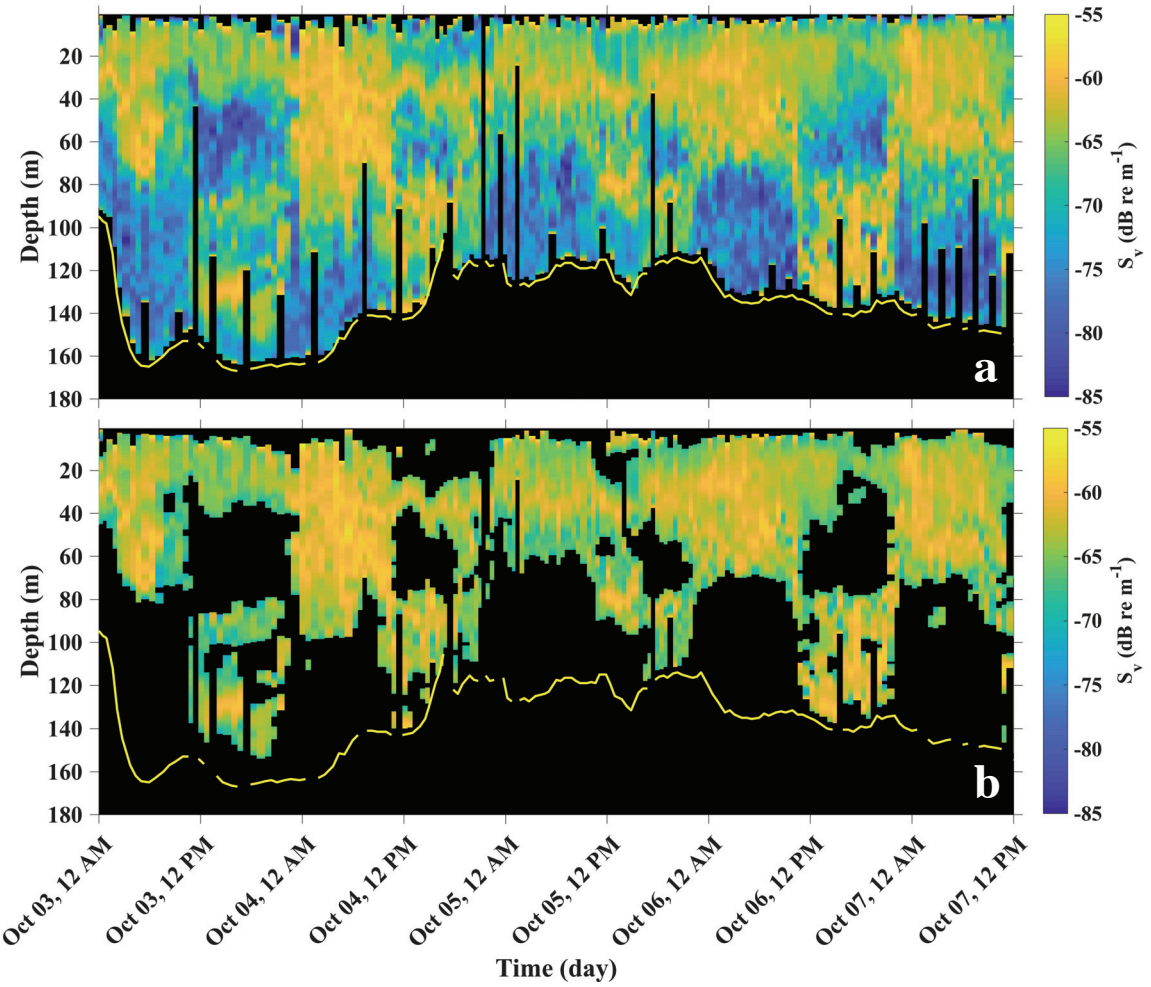

Figure 3.14. Example echogram for profiles collected between 3-7 October while the glider was over the central basin, moving into the southern basin. Top panel (a) shows backscatter (S_v) for entire profile, and bottom panel (b) shows the backscatter in SLs identified in each profile. Yellow line is the acoustically-derived seafloor depth. Black data points below seafloor are no data collected; black data points above seafloor are data points with S_v weaker than the BBL.

3.4.4 Calculation of SL Metrics

All data between each pair of upper and lower SL boundaries, including the data-points of the boundaries themselves, were used to calculate the SL metrics from the unfiltered S_v data with the noise floor constant inserted into missing values. Three SL metrics were calculated as follows for each SL in each glider profile:

1. Average euphausiid concentration (m^{-3}) was calculated by taking the average over all data-points within the SL as,

$$\overline{N}_{SL_{i,j}} = \frac{1}{Q}\sum_{p=1}^{Q} N_{j_{SL(i)}} \tag{3.6}$$

   where $SL_{i,j}$ is the i^{th} SL in the j^{th} glider profile; and has a total of Q depth bins (p) in that layer.

2. Integrated euphausiid concentration ($layer^{-1}$ m^{-2}) was calculated by taking the sum of concentrations over the data-points in the SL as,

$$\sum N_{SL_{i,j}} = \frac{\sum_{p=1}^{Q} N_{j_{SL(i)}}}{2} \tag{3.7}$$

   where the metric is referenced to meters by dividing the sum over 0.5 m binned concentration values by two.

3. Layer thickness (m) was calculated by taking the difference between the lower and upper SL boundary depths as,

$$\Delta Z_{SL_{i,j}} = Z_{UB_{i,j}} - Z_{LB_{i,j}} \tag{3.8}$$

   where Z is depth, UB is the upper boundary of the SL, and LB is the lower boundary of the SL.

The descriptive metrics for euphausiid SLs defined here are used for all subsequent data analysis presented and referred to in Chapters 4 and 5. The variation in the SL metrics and that of the water mass properties measured simultaneously by the glider are presented in the next chapter.

Chapter 4

Variation in SL Metrics and Water Mass Properties

In Chapter 4, I characterize spatial and temporal variation in euphausiid abundance using the scattering layer (SL) metric data derived from the echosounder observations in Chapter 3 (Sections 4.1.1, 4.2.1; addressing Thesis Objective 1). Next, I investigate the temporal and spatial patterns in the water mass properties measured by the glider CTD, and explain how those properties indicate water mass transport in the Basin (Section 4.1.2, 4.2.2). Finally, two analyses are performed to explain variation in zooplankton concentrations and distributions (Thesis Objective 2). First, I use multiple regression to identify the glider-derived environmental variables that best explain variation in each SL metric (Section 4.1.3a, 4.2.3). Second, to put the regression results into spatial context in Roseway Basin, I compare the SL metrics among inferred water masses identified with a cluster analysis (Section 4.1.3b, 4.2.3).

4.1 Methods

4.1.1 Analytical Methods for SL Metrics

4.1.1a Preparation of SL Metrics for Characterization and Modelling

In this section, the dataset was constrained so that only SL metrics representing the time and position in the water column where there was the most confidence that the majority of acoustic backscatter was from euphausiids was used further analysis. To achieve this, first, only the SL metrics from the shallowest scattering layer, within the upper 100 m, was used for analysis because euphausiid concentrations were elevated and large copepod concentrations were at their lowest in the BIONESS samples above 100 m (Fig. 3.3). In addition, the majority of SLs identified in the glider profiles collected at night were within the upper 50 m of the water column (Fig. 4.1). Retaining only the night-time surface SLs uses data from acoustic measurements in which there is the most confidence that

euphausiids are the primary scattering targets, as at other times (*i.e.,* daytime when euphausiids and copepods form mixed deep layers or at dawn and dusk when euphausiids and other zooplankton migrate to and from the surface) SLs contain a more mixed assemblage of zooplankton.

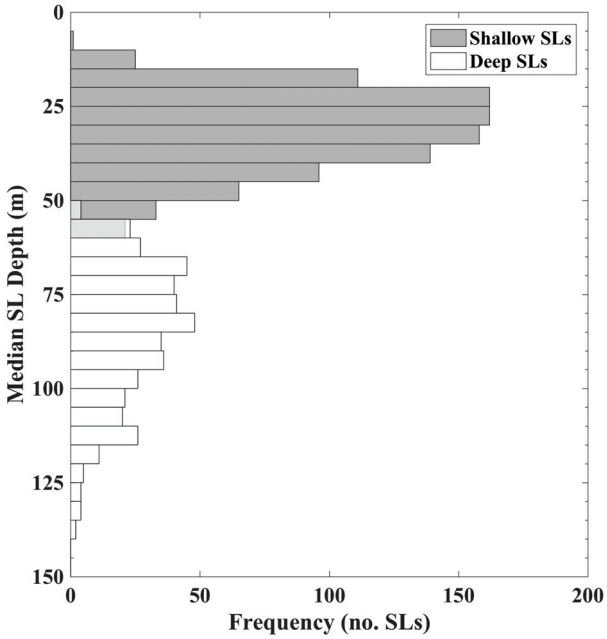

Figure 4.1. Frequency distribution of median depths for shallow (grey) and deep (white) SLs from glider profiles collected at night. Shallow SLs were defined as the shallowest SL with a thickness > 1 m, and deep SLs were defined as the SL (after identification of the shallow SL) with the highest integrated S_v from among any remaining SLs in the profile.

Next, SL metrics calculated from profiles where the glider made an early inflection were removed from the dataset (see Chapter 2, section 2.1.2). An early inflection was identified as any profile where, while on a downcast, the glider turned around and began an upcast 10 m or more from the lower boundary of the shallow SL in that profile (when compared to the lower SL boundaries identified in the immediately adjacent profiles). This cut-off ensured that metrics from SLs that were largely unsampled were omitted, and that if only a small portion of the SL was not sampled, it was still included in the SL metrics dataset.

Finally, to reduce the influence of small-scale (< 1 km) patchiness (*i.e.,* noise) and autocorrelation between consecutive glider profiles (*Ross et al.* 2017), the SL metrics were

averaged among profiles collected during each night-time period. Taking nightly averages reduced the total sample size from 989 profiles to 58 nightly averages of SL metrics over night-time profiles (transit 1 = 32 nightly averages; transit 2 = 26 nightly averages). This reduced dataset was used for all subsequent analyses and will be referred to as the SL metrics hereafter.

4.1.1b Statistical Analysis for SL Metric Characterization

A two-sample *F* test for homogeneity of variance was applied to test whether the use of normal statistics (assuming equal variance) was appropriate for analysing the SL metrics. The *F* test showed that while the variance for SL thickness was not significantly different between glider transits ($p = 0.33$), the variance for SL average and integrated concentration were (both p-values $<< 0.01$). Consequent to the results of the *F* test, two-tailed unbalanced Student's t-tests compared the overall mean for each SL metric, not assuming equal variance for the SL average or integrated concentrations, to determine if significant variation occurred in the SL metrics between transit 1 and transit 2. The t-tests for the SL average and integrated concentrations use the Satterthwaite-Welch adjustment for samples with unequal variance to obtain the effective degrees of freedom (*Satterthwaite* 1946; *Welch* 1947). There were three data-points representing the glider's traversal along the southeast margin of the basin between transit 1 and transit 2 return to Waypoint A (Fig. 2.2); these data were not included in the analysis. Least-squares restricted cubic splines were also fitted to plots of each SL metric against the across-basin coordinate (NW-SE; see definition in Fig. 2.3 and example Fig. 4.3, below) to visualize variation in the SL metrics over space in the basin.

4.1.2 Analytical Methods for Water Mass Properties

4.1.2a Preparation of CTD and Positional Data for Analysis

To allow the comparison of the CTD data to the echosounder-derived SL metrics, salinity, temperature, positional coordinates (rotated and standard), and time were averaged over all profiles belonging to each night-time period. For the time and position data, where the average over each glider downcast was retained per profile, and this resulted in a single

value date and position for each nightly average. For the temperature and salinity data, nightly averaging was applied across profiles and over 10 m depth ranges from the surface to the deepest measured depth, ~180 m, giving a total of 18 vertical depth ranges. All subsequent characterization and analyses were performed on these nightly- and depth-bin-averaged data.

4.1.2b Plotting and Analysis to Characterize Water Mass Properties

Temperature-salinity (T-S) diagrams were constructed with color-maps of depth, time, and along-basin position to visualize the variation in temperature and salinity over depth, time, and position in the basin. Annual mean values for water mass endmembers expected at the Halifax Line (*Dever et al.* 2016), located north of Roseway Basin on the Scotian Shelf, were plotted with the glider data to reference the measurements of temperature and salinity on the diagrams to known water masses on the Scotian Shelf. These endmembers included the Cabot Straight subsurface (CBSs; $T = 3.0 \pm 2.9$, $S = 31.6 \pm 0.6$), Cabot Straight Cold Intermediate Layer (CBS-CIL; $T = 1.8 \pm 1.1$, $S = 32.4 \pm 0.5$), and Warm Slope Water (WSW; $T = 11.7 \pm 1.8$, $S = 35.5 \pm 0.2$) endmember points defined in *Dever et al.* (2016).

Next, two depth ranges, 10–20 m and 90–100 m, were selected from among the ten-meter averages over each night-time period for further analysis because they, respectively, represent the variation in the deep and shallow water mass properties. The 90–100 m depth range was used to represent the deep water because it included data coverage across all locations that the glider transited in the basin. The temperature and salinity in the 90–100 m depth range were, respectively, found to be significantly correlated down to the deepest measured depths in the 170–180 m depth range ($p < 0.01$), supporting the assumption that this depth range is representative of variation in the deep basin water.

Shallow (10–20 m) salinity and deep (90–100 m) temperature were used in an agglomerative hierarchical cluster analysis to identify the spatial structure in the temperature and salinity data that indicated water masses in the basin. Salinity was used to represent shallow water mass variation because it is more conservative over depth than temperature, which is subject to atmospheric heat flux, and thus represents water mass variation and not seasonal heating/cooling of the surface water. Additionally, while salinity was correlated over all depths ($p < 0.01$), the shallow salinity and deep temperature were

found to be uncorrelated ($p = 0.9$), prompting the application of cluster analysis to the deep 90–100 m temperature data as well.

The cluster analysis uses an algorithm with a bottom-up approach that iteratively merges the most similar clusters from the dataset (with N data points): in the first iteration, every data point is identified as a separate 'cluster', then the pair of clusters with the shortest Euclidean distance are assigned to a new combined 'cluster'. The algorithm continues in this way, until only one cluster remains, consisting of all data points. A dendrogram shows the relationships between joined clusters at every iteration by the distance at which each cluster pair was joined, and thus allows an assessment of the structure within a dataset at different scales. The algorithm was used on the shallow salinity and deep temperature data for both transits together, without providing any spatial coordinate information. The coordinates belonging to the points in each identified cluster were then mapped by transit, to show the spatial structure in water mass properties identified in the cluster analysis during each glider transit of the basin.

4.1.3 Analytical Methods for Covariation Between SL Metrics and Glider-Derived Environmental Variables

4.1.3a Construction of Multiple Regression Models

Multiple regression models were constructed to identify the environmental variables that explained statistically significant variation in each SL metric. A bi-directional stepwise approach was employed to select the best-fit model with for each SL metric. That is, for each SL metric, models were constructed in a forward stepwise manner by starting with and empty model (intercept term only, no variables) and sequentially adding independent variables until no further improvement to fit could be achieved; conversely, models were also constructed in a backwards step-wise manner by starting with the full model (all independent variables and intercept term included) and sequentially removing variables until no further improvement could be made to the model fit.

Akaike's Information Criterion (AIC) was used to assess model goodness-of-fit at each step-wise iteration. The AIC is used to reference improvement from the initial model (either empty or full) and considers the trade-off between improving model goodness-of-fit and reducing degrees of freedom with each additional variable. The model improvement

at each step-wise iteration was assessed with a threshold Δ-AIC value of 2 (after *Carruthers et al.* 2008); where Δ-AIC is the difference between the AIC of the initial model and the AIC of the current model. If the same goodness of fit was achieved for models from both step-wise procedures and these models had two different sets of independent variables, the more parsimonious model (fewest independent variables with equivalent goodness-of fit) was selected as the final best-fit model for the SL metric in question.

A test for homogeneity of variance was applied by plotting the residuals in each metric from regressions against the data for shallow salinity (any independent variable would have worked for this application) against the fitted values from the initial set of models. All three metrics were found to have unequal variance across the range of dependent variables. To account for this, the $\log_{10}$ transform of each SL metric was used for final model construction (after Warton et al. 2016).

The environmental variables to be included in the models were: shallow salinity (psu, from 10-20 m depth), deep temperature °C and salinity psu (both 90-100 m depth), along- and across-basin coordinate (rel ° Lon and rel ° Lat, respectively) and the acoustically-derived estimates of seafloor depth (m). The shallow temperature was not included, as it did not represent variation in water mass (see section 4.2.2a). To ensure that the independent variables used in the models were not significantly multicollinear, the variance inflation factor (VIF) was calculated for each independent variable. The VIF for each independent variable is calculated as $VIF = \frac{1}{1-R_y^2}$; where R_y^2 is the coefficient of determination for a regression of one independent variable against all other independent variables. A VIF cut-off value of five was selected for determining if substantial multicollinearity was present among the independent variables. VIF cut-offs between one and 10 are not uncommon in the literature (*O'Brien* 2007), and five was selected as an intermediate value; this VIF cut-off corresponds to < 0.8, or at least 20% of any included independent variable must not be accounted for among other included variables.

All initial independent variables had VIF values less than 5, and thus at this cut-off, all were determined to be suitable for use in the multiple regression models. The variables with the highest collinearity were the shallow depth-range salinity, and the deep depth-range salinity and temperature.

4.1.3b Comparison of SL Metrics Between Temperature and Salinity Clusters

An unbalanced two-tailed Student's t-test (that did not expect equal variance between samples; see section 4.4.4b) was used to test for significant differences in the means of each SL metric that occurred in the corresponding positions of the shallow salinity and deep temperature clusters. This step allowed a determination of whether spatial structure of the water masses identified with the cluster analysis could explain variation in the SL metrics. A total of six t-tests were conducted, one for each of the three SL metrics for the clusters of both shallow salinity and deep temperature.

4.2 Results

4.2.1 Statistical Analysis of SL Metrics

The glider encountered strong variation in SLs within and between transits of Roseway Basin during the survey. One of the most prominent features of the glider's acoustic dataset is a significant decrease in estimated average and integrated euphausiid SL concentrations between transit 1 and transit 2 (Fig. 4.2, 4.3; $p << 0.001$ for both metrics; Average concentration: $t = 3.1$, 54 df; Integrated concentration: $t = 5.4$, 51 df). In contrast, there was no significant change in SL thickness between transits (Fig. 4.2, 4.4; $p = 0.86$, $t = 0.2$, 56 df). Average SL concentration decreased by 41% from 46.6 ± 16.9 ind m^{-3} to 27.4 ± 9.7 ind m^{-3}, and SL integrated concentration decreased by 40% from ~ 5,600 ± 3,200 ind m^{-3} to ~ 3,400 ± 2,100 ind m^{-3} between transits. The standard deviation (SD) in both concentration metrics was substantially lower in transit 2 than in transit 1; average and integrated concentration SD decreased by 43%, and by 26%, respectively (Fig. 4.2).

The basin-scale decrease in average and integrated euphausiid concentrations between transits is evident in the time series of these metrics (Fig. 4.4). The highest average and integrated euphausiid concentrations occurred over the central deep basin (See location reference in Fig. 4.6) between ~ Oct 2–6 during transit 1 (over a seafloor of approximately 150 m depth, Fig. 4.3; see echogram for this period Fig. 3.13). These high concentration layers were up to ~ 120 m thick and contained concentrations of up to 92 ind m^{-3} and ~15,400 ind $layer^{-1}$ m^{-2} (Fig. 4.3). Around Oct 7, when the glider was in the southern end of the basin and was over shallower waters (approximately 100 m depth), average and

integrated concentration began to steadily decrease over a period of approximately 28 days (spanning between transit 1 and transit 2) to ~ 12 ind m^{-3} and ~ 770 ind $layer^{-1}$ m^{-2}; the thickness of the SLs at the end of this period was also correspondingly low, at ~ 30 m (Fig. 4.4). The decreasing trend continued through the end of transit 1, and is evident on maps of the concentration metrics (particularly the average concentrations in the far-southern section of transit 1; Fig. 4.3), and continued during transit 2 as well, until around November 5. Towards the end of transit 2, the decrease in the concentration metrics ceases, when the glider is over the central basin and southeast basin margin.

There was also variation in all three SL metrics within each glider transit, especially in the across-basin direction (Fig. 4.5). Generally, over both transits thicker SLs with higher euphausiid concentrations tended to occur over the central deep basin, and thinner SLs with lower concentrations over the northwest and southeast basin margins. The largest decrease in SL average concentration between transits occurred over the northwestern margin (~77.95 rel ° Lat, in the across-basin direction), with ~ 30 ind m^{-3} fewer euphausiids per SL (Fig 4.5b). Similarly, the largest decrease in SL integrated concentration occurred over the northwest margin, with ~1,880 ind $layer^{-1}$ m^{-2} few euphausiids; however, in contrast to the average concentration between transits in the across-basin dimension, integrated concentration remained relatively unchanged over both the southeastern margin and the central basin (Fig 4.5c). And, contrary to the lack of change overall between transits, SL thickness experienced an increase of ~ 13 m over both the central basin and southeastern margin (Fig. 4.5a).

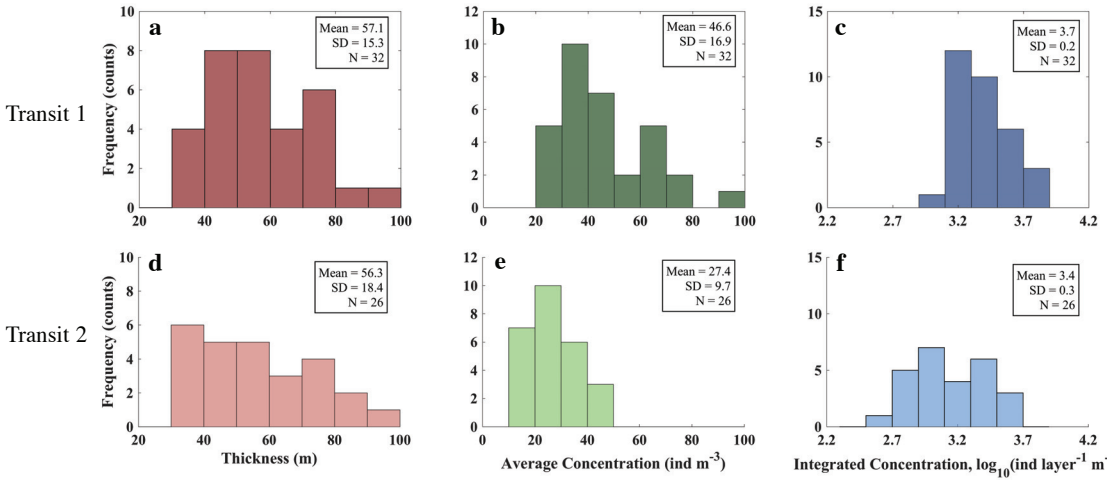

Figure 4.2. Frequency distributions of three descriptive metrics that characterize the nighttime surface euphausiid SL in Roseway Basin over approximately one-month time periods during transit 1 (a-c) and transit 2 (d-f). Top row for transit 1, layer thickness (a), average concentration (b), and integrated concentration (c). Bottom row same as top row for transit 2 SL metrics (d-f). Note that integrated concentration is plotted on a log-scale.

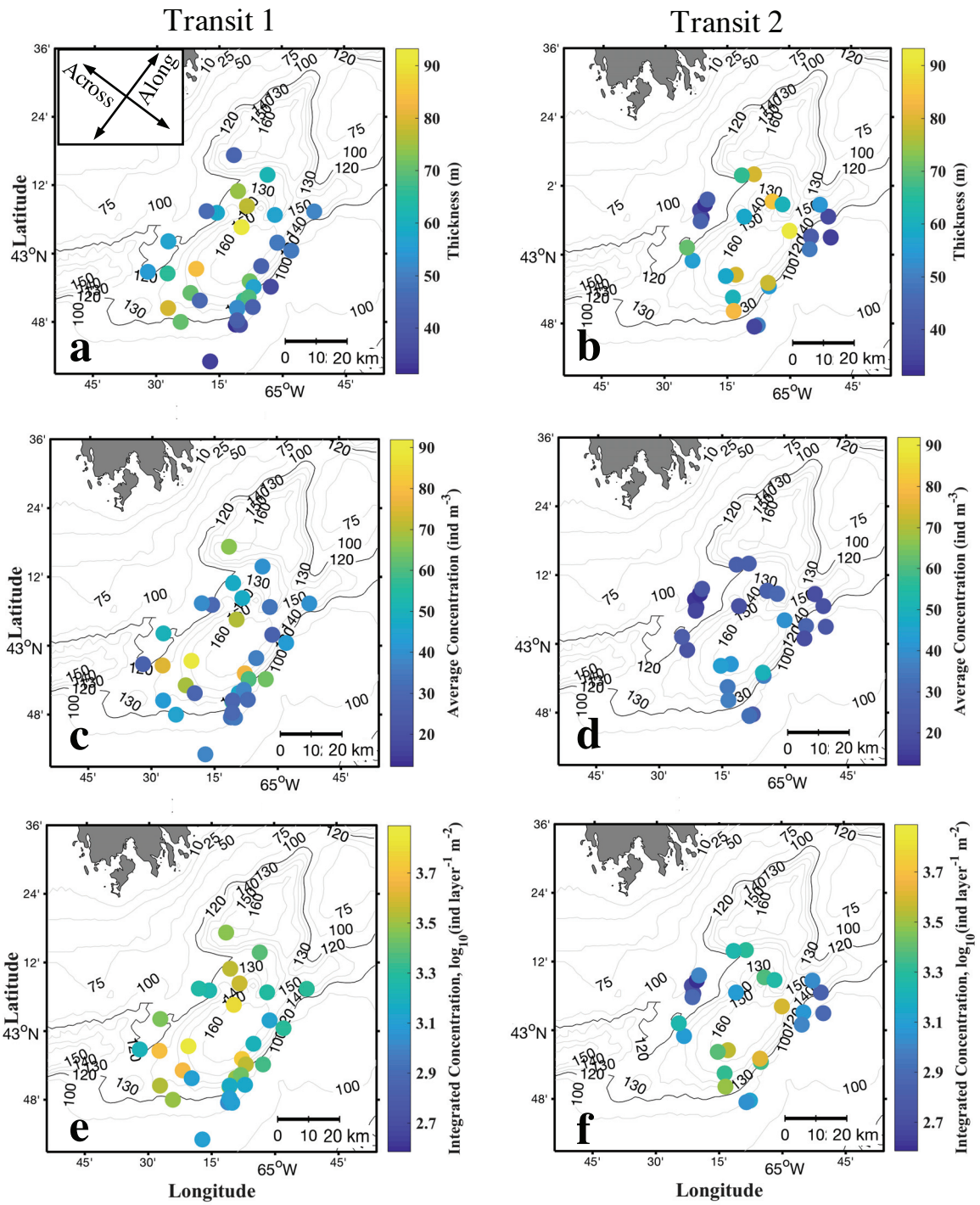

Figure 4.3. Maps of nightly averages over for each SL metric during each transit; left panels are transit 1, right panels are transit 2. Metrics shown are layer thickness (a-b, top row), average concentration (c-d, middle row), and integrated concentration (e-f, bottom row). Note that integrated concentration is plotted on a log-scale. The position of each point is the average over coordinates from all profiles for each night. An example of the orientation of the along- and across-basin coordinates is shown as an inset at the top of (a).

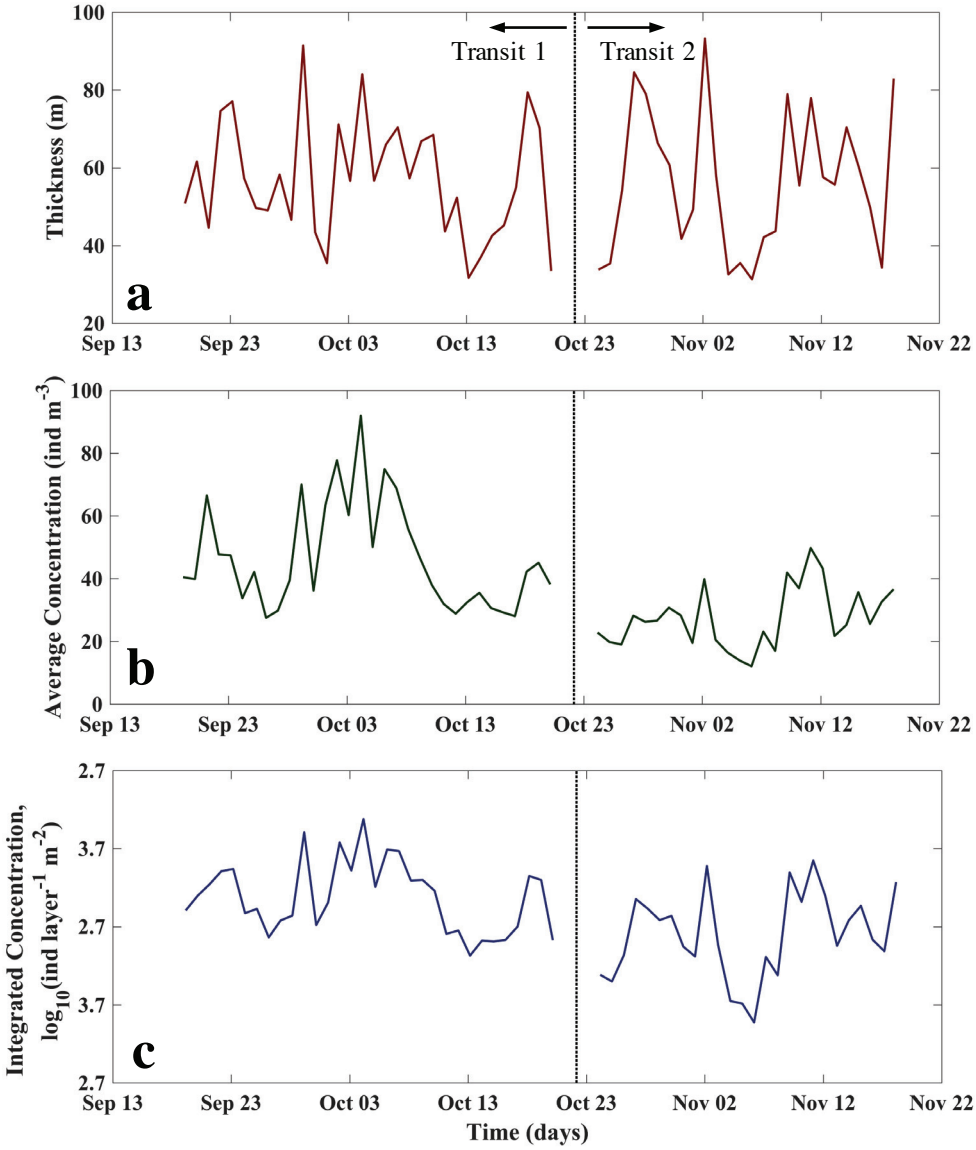

Figure 4.4. Time series for each SL metric over both transits of Roseway Basin; (a) layer thickness, (b) average concentration, and (c) integrated concentration. Dashed line in each panel indicates the end of transit 1 and the beginning of transit 2, while the glider regained position at waypoint A of the survey plan. Note that integrated concentration is plotted on a log-scale.

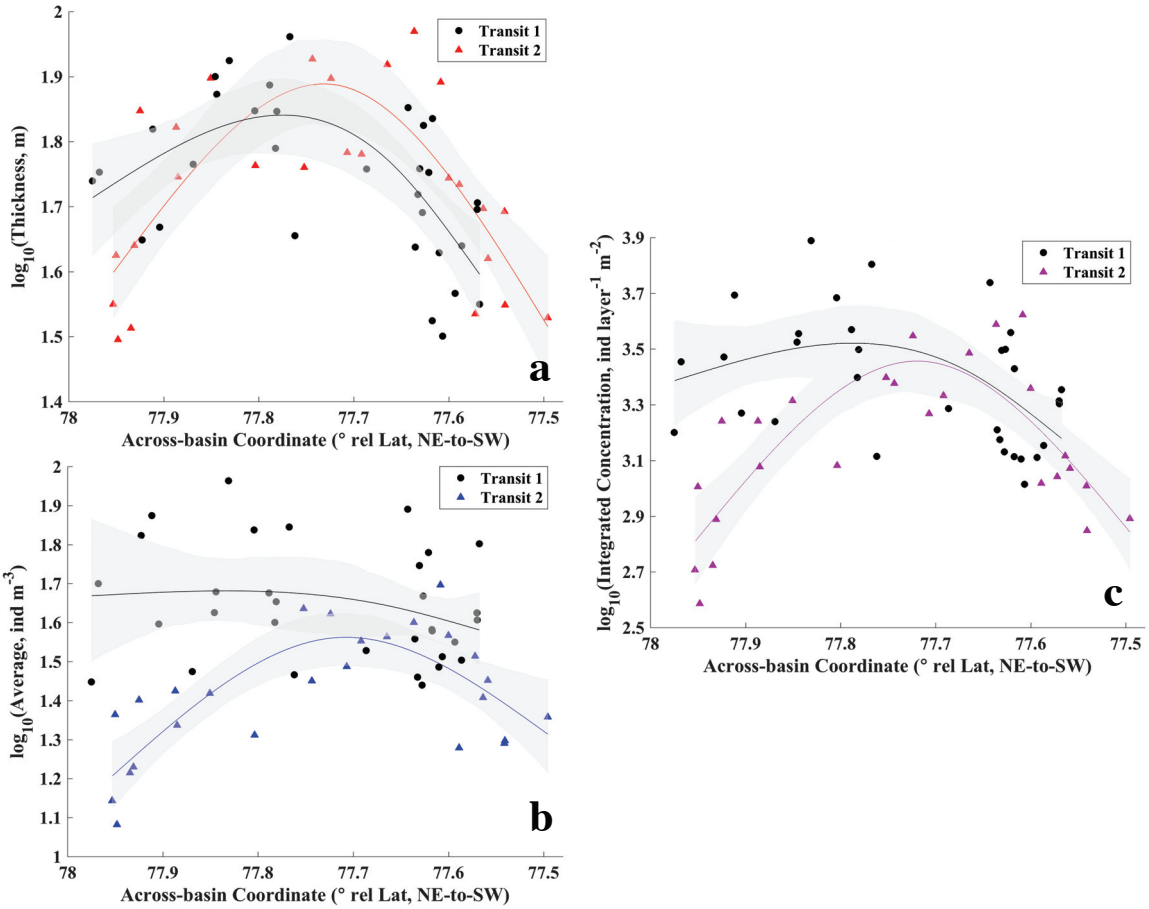

Figure 4.5. Least-squares restricted cubic spline fits for $\log_{10}$ transforms of SL thickness (a), integrated concentration (b), and average concentration (c) against the across-basin coordinates during transit 1 (black dots) and transit 2 (colored triangles). The across-basin axis (x-axis) is oriented with the NW margin on the left (higher numbers) and the SE margin on the right (lower numbers). Fig. 4.6 shows the orientation of the across-basin axis and the approximate locations of the 78 and 77.5 across-basin coordinates on a map of Roseway.

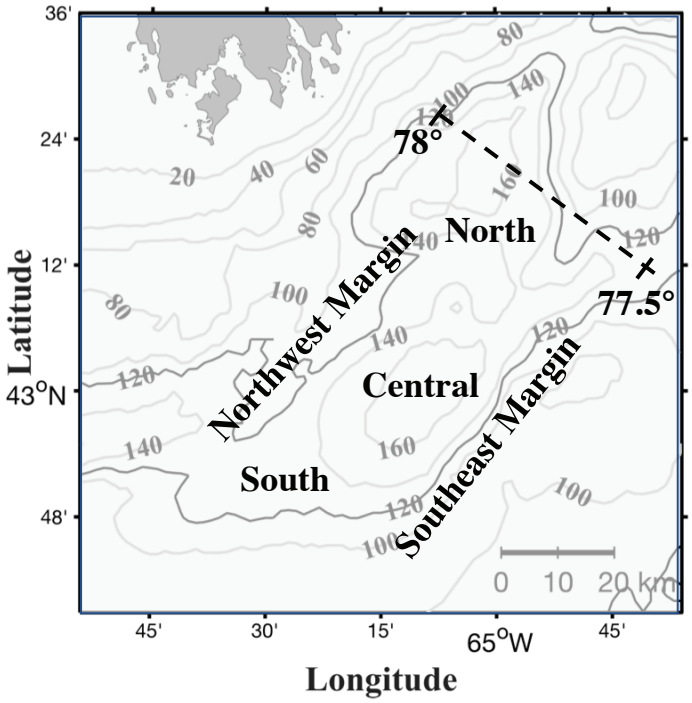

Figure. 4.6. Map showing regions referred to in the text and the locations of the 78° and 77.5° rel Lat across-basin coordinates used for the spline fits in Fig. 4.5.

4.2.2 Statistical Analysis of Water Mass Properties

Temperature and salinity varied over the glider track and throughout the water column during each transit. Water in the basin became colder and fresher over most of the water column over time. The average water column temperature cooled by ~4.8 °C (from 16.8 ± 1.3 °C to 12.0 ± 1.2 °C), and average water column salinity decreased by 0.6 psu (from 31.1 ± 0.7 psu to 30.53 ± 0.3 psu) between transit 1 and transit 2. The amplitudes of variation in both temperature and salinity over depth also decreased, yielding a more well-mixed water column in transit 2 relative to transit 1. In addition to the global cooling and freshening trend of the water mass properties in Roseway, there were also strong spatial variations in both the shallow and deep waters during each glider transit; these are described in the following two sections.

4.2.2a Near-Surface Variation in Water Mass Properties

Shallow water within the upper 20 m consistently cooled during both transits, and initially freshened during transit 1, before stabilizing in transit 2 (Figs. 4.7-4.9). The cooling trend

in shallow water continued steadily during transit 2 as well (Fig. 4.7). This almost linear decrease in temperature in near-surface waters throughout the survey transits can be explained by seasonal atmospheric cooling, and so is not representative of near-surface variation in water masses. For salinity, the general freshening trend was not sustained during transit 2 and overall salinity did not vary substantially for the remainder of this transit (Fig. 4.7), except for a notable period during approximately three days when the glider was over the northern side of the southeast margin (Fig. 4.8; see location reference in Fig. 4.6) and the water was considerably saltier, not just at the surface, but throughout the water column (Fig. 4.7). The freshest water measured in transit 1 was isolated over the far southern end of the basin (Fig. 4.8). Between transits, the strongest freshening in shallow water was over the northwest margin, and there was little to no change in salinity over the southeast margin (Fig. 4.10a).

4.2.2b Deep Variation in Water Mass Properties

Deep water initially warmed and freshened in transit 1, then cooled and experienced increased vertical variation in salinity during transit 2. For temperature, excepting the deepest waters (~120 m and deeper), which remained between 7-8 °C throughout the survey, deep water between 80-120 m warmed during transit 1 by around 3.5 °C (from ~5.5 °C to ~9 °C), then stabilized in transit 2 at around 6 °C (Fig. 4.7). Around this ~ 6 °C average temperature, deeper water (> 60 m depth) was more variable throughout the basin during transit 2, varying similarly to shallow salinity (Fig. 4.7). In contrast to the increase in deep temperature during transit 1, deep salinity (water deeper than ~120 m) decreased by around 2 psu between transits.

In terms of variation over space between transits, the strongest freshening of deep water (in the 90-100 m depth range; as previously selected for more detailed characterization) occurred over the central basin (~77.75 rel ° Lat, in the across-basin) and the least freshening occurred over the south margin between transits (~77.55 rel ° Lat, Fig. 4.9). During the warming of deep water in transit 1, the warmest water was consistently measured along the southeast margin (Fig. 4.9). Then, deep waters cooled in the first three days of transit 2, while the glider was still in the northern end of the basin (Fig. 4.8, 4.9),

and deep temperature remained cool throughout the basin except over the southeast margin, with the coldest water measured over the northern end of the basin (Fig. 4.7, 4.9). The deep water encountered by the glider during transit 2 over the southeast margin was much warmer than anywhere else in the basin; ~ 9.5 °C over the southeast margin relative to ~ 5-6 °C over the northwest and central basin. This deep, warm southeastern slope water was measured over the same area where the warmest water in transit 1 had been found (Fig. 4.10c, 4.9). The first pass over this anomalously warm water was also simultaneous to the previously described increase in salinity throughout the water column (Fig. 4.7).

In contrast to the parts of the glider track with warmer water, there was a cold intermediate layer (CIL) present briefly during the first ~ 4 days of the transit 1 (around Sept. 19-22), then twice again for around 8 days each during transit 2 (from approximately Oct 24-31 and again from Nov 8-15; Fig. 4.7). The CIL consisted of water between 4-6 °C at depths between 60-110 m, and was detected each time the glider was over the northern end of the basin. Between transits, deep temperature cooled over the central and northwest margins, while the deep water over the southeast margin warmed, with the warmest deep water over the entire survey occurring over the southeast margin in transit 2 (Fig. 4.10c).

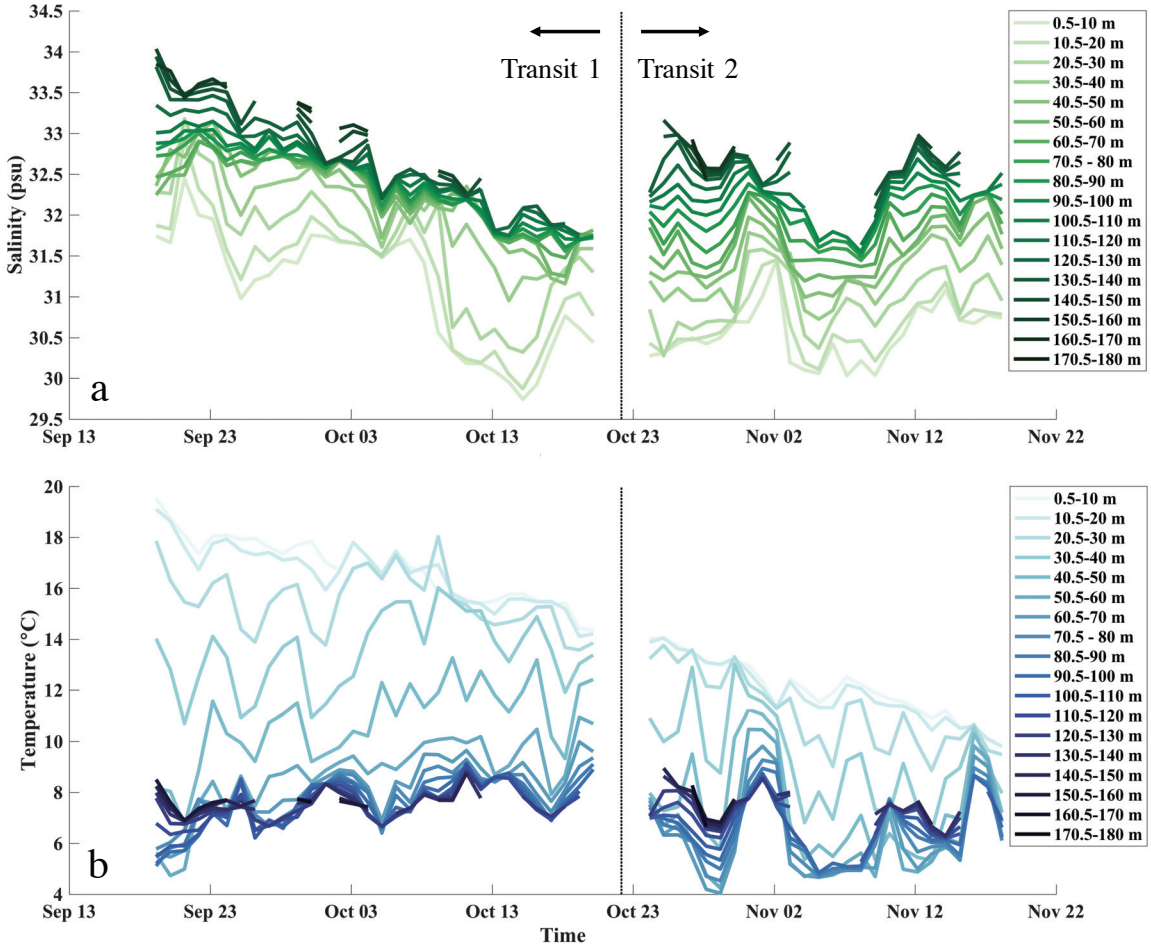

Figure 4.7. Time series of (a) temperature and (b) salinity for nightly profile averages over 10 m vertical averages from 0-180 m during the first and second glider transits of Roseway Basin. Gaps in the lines for deeper depth ranges indicate no data at those depths (glider in shallow water). Dashed vertical line indicates interval of two days between transit 1 and transit 2.

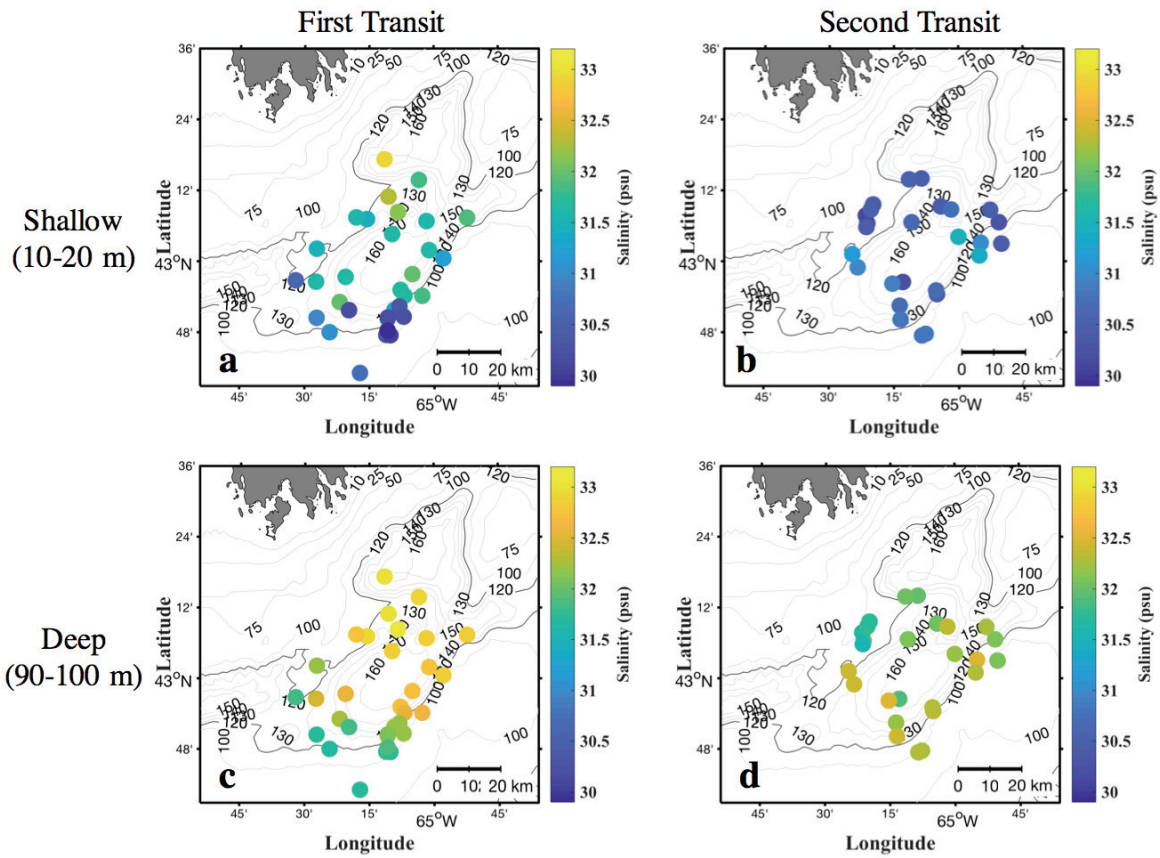

Figure 4.8. Maps of salinity for the (a-b) shallow 10-20 m depth range, and (c-d) the deep 90-100 m depth range over both glider transits of Roseway Basin, averaged over night-time profiles.

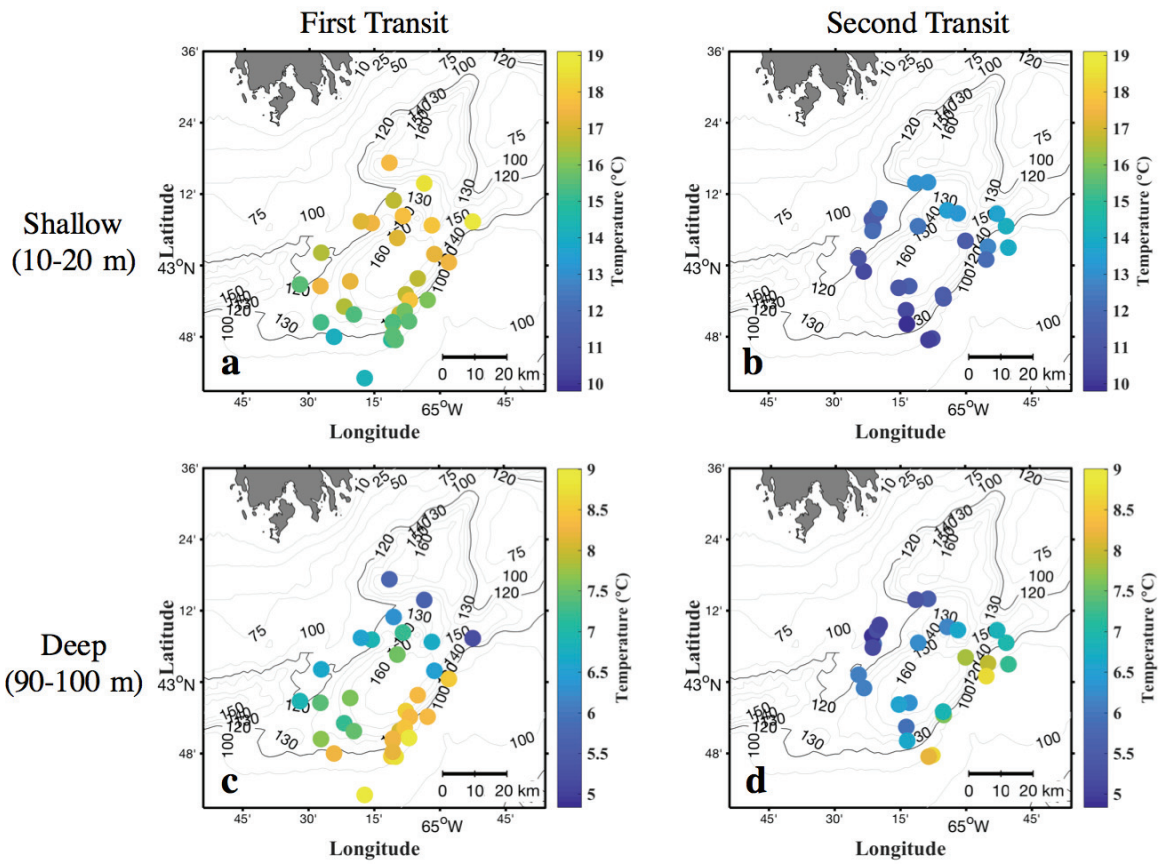

Figure 4.9. Maps of temperature for the (a-b) shallow 10-20 m depth range, and (c-d) the deep 90-100 m depth range over both glider transits of Roseway Basin, averaged over night-time profiles. Note the difference between color bar scales between the shallow and deep depth ranges.

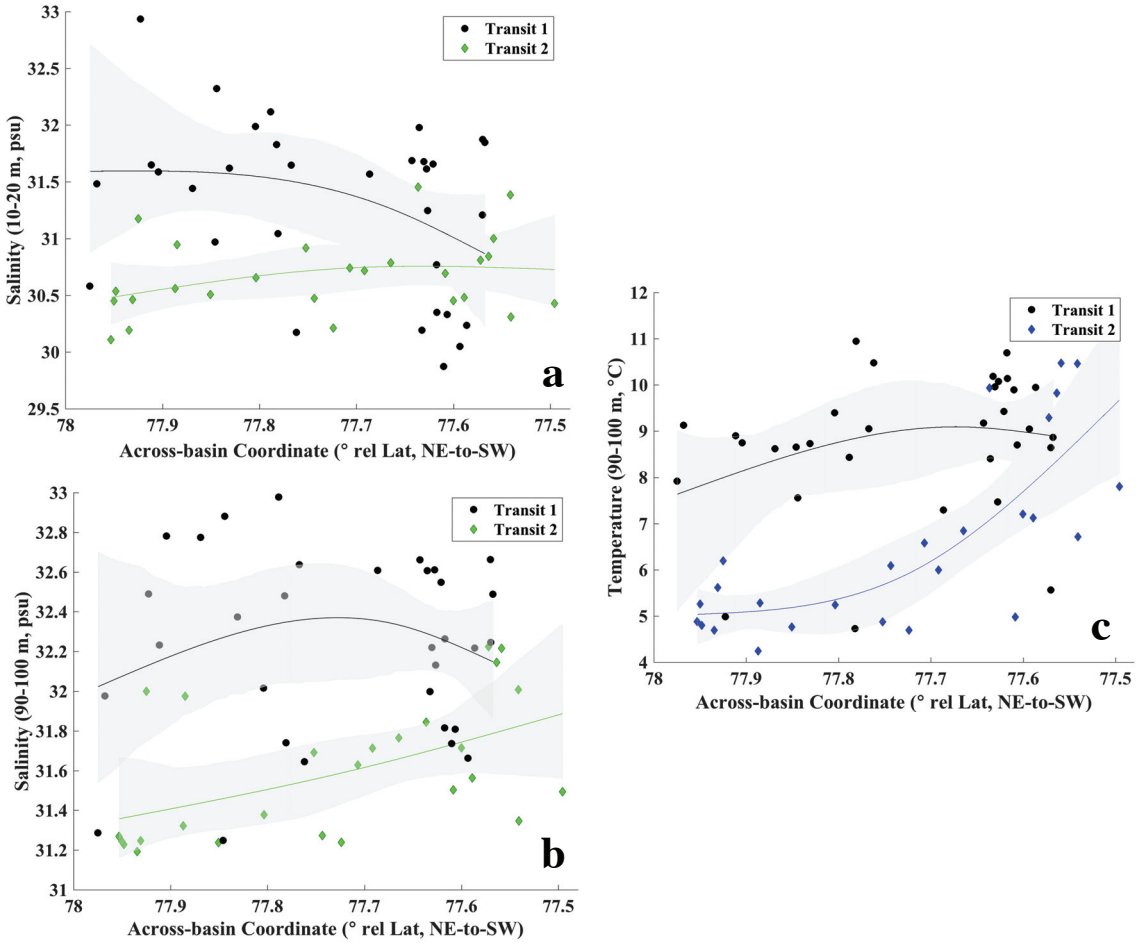

Figure 4.10. Least-squares restricted cubic spline fits for $\log_{10}$ transforms of shallow salinity (a; at 10-20 m depth), deep salinity (b; 90-100 m depth), and deep temperature (c; 90-100 m depth) against across-basin coordinates during transit 1 (black dots) and transit 2 (colored diamonds). Shallow temperature (10-20 m depth) is not shown as its variation does not represent variation in water mass (see text). The across-basin axis (x-axis) is oriented with the NW margin on the left (higher numbers) and the SE margin on the right (lower numbers).

4.2.2c Inferring Water Masses from Expected Endmembers and Cluster Analysis Results

All water measured during the survey was considerably warmer than the expected endmember values for water masses. Salinity throughout the water column was within the range of the Cabot Straight subsurface (CBSs) and Cabot Straight Cold Intermediate Layer (CBS-CIL; combined ranges of T: 1.8–3 °C, S: 31–33), and approached but never reached the saltiness of the Warm Slope Water (WSW; T = 11.7, S = 35.5) (Fig. 4.11). Only water deeper than 60 m closely approached the ranges expected for Scotian Shelf endmembers. The endmembers closest to the glider measurements of deep salinity and temperature (> 60 m) are the CBSs and the WSW, however it appears that any WSW in Roseway was a mixture of WSW and fresher water.

The cluster analysis revealed spatial structure in shallow salinity (10-20 m) and deep temperature (90-100 m) suggesting the presence of two water masses in the shallow and deep depth ranges (Fig. 4.12, 4.13), with different spatial patterning over the basin between depth ranges and properties (Fig. 4.14). The shallow temperature contained a fresh cluster (average over data assigned to cluster = 30.5 ± 0.3 psu) and a saltier cluster (average over data assigned to cluster = 31.7 ± 0.4 psu). The shallow-fresh cluster was only present in transit 1 in the far south end of the basin when the glider was at the end of the transit and during transit 2 at one location on the southeast margin; during both transits the shallow-salty cluster was present everywhere else. For the deep temperature, two clusters were also identified, a warmer cluster (average over data assigned to cluster = 8.2 ± 0.5 °C), and a cooler cluster (average over data assigned to cluster = 6.2 ± 0.7 °C).

The deep temperature clusters followed a different spatial pattern than the shallow salinity clusters. The deep-warm cluster was found along the southeast margin in both transits, and the deep-cool cluster was found everywhere else. There was a substantial decrease in the spatial coverage of the deep-warm cluster between transits. These results are consistent with the patterns of temperature and salinity encountered by the glider as shown in maps of these variables (Fig. 4.14a,b *vs* Fig. 4.8a,b for shallow salinity, and Fig. 4.14c,d *vs* Fig. 4.9c,d). The WSW (slope water mass) likely influences the deep-warm and shallow-salty clusters, and likewise, the CBSs (shelf water mass) likely influences the deep-cool and shallow-fresh, clusters.

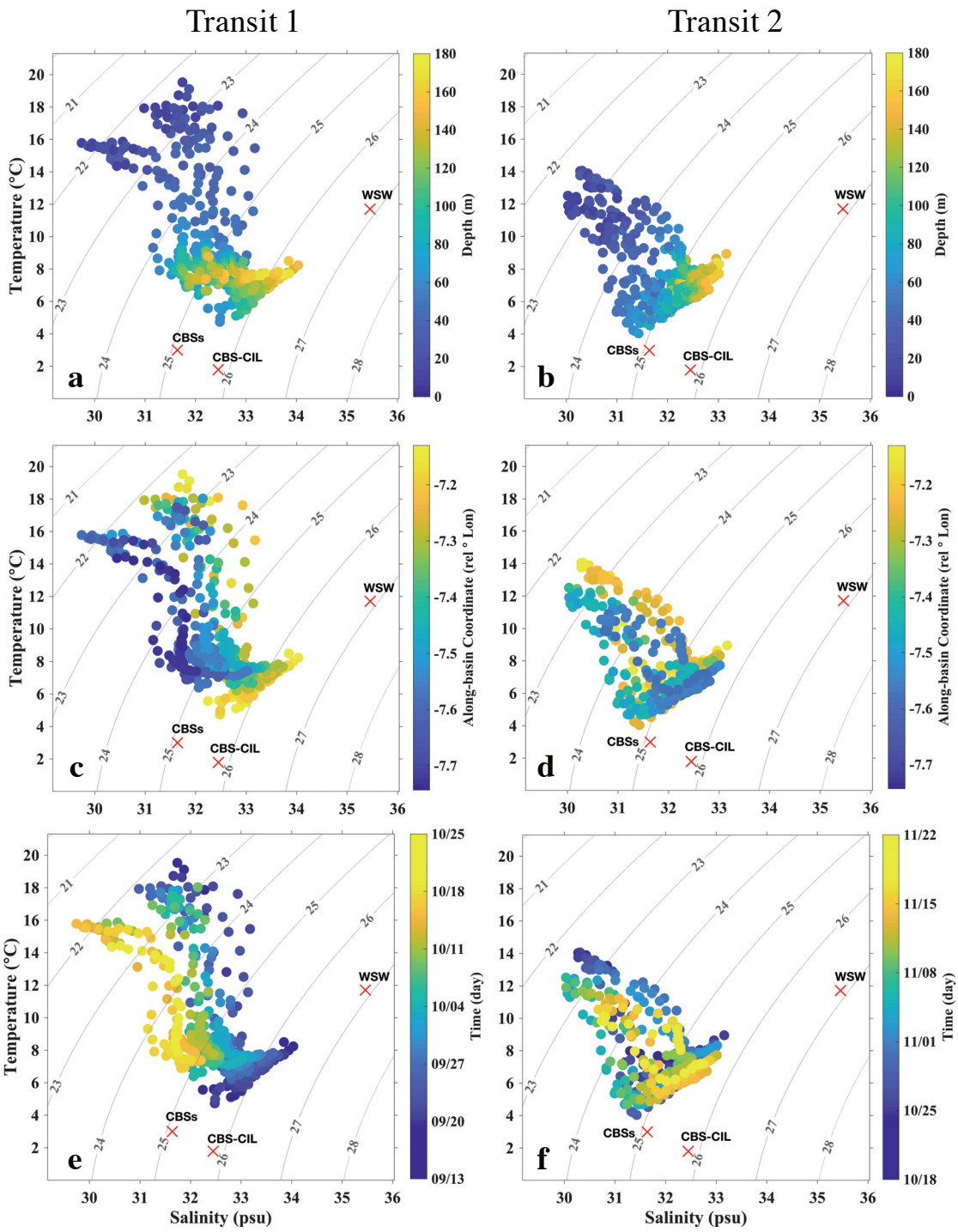

Figure 4.11. Temperature-salinity diagrams for transit 1 (left panels) and transit 2 (right panels) in Roseway Basin. Color maps for each diagram are: depth (m) (a-b), time (days) (c-d), and along-basin coordinate (rel ° Lon; where colors run cool to warm and values run toward zero as moving northeast to southwest (e-f). Annual mean Scotian Shelf water mass endmembers (WSW, CBSs, and CBS-CIL) from *Dever et al.* (2016) are indicated as red crosses in each panel.

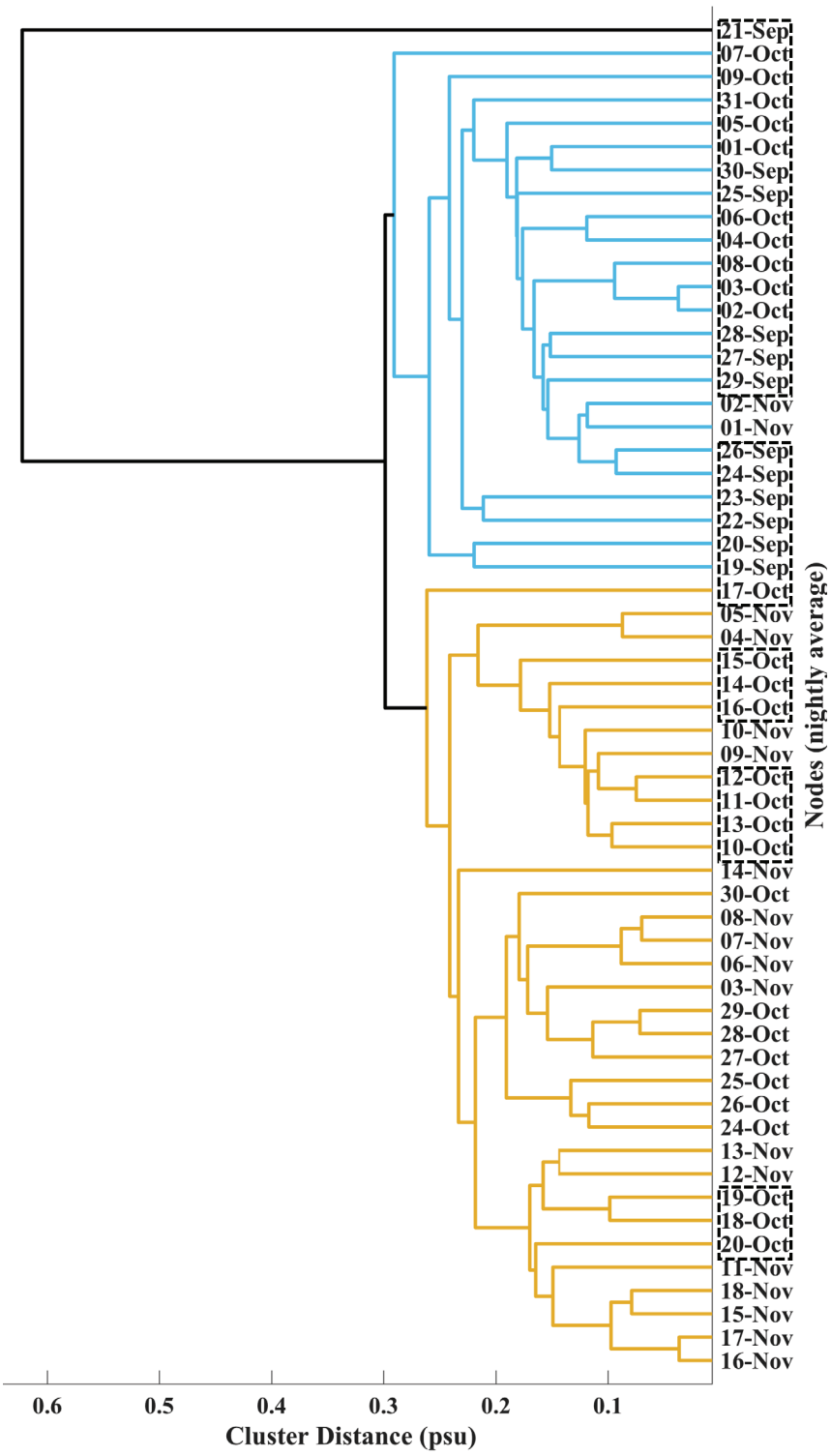

Figure 4.12. Dendrogram for results of cluster analysis on data for shallow salinity (10–20 m). The two primary clusters that part out the data are highlighted; a fresh cluster (30.5 ± 0.3 psu) is shown in light blue, and a salty cluster (31.7 ± 0.4 psu) is shown in yellow. Dates for each nightly average are shown at the end of each branch (nodes) to indicate each nightly averaged data point. Points from transit 1 are outlined in a dashed box and points from transit 2 are not boxed.

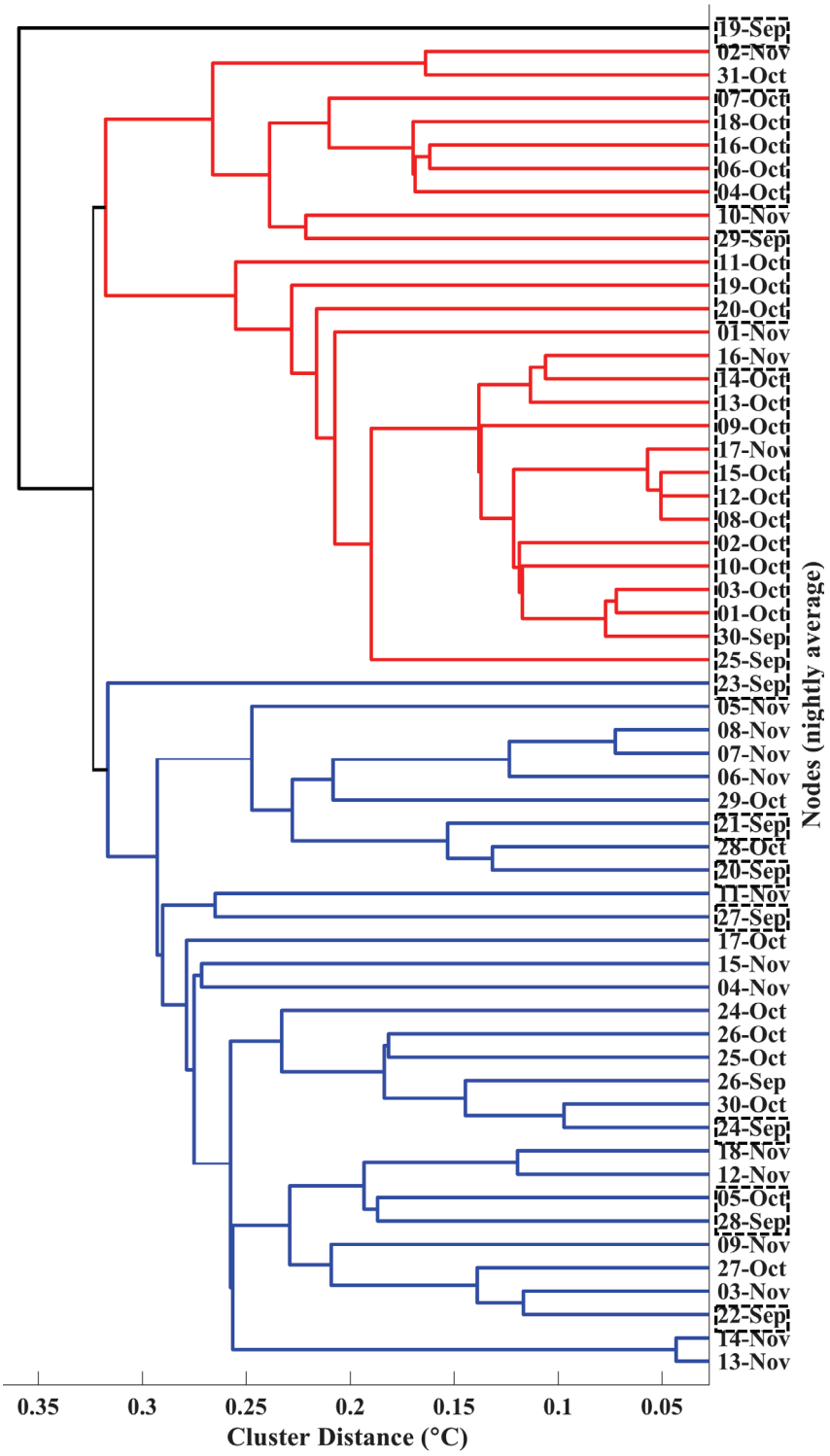

Figure 4.13. Dendrogram for results of cluster analysis on data for deep temperature (90–100 m). The two primary clusters that part out the data are each highlighted; a cool cluster (6.2 ± 0.7 °C) is shown in blue, and a warm cluster (8.2 ± 0.5 °C) is shown in red. Dates shown for each nightly average are shown at the end of each branch (nodes) to indicate each nightly averaged data point. Points from transit 1 are outlined in a dashed box and points from transit 2 are not boxed.

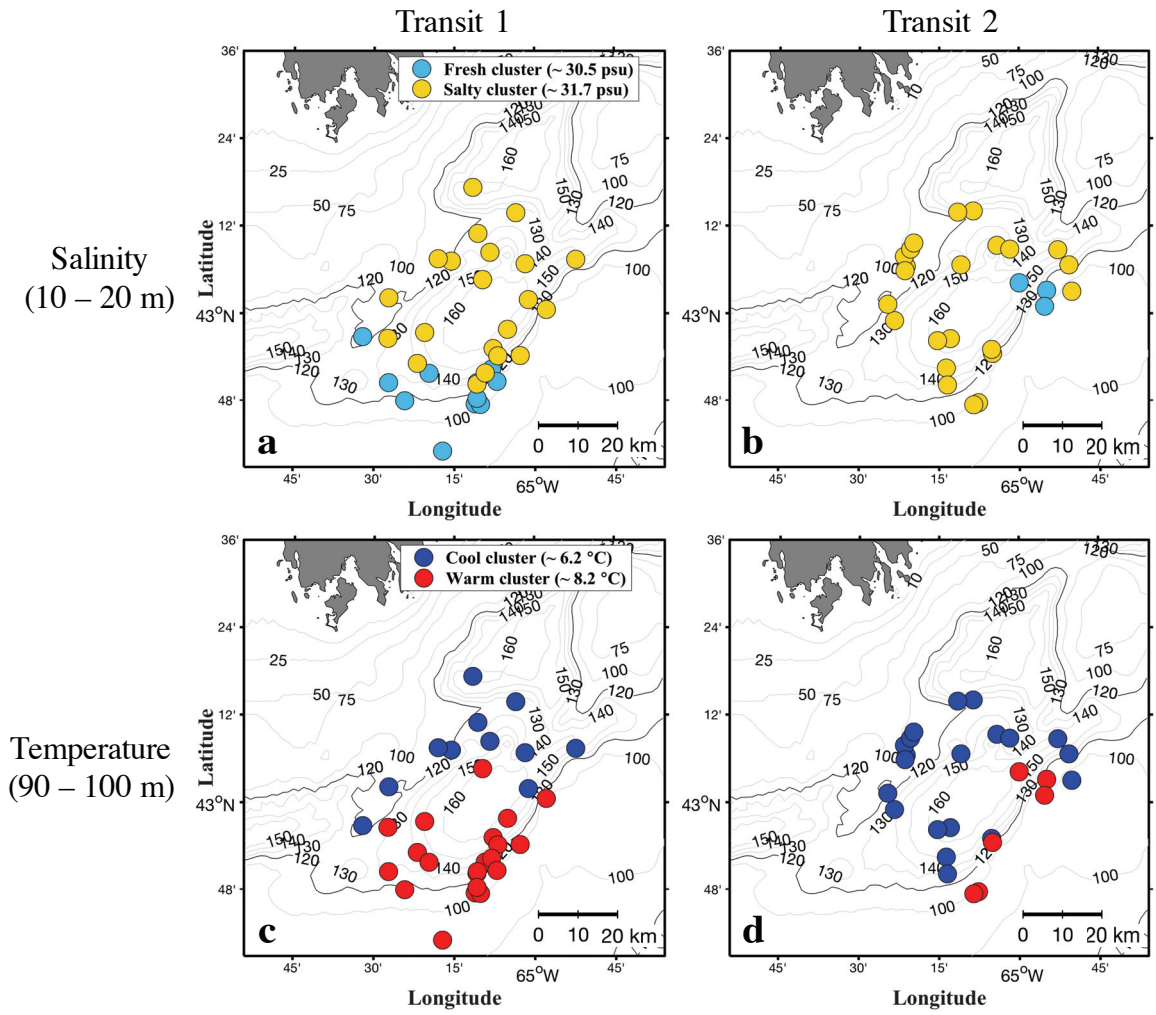

Figure 4.14. Maps of clusters identified for shallow salinity (10–20 m) for transit 1 (a) and transit 2 (b), and for deep temperature (90–100 m) for transit 1 (c) and transit 2 (d). Positions for nightly averages of salinity in the 'salty' cluster (31.7 ± 0.4 psu) are indicated as yellow points, and for the 'fresh' cluster (30.5 ± 0.3) are indicated as light blue points in (a) and (b). Positions for nightly averages of temperature for the 'cool' cluster are indicated as blue points, and for the 'warm' cluster are indicated as red points in (c) and (d). Positions of each cluster point are the same as for the temperature and salinity measurements used in the cluster analysis.

4.2.3 Statistical Analysis for Covariation Between SL Metrics and Environmental Variables

Layer thickness:

The strongest predictors of SL thickness in the best-fit multiple regression model were seafloor depth and along-basin coordinate (Table 4.1), and no significant relationships were found with water mass properties. The models showed that thicker SLs tended to occur more often over deeper regions of the basin, and toward the northeast (negative coefficient for the along-basin coordinate indicates thicker layers from southwest to northeast). Overall, the best-fit multiple regression model explained 52% of the total variation in layer thickness.

The layer thickness metric did not significantly change between deep temperature ($p = 0.84$) or shallow salinity clusters ($p = 0.14$; Table 4.2); this is not surprising, as seafloor depth and position were the most important variables for explaining variation in this metric, not water mass properties.

Average and integrated concentration:

The strongest predictors of SL average and integrated concentration in the best-fit multiple regression models for both metrics were deep temperature, shallow salinity, seafloor depth, and along-basin coordinate (Tables 4.3, 4.4). Higher average and integrated concentrations of euphausiids were predicted by the models to occur in warmer, saltier water, over regions with deeper seafloor depths, and toward the northern end of the basin. The best-fit multiple regression models for average and integrated concentration explained 69% and 68% of the total variation in each of these metrics, respectively.

Both SL average and integrated concentrations also had some association with water mass spatial structure identified in the cluster analysis (Table 4.2); significantly higher average ($p < 0.01$) and integrated ($p < 0.01$) euphausiid concentrations were present in the saltier shallow cluster, and higher average (<0.01), but not integrated ($p = 0.04$), concentrations were found in the warmer deep cluster.

Table 4.1. Best-fit multiple regression model summary for SL thickness metric. Model adjusted-$R^2 = 0.52$; p-value = 4.9×10^{-10}; error degrees of freedom = 55; dispersion = 0.008; ΔAIC = -2.93.

Variable	Coefficient Estimate	SE	p-value
Seafloor Depth	0.004	5.6×10^{-4}	< 0.001
Along-basin coordinate	-0.22	0.08	0.001

Table 4.2. Results for t-tests comparing magnitude of SL metrics in corresponding positions to the shallow salinity and deep temperature clusters over both glider transits. df = error degrees of freedom.

	Metric	Test Statistic	df	p-value
Shallow Salinity (10-20 m)	Layer Thickness	-1.5	52.1	0.1
	Average Concentration	-5.0	31.4	< 0.001
	Integrated Concentration	-4.3	52.1	< 0.001
Deep Temperature (90-100 m)	Layer Thickness	0.2	52.2	0.8
	Average Concentration	-3.2	45.1	0.002
	Integrated Concentration	-2.1	55.2	0.04

Table 4.3. Best-fit multiple regression model summary for SL average concentration metric. Model adjusted-$R^2 = 0.69$; p-value = 1.3×10^{-13}; error degrees of freedom = 53; dispersion = 0.01; ΔAIC = 0.34.

Variable	Coefficient Estimate	SE	p-value
Deep Temperature	0.52	0.013	< 0.001
Shallow Salinity	0.15	0.023	< 0.001
Seafloor Depth	0.003	0.001	< 0.001
Along-basin coordinate	-0.41	0.10	< 0.001

Table 4.4. Best-fit multiple regression model summary for SL integrated concentration metric. Model adjusted-R^2 = 0.68; p-value = 2 x 10^{-13}; error degrees of freedom = 53; dispersion = 0.02; ΔAIC = -5.7.

Variable	Coefficient Estimate	SE	p-value
Deep Temperature	0.048	0.019	0.016
Shallow Salinity	0.17	0.034	< 0.001
Seafloor Depth	0.007	0.001	< 0.001
Along-basin coordinate	-0.64	0.14	< 0.001

Chapter 5

Discussion

Overall, the measurements from the glider echosounder were successfully able to characterize variation in the baleen whale prey-field in space and time in Roseway Basin, thus achieving the goal of this thesis. Results demonstrated that variation in transport of water masses evident in the hydrography can explain some variation in euphausiid scattering layer (SL) concentration and distribution. Euphausiid SLs in surface waters of Roseway Basin contained sufficient concentrations of euphausiids to suggest that, in comparison to other known habitats, the Basin is conceivably a feeding habitat for baleen whales. The novel use of a glider for integrated monitoring of Roseway Basin revealed new insight to the variations of baleen whale prey-fields in this location and facilitated the formation of new hypotheses to motivate future research.

5.1 Seasonal Variation in Nova Scotia Current Explains Basin-Scale Variation in Euphausiid Concentrations

A seasonal (late-autumn) increase in volume transport of the Nova Scotia coastal current (NSC) on the Scotian Shelf can explain the change in water masses that co-occurred with a decline in euphausiid concentrations measured between transit 1 (October) and transit 2 (November). The transition from warmer-saltier to cooler-fresher water throughout the water column between glider transits can be attributed to a seasonal pulse of Cabot Strait Water (CSW; referred to as CBSs by *Dever et al.* 2016) originating in the Gulf of St. Lawrence (GoSL). This cold, fresh water is formed at its source in the Cabot Strait during the spring freshet, which occurs when meltwater from the St. Lawrence river increases the freshwater discharge into the GoSL (*Banks* 1966; *Galbraith et al.* 2013). The CSW is then transported by the NSC around Cape Breton and southwest along the Nova Scotia coast, taking about 3–4 months to arrive on the central and western Scotian Shelf (*Hannah et al.* 2001; *Dever et al.* 2016). The seasonal presence of CSW is marked over the central to western Scotian Shelf by the near-simultaneous cooling and freshening of coastal waters

influenced by the NSC (*Smith* 1983; *Dever et al.* 2016). The conclusion that CSW was the origin of the cold, fresh water mass in Roseway Basin is based on three main results: (1) cooling and freshening of the water column to 4 °C and 31.5, which is the T-S signature of Cabot Strait water (Fig. 4.11), (2) the time of arrival (mid-October) which is consistent with an autumn arrival of the spring GoSL freshet (Fig. 4.7, *Smith 1983*; *Dever et al. 2016*), and (3) the across-basin distribution of water masses, which demonstrated that water cooled and freshened on the northwest margin, closest to the Nova Scotia coastline and NSC, but not on the southeast margin, closest to the shelf-break and furthest from the NSC (Fig. 4.10, *Davies et al.* 2014). Typically, the deep water of Scotian Shelf basins, including Roseway Basin, is comprised of Warm Slope Water (WSW*, Davies et al.* 2014, *Petrie & Drinkwater* 1993). Moreover, flushing of the deep basin water up to 180 m depth with CSW had not to our knowledge been observed in Roseway Basin before because oceanographic measurements have primarily been taken during the August-September period (*Davies et al.* 2014; *Davies et al.* 2015, *Baumgartner et al.* 2003).

Concentrations of euphausiid species in the shallow night-time SLs, *M. norvegica* and *T. inermis*, were higher in WSW than CSW. Multiple regression models and the cluster analysis both showed that elevated euphausiid concentrations occurred over deeper regions of the basin and with the presence of warmer and saltier water. The across-basin spline curves also showed that euphausiid concentrations declined more in areas closer to the coast (northwest basin margin) than elsewhere in the basin, which indicates this decline was related to changes in the coastal water mass. These patterns are in good agreement with observations in the literature. Both *M. norvegica* and *T. inermis* are most often found at depth, in channels, deep basins, or near the shelf break across continental shelf regions (*Hjort & Ruud* 1929; *DFO*, 1996; *Melle et al.* 2004; *Pinchuk & Hopcroft* 2010), which implies an association with slope water because these are also the same regions where WSW is the dominant water mass (*Gatien* 1976; *Petrie & Drinkwater* 1993). Further, WSW can be a source of euphausiids to other locations in the Scotian Shelf and to surrounding areas, such as the Gulf of Maine (*Wiebe et al.* 1987). Finally, these associations suggest that the advection of the slope water mass impacts the spatial and temporal variation in euphausiid concentrations. Consequently, the northeast-to-southwest influx of cooler and fresher water to Roseway Basin combined with the association

between euphausiids and warm, salty slope water and the dramatic reduction in overall concentrations of euphausiids between glider transits provides evidence for the hypothesis that the autumn arrival of the spring freshet from the St. Lawrence River in Roseway displaced slope water from the basin along with the associated high concentrations of euphausiids. Because the spring freshet is an annual event over the Scotian Shelf, the changes in concentration and distribution of euphausiids in Roseway could also be an annual event.

5.2 Roseway Basin Represents Potential Feeding Habitat for Baleen Whales

Determining if Roseway Basin represents feeding habitat for euphausiid-eating baleen whales was a key motivation for this study. There are three characteristics of the euphausiid prey-field that can be used to determine if Roseway could support feeding whales. First, the concentrations of euphausiids need to be much higher than typical average concentrations in the ocean because they must meet the minimum energetic requirements for baleen whales (*Kenney et al.* 1986; *Piatt & Methven* 1992). Second, the persistence of elevated euphausiid concentrations is important, because highly ephemeral food patches may not persist long enough for migratory whales to find them before they are gone. Third, the vertical and horizontal distribution of regions with elevated euphausiid concentrations must be considered, because diving and searching for food are both energetically costly (*Goldbogen et al.* 2006; *Goldbogen et al.* 2011). The glider measurements of euphausiid concentrations include information on all three of these characteristics of baleen whale feeding habitat, and the context and implications of these findings is presented below.

The glider estimates of euphausiid concentrations in Roseway Basin are comparable to those reported in known baleen whale feeding habitats globally (Table 5.1), albeit they are closer to the low end of concentrations in which baleen whales are known to forage. The maximum estimated euphausiid biomass in Roseway over the entire survey in a night-time shallow SL, converted to units of g m^{-3} for comparability to the literature[2,3], was ~ 7 g m^{-3} or layer integrated as ~ 1,240 g m^{-2}. These biomass levels were encountered

[2] *Mauchline* (1967) for *M. norvegica* as 0.156 g ind^{-1}
[3] *Mauchline* (1967) for *T. inermis* as 0.012 g ind^{-1}

by the glider in transit 1 over the central deep basin. During transit 2, the maximum biomass was only half that in transit 1. However, it must be noted that the euphausiid concentration estimates, considering the sources of uncertainty discussed in section 3.3.5, could vary by as much as an order of magnitude. The estimated euphausiid biomass observed in this study during transit 1, withstanding the uncertainty around the estimates, is similar to those reported for known baleen whale feeding habitats. Furthermore, the wide range of reported concentrations for known habitats does not preclude the lower concentrations of euphausiids measured in transit 2, after the shift in water masses in the basin. For example, biomass measured acoustically the St. Lawrence Estuary (SLE), a blue whale critical feeding habitat, contains biomass ranging from ca. 2 - 250 g m^{-3} (*Lavoie et al.* 2000), and in some cases extremely dense aggregations of ca. 500 g m^{-3*} have been reported (*Cotté & Simard* 2005). Layer-integrated biomass in Roseway was also comparable to the lower acoustic estimates from the Western Antarctic Peninsula (WAP), where column-integrated biomass[4] of *Euphausiia superba* were found ranging from 168 g m^{-2} up to 9,800 g m^{-2}, representing over 50-fold variation in concentrations (*Wiebe et al.* 2011). Thus, the estimated euphausiid concentrations measured in Roseway were the same order of magnitude of those from known whale feeding habitats, which suggests that Roseway may be a viable baleen whale feeding habitat on the Scotian Shelf.

[4] *Gierak* (2013) for *E. superba* as 2 g ind^{-1}

Table 5.1. Euphausiid concentrations reported from aggregations in known baleen whale feeding habitats. Footnotes are for reported values that were converted from individuals to average biomass (g), to allow comparison across studies. Minimum and maximum values from SLs over both transits from this study are also listed here. CCS = California Current System; SLE = St. Lawrence Estuary; WAP = Western Antarctic Peninsula.

Study	Location	Method	Species	Concentration
This Study[1,2]	*Scotian Shelf*	*Acoustic*	*Mn, Ti*	*1–7 g m*$^{-3}$
				61.6–1,240 g m^{-2}
***Nicol* (1986)**[1]	Bay of Fundy	Aerial photos	Mn	2.5–121 g m^{-3}
***Croll et al.* (2005)**	CCS	Acoustic	Ts, Ep	260–1,850 g m^{-2}
***Ressler et al.* (2005)**[5]	CCS	Acoustic	Ts	0.6–316 g m^{-2}
***Lavoie et al.* (2000)**	SLE	Acoustic	Tr	2–250 g m^{-3}
***Cotté & Simard* (2005)**	SLE	Acoustic	Mn, Tr	4–500 g m^{-3}
***Nowacek et al.* (2011)**[3]	WAP	Acoustic	Es	340–4,000 g m^{-3}
***Wiebe et al.* (2011)**[3]	WAP	Acoustic	Es	168–9,800 g m^{-2}

The variation in euphausiid concentration between water masses revealed in this study showed that transport of euphausiids in water masses can affect the persistence of prey-fields in Roseway. Thus, one important timescale for the persistence of elevated euphausiid concentrations appears to depend on processes that affect transport of these water masses. Temporal persistence of high concentrations of euphausiids was low (not more than a few weeks), relative to the baleen whale feeding season on the Scotian Shelf, which is typically June through October, coincident with the seasonal cycle of ocean productivity (*Baumgartner & Mate* 2005; *Michaud & Taggart* 2007). However, these dense SLs could have formed and persisted for days or longer before the arrival of the glider in Roseway. The least change in both water masses and euphausiid concentrations was over the furthest part of the basin from the coastal current influence (southeast margin), and contrastingly the most change was over the closest part of the basin to the coastal current (northwest margin). These observations suggest that there may be a persistent, albeit low-concentration, prey-field that exists along the southeast margin in Roseway, and a more ephemeral high-concentration zone toward the northwest margin. Additionally, the

[5] *Abraham & Sydeman* (2006) for *T. spinifera* as 0.1 g ind^{-1}

associations between euphausiid concentrations and water masses imply that Roseway Basin could be a more persistent feeding habitat for whales through the summer months, while the influence of slope water is typically stronger across the Scotian Shelf (*Petrie & Drinkwater* 1993; *Dever et al.* 2016). If this is true, the glider survey may not have measured a consistent feature that characterizes prey-field persistence in Roseway, but a marked seasonal shift in euphausiid concentration from increased shelf water influence with the arrival of the spring freshet in the NSC.

In terms of euphausiid distributions in the basin, Roseway appeared to retain euphausiid biomass at elevated concentrations relative to the immediately surrounding shelf (100-120 m isobaths). Euphausiid concentration was higher in the WSW mass and over deeper bathymetry in this study, and euphausiid concentrations and SL thickness within the basin (at depths > 120 m) were consistently higher than those measured over the shallow shelf outside the basin (depths of ~ 100 m) during the entire glider survey. These results imply that the basin may represent a bathymetrically constrained feeding habitat on the Scotian Shelf for whales. There could be two reasons for this; physical and biological. From the physical standpoint, euphausiids could be retained as a result of deep basin bathymetry combined with geostrophic gyre-like circulation within the Basin (*Herman et al.* 1991). From a biological standpoint, euphausiids feed on diapausing copepods while at depth during the day (*Sameoto* 1980; *Kaartvedt et al.* 2002). Significant concentrations of diapausing, stage-V, *C. finmarchicus* were measured by *Davies et al.* (2014, 2015) at the 100–130 m depth range in Roseway, and these concentrations occurred only within the basin and not over the surrounding shelf. Since all Scotian Shelf basins are known to retain zooplankton biomass and have gyre-like circulation, the implication from the results in Roseway is that all Scotian Shelf basins have the potential to be viable baleen whale feeding habitat.

5.3 Future Research: Integrated Habitat Monitoring with Ocean Gliders

A critical objective of the WHaLE project is to determine if variation in the presence of baleen whales is explained by variation in their prey-field, and the results of this study permit this investigation for Roseway Basin. Passive acoustic monitoring (PAM) was included in the instrument suite integrated on the glider. Comparisons between the acoustic

whale detections and the euphausiid SL metrics developed in this study could be used to test hypotheses about habitat use by whales in Roseway Basin. Given the variation in euphausiid distributions during the glider survey, whales that feed on euphausiids might be expected to have a more persistent presence during during September to early October (transit 1), particularly in the south-central basin, where the glider encountered the highest concentrations in the first few days of October. Acoustic presence may also be expected to decline during the water mass transition, when strong cooling and freshening transition toward the end of transit 1 and between transits when euphausiid concentrations declined. Moreover, a decline in whale detections may be more dramatic on the northwestern basin margin, where the changes in euphausiid concentration between transits were most apparent. The ability to make inferences about the variation in predator presence that is informed by monitoring of prey-field variation will be valuable for future whale ecology studies in Roseway, and could also be applied to other known or suspected baleen whale feeding habitats.

In addition to extending the results of this study to other habitat monitoring questions, future work may be able to answer questions that have emerged from this study, such as whether the autumn decrease in euphausiid concentrations in Roseway is a persistent, seasonal feature of variation in this location. Repeated sampling over one or more years during a similar period to the glider survey presented in this study would verify if the pattern is persistent annually or was an ephemeral observation. Additionally, repeated sampling of Roseway combined with a wider survey coverage outside of the basin could determine whether this location represents a persistent retention hotspot for euphausiid concentrations on the Scotian Shelf. The answers to these questions have implications for Roseway Basin's viability as a whale feeding habitat. Specifically, for the freshet hypothesis presented above, this would illustrate part of the time-scale of habitat suitability for this location, and could allow inferences about the variation in prey-fields from interannual variations in the freshet strength.

Finally, verification of the zooplankton species assemblage in the SLs was a large source of uncertainty in the estimates of euphausiid concentrations for this study. Improved groundtruthing data and coordinated glider sampling in future work would help mitigate this issue for future studies. This might include net samples collected during both the day

and at night (only night-time tows were available for the net-acoustics comparison for this study) and tows taken at several stations over a larger area of the basin to resolve diel changes and to quantify spatial patchiness in the *in-situ* SL species composition. Another approach is the use of depth-dependent TS values to decrease uncertainty when estimating concentrations. This would contribute to increasing confidence in estimated concentrations to determine prey-field viability in Roseway, because while absolute values were presented in this thesis, there was considerable uncertainty around these values.

5.4 Conclusions and Significance

The glider echosounder measurements provided information on the spatial and temporal variation of baleen whale prey-fields throughout Roseway Basin, which fulfills this thesis' goal of using of an ocean glider to conduct integrated habitat monitoring of Roseway Basin. This was the first study of zooplankton ecology using ocean gliders conducted on the Scotian Shelf. The survey in Roseway, which included use of PAM to listen for the acoustic presence of whales, allowed simultaneous data collection of the oceanography, the whales, and their prey. The glider successfully resolved time and space variation in water mass properties and backscatter, suggesting that advection of water masses play a role in the redistribution of euphausiid biomass in Roseway Basin over the basin-scale and smaller patch scales, and over periods of one month or less.

The results of this study have also raised process-based questions that are relevant to baleen whale habitat monitoring that can be tested by future work. This thesis supports other MEOPAR WHaLE sub-projects that involve integrated whale habitat monitoring being conducted by project members on both the east and west coasts of Canada. Successfully monitoring multiple aspects of whale habitat, as was achieved here, is of key importance for comprehensive habitat characterization, and has wide-reaching applicability for baleen whale conservation efforts on the Scotian Shelf. And, in a broader context than that of baleen whales and their prey-fields, the integrated oceanographic information provided by the glider is an important contribution to the knowledge of euphausiid ecology on the Scotian Shelf, as no previous study in this region has looked beyond the concentrations of animals in a sampling location and into the processes that drive variation in those concentrations.

References

Abraham CL, Sydeman WJ. 2006. Prey-switching by Cassin's auklet *Ptychoramphus aleuticus* reveals seasonal climate-related cycles of *Euphausia pacifica* and *Thysanoessa spinifera*. Mar Ecol Prog Ser, 313, 271-283.

Allard K, Gjerdrum C. Unpublished working paper. Using marine bird distribution and abundance toward assessment of important marine habitat locations. Presented at the CSAS Regional Science Advisory Process held during February 18-20, 2014, in Halifax, Nova Scotia.

Banks RE. 1966. The cold layer in the Gulf of St. Lawrence. J Geophys Res, 71(6), 1603-1610.

Baumgartner MF, Mate BR. 2005. Summer and fall habitat of North Atlantic right whales (*Eubalaena glacialis*) inferred from satellite telemetry. Can J Fish Aquat Sci, 62(3), 527-543.

Baumgartner MF, Cole TV, Clapham PJ, Mate BR. 2003. North Atlantic right whale habitat in the lower Bay of Fundy and on the SW Scotian Shelf during 1999–2001. Mar Ecol Prog Ser, 264, 137-154.

Becker KN, Warren JD. 2014. Material properties of Northeast Pacific zooplankton. ICES J Mar Sci, 71(9), 2550-2563.

Blaxter JH, Douglas B, Tyler PA, Mauchline J. 1998. The biology of calanoid copepods (Vol. 33). Academic Press.

Brown M, Fenton D, Smedbol,K, Merriman C, Robichaud-Leblanc K, and Conway J. 2009. Recovery Strategy for the North Atlantic Right Whale (*Eubalaena glacialis*) in Atlantic Canadian waters. Species at Risk Act Recov Strat Ser vi + 66 p.

Carruthers E, Lewis K, McCue T, Westley P. 2008. Generalized linear models: model selection, diagnostics, and overdispersion. Memorial University of Newfoundland.

Chu D, Foote KG, Stanton TK. 1993. Further analysis of target strength measurements of Antarctic krill at 38 and 120 kHz: Comparison with deformed cylinder model and inference of orientation distribution. J Acoust Soc Am, 93(5), 2985-2988

Cochrane NA, Sameoto DD, Herman AW. 2000. Scotian Shelf euphausiid and silver hake population changes during 1984–1996 measured by multi-frequency acoustics. ICES J Mar Sci, 57(1), 122-132.

Cochrane NA, Sameoto DD, Belliveau DJ. 1994. Temporal variability of euphausiid concentrations in a Nova Scotia shelf basin using a bottom-mounted acoustic Doppler current profiler. Mar Ecol Prog Ser, 55-66.

Cochrane NA, Sameoto D, Herman AW, Neilson J. 1991. Multiple-frequency acoustic backscattering and zooplankton aggregations in the inner Scotian Shelf basins. Can J Fish Aquat Sci, 48(3), 340-355.

Cotté C, Simard Y. 2005. Formation of dense krill patches under tidal forcing at whale feeding hot spots in the St. Lawrence Estuary. Mar Ecol Prog Ser, 288, 199-210.

Croll DA, Marinovic B, Benson S, Chavez FP, Black N, Ternullo R,Tershy R. 2005. From wind to whales: trophic links in a coastal upwelling system. Mar Ecol Prog Ser, 289, 117-130.

Davies KTA, Ross T, Taggart CT. 2013. Tidal and subtidal currents affect deep aggregations of right whale prey, *Calanus* spp., along a shelf-basin margin. Mar Ecol Prog Ser, 479, 263–282. https://doi.org/10.3354/meps10189

Davies KTA, Taggart CT, Smedbol RK. 2014. Water mass structure defines the diapausing copepod distribution in a right whale habitat on the Scotian Shelf. Mar Ecol Prog Ser, 497, 69–85. https://doi.org/10.3354/meps10584

Davies KTA, Taggart CT, Smedbol RK. 2015. Interannual variation in diapausing copepods and associated water masses in a continental shelf basin, and implications for copepod buoyancy. J Marine Syst, 151, 35–46. https://doi.org/10.1016/j.jmarsys.2015.06.001

Department of Fisheries and Oceans. 2007. Recovery potential assessment for right whale (Western North Atlantic population). DFO Can Sci Advis Sec Sci Advis Rep. 2007/027.

Department of Fisheries and Oceans. 1996. Krill on the Scotian Shelf. DFO Atlantic Fisheries Stock Status Report. 96/106E.

Doherty P, Horsman T. 2007. Ecologically and biologically significant areas of the Scotian Shelf and environs: A compilation of scientific expert opinion. Can Tech Rep Fish Aquat Sci 2774: xii + 57 p.

Fisheries and Oceans Canada. 2014. Recovery Strategy for the North Atlantic Right Whale (*Eubalaena glacialis*) in Atlantic Canadian Waters [Final]. Species at Risk Act Recovery Strategy Series. Fisheries and Oceans Canada, Ottawa. vii + 68 pp.

Fleminger A, Clutter RI. 1965. Avoidance of towed nets by zooplankton. Limnol Oceanogr, 10(1), 96-104.

Francois RE, Garrison GR. 1982. Sound absorption based on ocean measurements. Part II: Boric acid contribution and equation for total absorption. J Acoust Soc Am, 72(6), 1879-1890.

Galbraith PS, Chassé J, Gilbert D, Larouche P, Brickman D, Pettigrew B, ... Lafleur C. 2013. Physical oceanographic conditions in the Gulf of St. Lawrence in 2012. Canadian Science Advisory Secretariat.

Garau B, Ruiz S, Zhang WG, Pascual A, Heslop E, Kerfoot J, Tintoré J. 2011. Thermal lag correction on slocum CTD glider data. J Atmos Ocean Tech, 28(9), 1065–1071. https://doi.org/10.1175/JTECH-D-10-05030.1

Gatien MG. 1976. A study in the slope water region south of Halifax. J Fish Res Board Can, 33(10), 2213-2217.

Gierak R. 2013. *Euphausia superba*. Animal Diversity Web. Accessed August 21, 2017 at http://animaldiversity.org/accounts/Euphausia_superba/

Goldbogen JA, Calambokidis J, Oleson E, Potvin J, Pyenson ND, Schorr G, Shadwick RE. 2011. Mechanics, hydrodynamics and energetics of blue whale lunge feeding: efficiency dependence on krill density. J Exp Biol, 214(1), 131-146.

Goldbogen JA, Calambokidis, J, Shadwick RE, Oleson EM, McDonald MA, Hildebrand JA. 2006. Kinematics of foraging dives and lunge-feeding in fin whales. J Exp Biol, 209(7), 1231-1244.

Greene CH, Wiebe PH, Burczynski J. 1989. Analyzing zooplankton size distributions using high-frequency sound. Limnol Oceanogr, 34(1), 129-139.

Hamner WM, Hamner PP. 2000. Behavior of Antarctic krill (*Euphausia superba*): schooling, foraging, and antipredatory behavior. Can J Fish Aquat Sci, 57(S3), 192-202.

Hannah CG, Shore JA, Loder JW, Naimie CE. 2001. Seasonal circulation on the western and central Scotian Shelf. J Phys Oceanogr, 31(2), 591-615.

Hardy SAC. 1936. Observations on the uneven distribution of oceanic plankton. University Press.

Hays GC. 2003. A review of the adaptive significance and ecosystem consequences of zooplankton diel vertical migrations. In Migrations and Dispersal of Marine Organisms (pp. 163-170). Springer, Dordrecht.

Herman AW, Cochrane NA, Sameoto DD. 1993. Detection and abundance estimation of euphausiids using an optical plankton counter. Mar Ecol Prog Ser, 165-173.

Herman AW. Sameoto DD, Shunnian C, Mitchell MR, Petrie B, Cochrane N. 1991. Sources of zooplankton on the Nova Scotia shelf and their aggregations within deep-shelf basins. Cont Shelf Res, 11(3), 211–238. https://doi.org/10.1016/0278-4343(91)90066-F

Hjort J, Ruud JT. 1929. Whaling and fishing in the North Atlantic. Rapp. P.-V. Réun. Int. Counc. Explor. Mer. 56, 5-123.

Hofmann EE, Murphy EJ. 2004. Advection, krill, and Antarctic marine ecosystems. Antarct Sci, 16(4), 487-499.

Hovekamp S. 1989. Avoidance of nets by *Euphausia pacifica* in Dabob Bay. J Plankton Res, 11(5), 907-924.

Hoyt E. 2012. Marine Protected Areas for Whales, Dolphins and Porpoises: A world handbook for cetacean habitat conservation and planning. Routledge.

Kaartvedt S, Larsen T, Hjelmseth K, Onsrud MS. 2002. Is the omnivorous krill *Meganyctiphanes norvegica* primarily a selectively feeding carnivore? Mar Ecol Prog Ser, 228, 193-204.

Kenney RD, Hyman MA, Owen RE, Scott GP, Winn HE. 1986. Estimation of prey densities required by western North Atlantic right whales. Mar Mammal Sci, 2(1), 1-13.

Lavery AC, Wiebe PH, Stanton TK, Lawson GL, Benfield MC, Copley N. 2007. Determining dominant scatterers of sound in mixed zooplankton populations. J Acoust Soc Am, 122(6), 3304–3326. https://doi.org/10.1121/1.2793613

Lavoie D, Simard Y, Saucier FJ. 2000. Aggregation and dispersion of krill at channel heads and shelf edges: the dynamics in the Saguenay-St. Lawrence Marine Park. Can J Fish Aquat Sci, 57(9), 1853-1869.

Lawson GL, Wiebe PH, Ashjian CJ, Stanton TK. 2008. Euphausiid distribution along the Western Antarctic Peninsula-Part B: Distribution of euphausiid aggregations and biomass, and associations with environmental features. Deep Sea Res Pt II, 55(3–4), 432–454. https://doi.org/10.1016/j.dsr2.2007.11.014

Loder JW, Han,G, Hannah CG, Greenberg DA, Smith PC. 1997. Hydrography and baroclinic circulation in the Scotian Shelf region: winter versus summer. Can J Fish Aquat Sci, 54(S1), 40-56.

Mackas DL, Kieser R, Saunders M, Yelland DR, Brown RM, Moore DF. 1997. Aggregation of euphausiids and Pacific hake (*Merluccius productus*) along the outer continental shelf off Vancouver Island. Can J Fish Aquat Sci, 54(9), 2080–2096. https://doi.org/10.1139/f97-113

Martin B, Kowarski K, Mouy X, Moors-Murphy H. 2014. Recording and identification of marine mammal vocalizations on the scotian shelf and slope. In Oceans-St. John's, 2014 (pp. 1-6). IEEE.

Mauchline J. 1967. Volume and weight characteristics of species of Euphausiacea. Crustaceana, 241-248.

Mauchline J. 1980. The biology of euphausiids. Adv Mar Biol, 18, 373-623.

Mauchline J, Fisher LR. 1969. The Biology of Euphausiids. FS Russell and M. Yonge, editors.

McDougall TJ, Barker PM. 2011. Getting started with TEOS-10 and the Gibbs Seawater (GSW) oceanographic toolbox. SCOR/IAPSO WG, 127, 1-28.

McLellan HJ. 1954. Temperature-salinity relations and mixing on the Scotian Shelf. J Fish Res Board Can, 11(4), 419-430.

Medwin H. 2005. Sounds in the sea: From ocean acoustics to acoustical oceanography. Cambridge University Press.

Medwin H, Clay CS. 1998. Fundamentals of Acoustical Oceanography Academic. New York, 24.

Melle W, Ellertsen B, Skjoldal HR. 2004. Zooplankton: the link to higher trophic levels. The Norwegian Sea Ecosystem, 137-202. Tapir Academic Press.

Michaud J, Taggart CT. 2007. Lipid and gross energy content of North Atlantic right whale food, Calanus finmarchicus, in the Bay of Fundy. Endanger Species Res.

Michaud J, Taggart T. 2011. Spatial variation in right whale food, *Calanus finmarchicus*, in the Bay of Fundy. Endanger Species Res, 15(3), 179-194.

Mitchell EDWARD, Kozicki VM, Reeves RR. 1986. Sightings of right whales, *Eubalaena glacialis*, on the Scotian Shelf, 1966–1972. Report of the International Whaling Commission (Special Issue 10), 83-107.

Morris DJ, Watkins JL, Ricketts, Buchholz CF, Priddle J. 1988. An assessment of the merits of length and weight measurements of Antarctic krill *Euphausia superba*. Brit Ant Surv Bull, 79: 27–50.

Nicol S. 1986. Shape, size and density of daytime surface swarms of the euphausiid *Meganyctiphanes norvegica* in the Bay of Fundy. J Plankton Res, 8(1), 29-39.

Nowacek DP, Friedlaender AS, Halpin P, Hazen, EL, Johnston DW, Read AJ, ... Zhu Y. 2011. Super-aggregations of krill and humpback whales in Wilhelmina Bay, Antarctic Peninsula. PLoS One, 6(4), e19173.

O'Brien, R. M. (2007). A caution regarding rules of thumb for variance inflation factors. *Quality & Quantity*, *41*(5), 673-690.

Patrician MR, Kenney RD. 2010. Using the Continuous Plankton Recorder to investigate the absence of North Atlantic right whales (*Eubalaena glacialis*) from the Roseway Basin foraging ground. J Plankton Res, 32(12), 1685–1695. https://doi.org/10.1093/plankt/fbq073

Petrie B, Drinkwater K. 1993. Temperature and salinity variability on the Scotian Shelf and in the Gulf of Maine 1945–1990. J Geophys Res: Oceans, 98(C11), 20079-20089

Piatt JF, Methven DA. 1992. Threshold foraging behavior of baleen whales. Mar Ecol Prog Ser, 205-210.

Pinchuk A, Hopcroft R. 2010. *Thysanoessa inermis*, Kroyer 1846. From: Arctic Ocean Diversity, webpage accessed August 7, 2017 from: http://www.arcodiv.org/watercolumn/euphausiid/Thysanoessa_inermis.html

Razouls C, de Bovée F, Kouwenberg J, Desreumaux N. 2005-2017. Diversity and Geographic Distribution of Marine Planktonic Copepods. Retrieved from http://copepodes.obs-banyuls.fr/en

Reid D, Scalabrin C, Petitgas P, Masse J, Aukland R, Carrera P, Georgakarakos S. 2000. Standard protocols for the analysis of school based data from echo sounder surveys. Fish Res, 47(2), 125-136.

Ressler PH, Brodeur RD, Peterson WT, Pierce SD, Vance PM, Røstad A, Barth JA. 2005. The spatial distribution of euphausiid aggregations in the Northern California Current during August 2000. Deep Sea Res Pt II, 52(1), 89-108.

Ringelberg J. 2009. Diel vertical migration of zooplankton in lakes and oceans: causal explanations and adaptive significances. Springer Science & Business Media.

Ross T, Craig SE, Comeau A, Davis R, Dever M, Beck M. 2017. Blooms and subsurface phytoplankton layers on the Scotian Shelf: Insights from profiling gliders. J Marine Syst, 172, 118-127.

Sameoto DD. 1980. Relationships between stomach contents and vertical migration in *Meganyctiphanes norvegica*, *Thysanoessa raschii* and *T. inermis* (Crustacea Euphausiacea). J Plankton Res, 2(2), 129-143.

Sameoto DD, Jaroszynski LO, Fraser WB. 1980. BIONESS, a new design in multiple net zooplankton samplers. Can J Fish Aquat Sci, 37(4), 722-724.

Sameoto D, Cochrane N, Herman A. 1993. Convergence of Acoustic, Optical, and Net-Catch Estimates of Euphausiid Abundance: Use of Artificial Light to Reduce Net. Can J Fish Aquat Sci, 50(2), 334–346. https://doi.org/10.1139/f93-039

Satterthwaite FE. 1946. An approximate distribution of estimates of variance components. Biometrics bull, 2(6), 110-114.

Schofield O, Kohut J, Aragon D, Creed L, Graver J, Haldeman C, Kerfoot J, Roarty, H, Jones C, Webb D, Glenn S. 2007. Slocum gliders: Robust and ready. J Field Robot, 24(6), pp.473-485.

Smith PC. 1983. The mean and seasonal circulation off southwest Nova Scotia. J Phys Oceanogr, 13(6), 1034-1054.

Stanton TK, Chu D. 2000. Review and recommendations for the modelling of acoustic scattering by fluid-like elongated zooplankton: euphausiids and copepods. ICES J Mar Sci, 57(4), 793-807.

Stanton TK, Chu D, Wiebe, PH. 1998b. Sound scattering by several zooplankton groups. II. Scattering models. J Acoust Soc Am, 103(1), 236-253.

Stanton TK, Chu D, Wiebe PH, Martin LV, Eastwood RL. 1998a. Sound scattering by several zooplankton groups. I. Experimental determination of dominant scattering mechanisms. J Acoust Soc Am, 103(1), 225–235.

Vagle S, Foote KG, Trevorrow MV, Farmer DM. 1996. A technique for calibration of monostatic echosounder systems. IEEE J Oceanic Eng, 21(3), 298-305.

Ward-Paige CA, Bundy A. 2016. Mapping biodiversity on the Scotian Shelf and in the Bay of Fundy. DFO Can Sci Advis Sec Res Doc, 2016/006.

Welch BL. 1947. The generalization of student's' problem when several different population variances are involved. Biometrika, 34(1/2), 28-35.

Wiebe PH, Ashjian CJ, Lawson GL, Piñones A, Copley NJ. 2011. Horizontal and vertical distribution of euphausiid species on the Western Antarctic Peninsula US GLOBEC Southern Ocean study site. Deep Sea Res Pt II, 58(13), 1630-1651.

Wiebe PH, Backus RH, Caron DA, Gilbert PM, Grassle JF, Powers K, Waterbury JB. 1987. Biological oceanography. In Milliman, J.D., Wright, W.R. (eds). The Marine Environment of the U.S. Atlantic Continental Slope and Rise. Junes and Bartlett, Boston/Woods Hole, M.A. pp 140-201.

Wiebe PH, Boyd SH, Davis BM., Cox JL. 1982. Avoidance of towed nets by the euphausiid *Nematoscelis megalops*. Fish. Bull, 80(1), 75-91.

Woodley TH, Gaskin DE. 1996. Environmental characteristics of North Atlantic right and fin whale habitat in the lower Bay of Fundy, Canada. Can J Zool, 74(1), 75-84.

Appendix A

Rare Zooplankton Taxa Collected in BIONESS Net Samples

Table A.1. Rare copepods and other zooplankton collected in the BIONESS net samples on 9 Oct 2025 in Roseway Basin.

	Taxa	Description
Rare Copepods	*Acartia danae*	
	Calocalanus pavo	
	Candacia armata	
	Corycaeus latus	
	Euterpina acutifrons	
	Mecynocera clausi	
	Mecynocera clausi	
	Microcalanus sp	
	Nannocalanus minor	
	Temora longicornus	
Other Zooplankton	*Beroe cucumis*	Ctenophore
	Beroe gracils	Ctenophore
	Bivalve larvae	
	Cladocera	
	Echinodermata larvae	
	Euphausiid egg	
	Euphausiid nauplii	
	Foraminifera	
	Fritillaria sp	Tunicate
	Gastropoda larvae	
	Isopoda	
	Oikiopleura sp	Tunicate
	Paraconchoecia spinifera	Ostrocod
	Parasagitta sp	Chaetognath
	Polychaeta larvae	
	Pseudosagitta maxima	Chaetognath
	Serratosagitta serrodentata	Chaetognath
	Siphonophore bract	
	Thalia democratica	Salp
	Tomopteris helgolandica	Polychaete